



Aristotle University of Thessaloniki
School of Science – Department of Physics
Section of Astrophysics, Astronomy and Mechanics
Laboratory of Astronomy

A WIDE-FIELD SURVEY FOR VARIABLE STARS



Diploma Thesis
by
Vasileios Karamanavis

Supervisor: Professor John H. Seiradakis

Thessaloniki, April 2011

Cover image: T Tauri stars and Hind's Variable Nebula. Image credit Don Goldman, APOD, 2007 December 13.

The orange star at the center of the image is T Tauri, prototype of the class of T Tauri variable stars. The nearby dusty, yellow cloud is Hind's Variable Nebula (NGC 1555/1554). Over 400 light-years away, at the edge of a molecular cloud, both star and nebula are seen to vary significantly in brightness but not necessarily at the same time, adding to the mystery of the intriguing region. T Tauri stars are now generally recognized as young (less than a few million years old), sun-like stars still in the early stages of formation. To further complicate the picture, infrared observations indicate that T Tauri itself is part of a multiple system and suggest that the associated Hind's Nebula may also contain a very young stellar object. This remarkable color image spans about 4 light-years across, at the estimated distance of T Tauri.

*To my parents and my brother,
who were always there for me...*

Abstract

This diploma thesis will focus on the use of wide-field instrumentation and associated analysis methods in order to facilitate the discovery of new variable stars. The thesis has been organised in the following way.

In Chapter one I give an introduction to the variable star nomenclature and taxonomy along with facts and figures of the variable star observations since the birth of astronomy.

Chapter 2 begins by laying out the theoretical dimensions of the research, and looks at how certain physical mechanisms, such as pulsations, eruptions, eclipses and rotation contribute to stellar variability.

Chapter 3 serves as a brief overview of the variable star classes and categories established to date. The classification scheme largely follows that of the General Catalogue of Variable Stars (GCVS).

In Chapter 4, I describe the observations as well as the instrumentation used and the field tests performed to determine its optimal configuration for the search of new variable stars.

Chapter 5 gives a detailed account of the data reduction and analysis procedure followed, with emphasis to the theoretical pieces of astronomical image manipulation including practical considerations. An overview of the reduction pipeline is presented, while I elaborate on the De-trending process, the TFA algorithm (Kovàcs et al. 2005) and the selection criteria for stellar variability namely the j-index (Stetson 1996) and the pulsation parameter (Viscum et al. 1997).

The last chapter contains the results and the final light curves of twenty-one (21) candidates that comply with our variability criteria, out of which sixteen (16) lack any bibliographic reference.

Περίληψη

Η διπλωματική αυτή εργασία επικεντρώνεται στην ανίχνευση μεταβλητών αστέρων με τη μέθοδο της ευρέως-πεδίου επισκόπησης (wide-field survey). Η οργάνωσή της ακολουθεί την παρακάτω δομή.

Στο Κεφάλαιο 1 γίνεται μια σύντομη περιγραφή της ταξινόμησης και της ονοματολογίας των μεταβλητών αστέρων και των κανόνων που τις διέπουν.

Στο Κεφάλαιο 2 περιγράφονται οι φυσικοί μηχανισμοί που συμβάλλουν ή και καθορίζουν τη μεταβλητότητα των αστέρων και τα χαρακτηριστικά της.

Στο τρίτο Κεφάλαιο γίνεται αναφορά στις σημαντικότερες κατηγορίες μεταβλητών αστέρων, στα φυσικά τους χαρακτηριστικά και στην παρατηρησιακή τους υπογραφή. Η ταξινόμηση ακολουθεί, κατα κύριο λόγο, αυτήν του General Catalogue of Variable Stars (GCVS).

Στο Κεφάλαιο 4 περιγράφω την δομή των παρατηρήσεων από τον Αστρονομικό Σταθμό Χολομώντα. Παρατείθενται επίσης τα αποτελέσματα των δοκιμών του εξοπλισμού ώστε να προσδιοριστεί η βέλτιστη διαμόρφωσή του για την επίτευξη των στόχων της εργασίας.

Το Κεφάλαιο 5 ασχολείται με την πλήρη περιγραφή της ανάλυσης των δεδομένων. Δίνεται έμφαση σε θεωρητικά κομμάτια καθώς επίσης και σε πρακτικές δυσκολίες. Παρουσιάζω ένα περίγραμμα του κώδικα ανάλυσης των δεδομένων και εστιάζω ειδικά στις διαδικασίες του De-trending με τον κώδικα TFA (Kovács et al. 2005) και της επιλογής των μεταβλητών αστέρων του δείγματος με χρήση των δεικτών μεταβλητότητας j -index (Stetson 1996) και pulsation parameter (Viskum et al. 1997).

Στο τελευταίο κεφάλαιο παρουσιάζω τις τελικές καμπύλες φωτός είκοσι ενός (21) υποψήφιων μεταβλητών αστέρων, για δέκα έξι (16) από τους οποίους δέν υπάρχουν βιβλιογραφικές αναφορές.

Acknowledgements

During the effort for the completion of this thesis many people have contributed in one or the other way. Stavros Avgoloupis and John H. Seiradakis were the first astronomy professors I met during my studies in the University of Thessaloniki. They have been the best examples for me to follow and they are the most inspiring mentors I have ever met. I would like to thank especially John H. Seiradakis for his guidance through my work; without his help this dissertation would have been a never land.

People like Dimitris Mislis, Stelios Pyrzas, Lilia Tremou and Ioannis Nestoras who started the whole observational journey at Mount Holomon have also a special place in our hearts and minds.

I am thankful to John Antoniadis, former colleague and good friend, for kindly making available to me the original version of the ThReT reduction pipeline and for the endless talks we had over issues concerning this diploma thesis.

Giannis Vakoulis, Kostas Kouroubatzakis, Thanasis Nitsos have proved to be valuable friends and irreplaceable co-observers during all of our observational attempts.

I would like to thank Panagiotis Ioannidis and Chryssa Avdelidou for obtaining the seeing data.

The completion of a large number of theses, along with mine, is due to the good will of the Faculty of Forestry and Natural Environment of the University of Thessaloniki, and the Taxiarchis forest manager G. Panourgias allowing us to use some of their space and infrastructure at Mt. Holomon.

Vaggelis Tsorlinis, the observatory technician, has helped me more than many times with technical issues that come up in every observational quest.

Finally but exceptionally, I am grateful to Nikoletta Filippou who has always been my driving force and inspiration, even in complicated times.

Contents

1	Introduction	1
1.1	Introduction	1
1.2	Variable Star Milestones	1
1.3	Nomenclature and Taxonomy	3
1.3.1	The General Catalogue of Variable Stars (GCVS)	4
2	Stellar Variability Mechanisms	7
2.1	Introduction	7
2.2	Intrinsic Variability	7
2.2.1	The Instability Strip	7
2.2.2	Pulsations	8
2.2.3	Eruptions	12
2.3	Extrinsic Variability	13
2.3.1	Eclipses and Binary Stars	13
2.3.2	Stellar Rotation	18
2.4	The Solar Case	19
2.4.1	Helioseismology	21
3	An Overview of Variable Stars	23
3.1	Introduction	23
3.2	Eclipsing Variable Stars	23
3.2.1	Algol Type Stars	23
3.2.2	β Lyrae Stars	25
3.2.3	RS Canum Venaticorum	25
3.2.4	Contact Binaries – W Ursae Majoris Variables (W UMa)	26
3.2.5	Transiting Extra-Solar Planets	27
3.3	Rotating Variable Stars	29
3.3.1	FK Comae Stars	29
3.3.2	BY Draconis Stars	29
3.3.3	Pulsars	29
3.4	Pulsating Variable Stars	31
3.4.1	Classical Cepheids	31
3.4.2	Population II Cepheids (W Virginis Stars)	31
3.4.3	RR Lyrae Stars	31
3.4.4	δ Scuti Variables	32
3.4.5	Rapidly Oscillating Peculiar Ap (roAp) Stars	33

3.4.6	β Cephei (β Canis Majoris) Stars	34
3.5	Eruptive Variable Stars	35
3.5.1	Flare Stars	35
3.5.2	Cataclysmic Variables (CVs) and Nova-like Stars	35
3.5.3	Symbiotic Binaries	36
3.5.4	Wolf–Rayet Stars	37
3.5.5	Supernovæ	37
3.6	Pre-Main Sequence Variable Stars	39
3.6.1	T Tauri Stars	39
3.6.2	Herbig Ae and Be Stars	40
3.6.3	Herbig–Haro Objects	40
3.7	X-ray Binaries	41
3.7.1	High-Mass X-ray Binaries	42
3.7.2	Low-Mass X-ray Binaries	43
4	Observations	45
4.1	Introduction	45
4.2	The Site of Observations	46
4.2.1	Seeing Measurements	46
4.3	Interesting Stellar Fields	47
4.4	Instrumentation and Equipment	52
4.4.1	The Camera	52
4.4.2	Tests of our CCD Camera	52
4.4.3	Telescopes and Mounts	56
5	Data Reduction and Analysis	61
5.1	Introduction	61
5.2	Outline of the Reduction Scheme	61
5.2.1	De-Biasing	63
5.2.2	Dark Current Correction	63
5.2.3	Flat-Fielding	63
5.2.4	Photometry	64
5.3	De-Trending the Time Series	64
5.3.1	The Trend Filtering Algorithm	64
5.4	Variability Criteria	66
5.4.1	The j-index	66
5.4.2	Pulsation parameter	66
5.5	ThReT Reduction & Analysis Pipeline	67
5.6	Astrometric Calibration	68
6	Results and Discussion	73
6.1	Introduction	73
6.2	The observations of 24 July 2009	73
6.2.1	Light Curves of Variable Stars within ExoField #1	77
6.3	Conclusions	85
6.4	Future Work	85
Querying the SIMBAD database	91	
Software	101	
Bibliography	115	

List of Figures

1.1.1 Man seeking the ultimate truth	2
2.2.1 Types of variable stars on the H-R diagram	8
2.2.2 One-dimensional oscillations	9
2.2.3 Two-dimensional oscillations	9
2.2.4 Non-radial pulsation modes for certain values of ℓ and m	10
2.2.5 Two versions of the H-R diagram containing well-known types of pulsating variables. Evolutionary tracks are also visible.	11
2.2.6 BO Microscopii flare and spots	13
2.3.1 The principle behind radial velocity determination.	14
2.3.2 Direct imaging of the binary star SR24 in the constellation of Ophiuchus. .	15
2.3.3 Roche equipotential surfaces.	16
2.3.4 Eclipse geometry.	17
2.3.5 The effect of starspots	18
2.3.7 The effect of rotation to a $20M_{\odot}$ star with a $Z=0.02$ at ZAMS	19
2.3.6 Distribution of calcium on the surface of the Ap star HR 3831	19
2.4.1 The butterfly diagram	20
2.4.2 Images of the solar surface.	22
3.1.1 The position of variable stars on the H-R diagram	24
3.2.1 Characteristic light curve of an Algol type variable	25
3.2.2 Characteristic light curve of a β Lyrae variable	26
3.2.3 Light curve and model of RS CVn system	27
3.2.4 The Roche potential	28
3.2.5 Light curve of an EW (or W UMa) system, GK Aqr	28
3.3.1 Activity of FK Comae Berenices	30
3.3.2 Typical pulse profile of a radiopulsar	30
3.4.1 Light curve, temperature, radius and radial velocity of δ Cephei	32
3.4.2 Light curves of RR Lyrae stars	33
3.4.3 Spectrum and light curve of a roAp star. The chemical peculiarities are visible.	34
3.5.1 Light curve of a CV star	37
3.5.2 Light curve of a symbiotic star, AX Persei	38
3.5.3 Large sample of SN light curves	39
3.6.1 A schematic of the T Tauri phenomenon	40
3.6.2 Herbig–Haro object number 211	41

3.6.3 A collection of HH objects	42
4.2.1 Map of the Chalkidiki region	46
4.2.2 Seeing conditions at Mt. Holomon.	48
4.2.3 Seeing conditions at Mt. Holomon (cont.).	49
4.2.4 Seeing conditions at Mt. Holomon (cont.).	50
4.2.5 Overall Seeing and Isoplanatic angle measurements	50
4.3.1 Visibility plot of the ExoField #1	51
4.4.1 Spectral response of the KAF-6303 chip.	53
4.4.2 Linearity diagram of the KAF-6303 chip.	54
4.4.3 Typical calibration frames acquired with both telescopes.	57
4.4.4 Images of ExoField #1 using both telescopes. The same star is marked for a comparison of the fields of view.	58
4.4.5 FWHM of the PSFs along the x and y axis of the CCD array, using the EPSILON-180ED telescope.	59
5.2.1 A road map of CCD photometry	62
5.6.1 1006 SIMBAD objects overplotted on ExoField #1	70
5.6.2 The structure of ThReT reduction and analysis pipeline	71
6.2.1 Standard deviation vs magnitude plot for the 24/07/2009 data prior to the application of the TFA algorithm	74
6.2.2 $\delta\sigma$ versus $\sigma(\text{non-TFA})$ plot for the 24/07/2009 data	74
6.2.3 Distribution of variability index j for the stars in ExoField #1	75
6.2.4 Histogram of j-index values of the stars within the field.	75
6.2.5 Distribution of the pulsation index in ExoField #1	76
6.2.6 Histogram of pulsation parameter values of the stars within the field.	76
6.2.7 Light curves	77
6.2.8 Light curves	78
6.2.9 Light curves	79
6.2.10 Light curves	80
6.2.11 Light curves	81
6.2.12 Light curves	82
6.2.13 Light curves	83
6.4.1 The Self-Organizing map	86
6.4.2 SOM@VizieR	86

List of Tables

4.1.1 A summary of the observations.	45
4.2.1 Holomon Astronomical Station geographical data.	47
4.3.1 ExoField #1 Data.	47
4.4.1 CCD camera and Sensor specifications.	52
4.4.2 The Celestron C11 Specifications.	56
4.4.3 Takahashi EPSILON-180ED Astrograph Specifications.	56
6.2.1 A catalogue of variable stars within ExoField #1.	84

1

Introduction

”Twinkle, twinkle, little star,
How I wonder what you are!
Up above the world so high,
Like a diamond in the sky!”

-An old but interesting
nursery rhyme

1.1 Introduction

SINCE the beginning of his existence man always looked up in the sky and wondered about the infinite beauty he observed. He was sailing among the twinkling beacons, now called stars, and the endless road of light and matter, our Milky Way. He observed the changes in the night and the day sky, which are considerably less, and tried to understand as many things as possible about his natural environment, using only his eyes. The invention of the telescope by Galileo is a great leap in the history of mankind, which opened new roads in the understanding of the universe and the position of man in it. Now humans are not the center but a small part, an important one, but still a small part of the universe.

All stars during the course of their lifetime display variations in brightness. Those that vary in brightness, in time scales of the order of the human life and in amplitude as much as to be detectable by the naked eye or any other means of observation, are characterized as variable stars. In general, each star's variations are characteristic of its evolutionary stage. Two important parameters are the overall amplitude as well as the duration of the duty cycle of the variability. The duty cycle, the amplitude and the shape of the light curve can be obtained by photometric observations.

1.2 Variable Star Milestones

The history of variable stars starts in the ancient world. The Greek astronomer Hipparchus (190 BC–120 BC), in 134 BC according to Pliny, first observed the appearance of a nova in the constellation of Scorpius. Hipparchus then compiled the first catalog of stars, probably inspired by that event. This nova observation is also confirmed by the Chinese astronomer She Ke who spotted the same event in the sky in the same position as Hipparchus in June 134 BC.

Arab astronomers also greatly contributed to variable star observations. They have probably identified the variations of brightness of β Persei, which was known as "al-ghūl",



Figure 1.1.1: Man seeking the ultimate truth about the universe and its well hidden secrets.

meaning the daemon star and is now known as Algol. In Greek mythology Algol is also linked with misfortune due to its variability.

Towards the end of the 16th century the first contemporary observations of variable stars were made. First, *Tycho Brahe's supernova* lit up in 1572. Some years later, in 1596, the irregular light variations of α Ceti were observed by David Fabricius. The star due to its abnormal behavior took the name Mira or Mirabilis (*the wonderful*).

Another supernova exploded in 1604. This time the constellation of Ophiuchus hosted the cataclysmic event. It was discovered in October 9, 1604 but it was already brighter than all other stars in the sky. Kepler was not the first to see it but he started a very thorough study, probably inspired by the work done by Tycho Brahe for SN 1572. The brightness was at first comparable to Mars but very soon it overwhelmed the brightness of Jupiter reaching a magnitude of -2.25, according to a calculation by W. Baade. *Kepler's supernova* was the last supernova to explode in our Galaxy.

At the end of the 18th century Edward Pigott (approx. 1753–1825) and John Goodricke (1764–86) contribute to the variable star research with their observations. Pigott established the variability of η Aquilae in 1784, of R Coronae Borealis in 1795, and of R Scuti in 1796. Goodricke is credited with the discovery of the periodicity of δ Cephei and β Lyrae in 1784, and of β Persei (Algol) in 1782–1783.

Friedrich Wilhelm Argelander based on his visual observations between 1852 and 1859 discovered a large number of new variable stars. Those observations led to the compilation of *Bonner Durchmusterung*, a star catalog that contained the position and brightness of thousands of stars. This was the last star catalog before the introduction of the photographic plate, which revolutionized astronomy and turned it into a quantitative science.

The invention of the photographic plate along with the construction of greater telescopes paved the way for a more systematic and refined study of variable stars. Spectra became largely available to researchers and thanks to the work of E. Pickering and his colleagues like Henrietta Leavitt or Annie Jump Cannon, thousands of spectra were analysed. The results led to the discovery of new classes of variables and the establishment of period-luminosity relation for Cepheid variables which set the scale of the Universe.

Today thousands of variable stars are known and classified. The General Catalog

of Variable Stars is the basic reference for anyone interested in this field. The constant advances in technology enable us to study variable stars well beyond the limits of our Galaxy. Almost every astronomical survey aims into detecting even the slightest variability in stars and other objects. Variability is the observational signature of many interesting phenomena, and we shall never cease to look for it.

1.3 Nomenclature and Taxonomy

There is a certain number of parameters which are used to classify variable stars. These parameters are deduced either photometrically or spectroscopically. Some important spectroscopic parameters are the spectral type, the chemical composition and the luminosity class. In principle the task of classification should be an easy one. Each star should fall into a category according to the values of those parameters. But the situation is very complicated. All of the parameters are not always present. This is because one can have only photometric or only spectroscopic data, or the quality is poor or the time resolution is not adequate for a conclusion to be drawn. Furthermore as technology advances and new instruments are used, more data are accumulated. Often some parameters point to one class, while some others point to another. This makes the borders between classes difficult to discern.

Another equally important issue is the nomenclature of variable stars. At first if an object that belongs to a constellation turned out to be a variable one, then the Bayer–Flamsteed notation was used, namely a greek or roman letter followed by the genitive of the name of the constellation it belongs to (e.g β Lyrae).

The star catalogue, known as *Bonner Durchmusterung (BD)*, compiled by Argelander contained a large number of variable sources. To tackle the problem of naming, Argelander introduced a new system for the stars without a Bayer–Flamsteed designation. According to this new scheme the roman capital letters starting from R (R, S, T, U, V, W, X, Y, Z) are used before the latin name of the constellation or the corresponding abbreviation (e.g U Gem).

The introduction of the photographic plate revolutionized data acquisition and consequently increased the number of known variable stars. Argelander's scheme was inadequate; an extension had to be made. *Astronomische Gesellschaft* extended it by adopting double roman letters from RR to RZ, SS to SZ etc. This first extension raised the number of variable stars per constellation from 9 to 54. When the number turned out to be insufficient a second extension was made, namely using the remaining letters, AA to AZ, BB to BZ etc, omitting J. The second extension raised the number to 334 variables per constellation.

A new nomenclature was proposed by the Dutch astronomer Nijland (Hoffmeister, 1984). The new system appeared as a uniform and concise counterpart to the doubly extended Argelander scheme. Nijland suggested that variables from R through QZ (all of the 334) should be renamed as V1, V2, ..., V334 and the subsequent variables would get an ever increasing designation *ad infinitum* (e.g V335, V336 etc.). The Nijland system was not accepted widely for reasons of consistency, since many names of variable stars based on the Argelander system were used to characterize whole classes of variables (e.g RR Lyr). However the system is in use for the variable stars in a constellation beyond QZ or V334.

Other objects that appear in a more dramatic way have different naming schemes. This is the case for Novae. Old novae are referred to as *Nova* and the genitive of the constellation in which they appeared, followed by the year of observation (e.g Nova Cygni 1600, or N Cygni 1600). If more than one novae erupt in the same year a number is added (e.g Nova Vul 1968, number 2). This system holds until a proper variable-star

designation is assigned (e.g Nova Vul 1968, number 2 has been renamed LU Vul). This procedure of renaming is not time consistent, meaning that the variable-star designation is chronologically irrelevant of the actual time of observation (e.g AT Sgr = Nova Sgr 1900, V737 Sgr = Nova Sgr 1933, V1016 Sgr = Nova Sgr 1899).

A similar system is used for supernovae. The year of observation and a latin character are used following the word *Supernova* or the abbreviation SN (e.g Supernova 1987a or SN 1987a). A variable star designation is not usually appended to Supernovae except for the well known galactic ones.

Other well known and widely used designations are HR, HD, R (Ratcliffe catalog) and He (Henize), followed by a number. These variable stars are noted in the corresponding catalogs.

1.3.1 The General Catalogue of Variable Stars (GCVS)

The primary bibliographical reference for the variable star researcher is the General Catalog of Variable Stars (GCVS). The GCVS is maintained and edited by the astronomical Institute of the Russian Academy of Sciences, at the Sternberg Astronomical Institute of the Moscow State University. The whole effort is under the auspices of the IAU Division of Variable Stars.

The most recent edition of the GCVS is the 4th ed. (GCVS4, Kholopov et al. 1985-1988), containing data about 28484 objects that are discovered since 1984. They all have the designation "variable star" and the data that are contained in the first three volumes I-III, are about variable stars in the Milky Way galaxy. The fourth volume of GCVS4 was published in 1994 and contains a table of all variables ordered by right ascension (B1950), a table of variables listed by variability type, and an extensive series of cross-identification tables to alternative designations. Volume V of GCVS4 contains extensive information on extragalactic variables. It actually consists of two catalogs. The first catalog, of variable stars in external galaxies contains 10979 variable stars in 35 stellar systems (including the Magellanic Clouds, the large galaxies in Andromeda and Triangulum, etc.). The second catalogue, of extragalactic supernovae includes 984 confirmed or suspected supernovae.

There exist also supplements to the GCVS, namely the *Name List of Variable Stars*, which appears in a regular basis in the *Information Bulletin on Variable Stars* (IBVS, IAU Commission 27 & 42). The *New catalog of Suspected Variables* is another well-known catalog compiled by Kukarkin et al. (1982) that contains data on 14811 objects that are not yet finally designated as variables prior to 1980. The *New Catalogue of Suspected Variable Stars. Supplement* is a compilation of 11206 stars suspected of variability and not finally designated as variables prior to 1997.

The GCVS4 utilizes a classification scheme according to variability type. Those types along with the stars they contain and their symbols are shown below, for a concise presentation refer to the original GCVS4.

1. Eruptive (FU, GCAS, I, IA, IB, IN, INA, INB, INT, IT, IN(YY), IS, ISA, ISB, RCB, RS, SDOR, UV, UVN, WR)
2. Pulsating (ACYG, BCEP, BCEPS, CEP, CEP(B), CW, CWA, CWB, DCEP, DCEPS, DSCT, DSCTC, GDOR, L, LB, LC, M, PVTEL, RPHS, RR, RR(B), RRAB, RRC, RV, RVA, RVB, SR, SRA, SRB, SRC, SRD, SXPHE, ZZ, ZZA, ZZB)
3. Rotating (ACV, ACVO, BY, ELL, FKCOM, PSR, SXARI)
4. Cataclysmic (explosive and nova-like) variables (N, NA, NB, NC, NL, NR, SN, SNI, SNII, UG, UGSS, UGSU, UGZ, ZAND)

5. Eclipsing binary systems (E, EA, EB, EW, GS, PN, RS, WD, WR, AR, D, DM, DS, DW, K, KE, KW, SD)
6. Intense variable X-ray sources (X, XB, XF, XI, XJ, XND, XNG, XP, XPR, XPRM, XM)
7. Other symbols (BLLAC, CST, GAL, L:, QSO, S, *, +, :)
8. The new variability types (ZZO, AM, R, BE, LBV, BLBOO, EP, SRS, LPB)

The GCVS is a rather systematic and well maintained effort of cataloging variable stars. The classification is based on sound observational facts and there is also a sense of criticism over them.

2

Stellar Variability Mechanisms

"Shake, rattle and roll"

-Bill Haley and His Comets,
a 1954 popular song

2.1 Introduction

NATURE'S way is definitely not a static one. The very essence of nature is change, variation, fluctuation; and She has many ways to accomplish that. In the stellar domain, variability is explained on the basis of many mechanisms, whose diversity spans from simple eclipses to exotic pulsations and eruptions on the surface of stars.

There are also times that more than one mechanism is responsible for a certain type of variability. This is when things get complicated from an observational, as well as from a theoretical point of view. Observationally, a modulation in a light curve due to a phenomenon other than the one which causes the initial, high amplitude variability is difficult to catch. In this case errors play a significant role, especially when the secondary variability is of low amplitude. Theoretically the interpretation of perplexed light curves is a puzzling task. The situations gets worse in case of a superposition of mechanisms. Nature has a clear aversion to sealed-off effects and mechanisms.

The known mechanisms responsible for stellar variability are discussed in this chapter. Unlike Nature's way, the discussion is done separately for each variability mechanism for reasons of clarity.

2.2 Intrinsic Variability

Stars of this kind vary due to physical activity of the star itself. There are many known types of intrinsic variables and not all of them share the same characteristics. The explanation of their variability is a great challenge and many things still remain unknown. The light variations can be periodic or quasi-periodic and this gives important insights to the study of stellar interiors.

2.2.1 The Instability Strip

As it can be seen in Figure 2.2.1 variable stars do not fall into random positions on the H-R diagram. Most of them are found in a narrow zone called the *instability strip*. The instability strip spans from around 600K to 1100K and it is nearly vertical. All stars within this zone pulsate radially. According to stellar evolution theory, pulsations are an

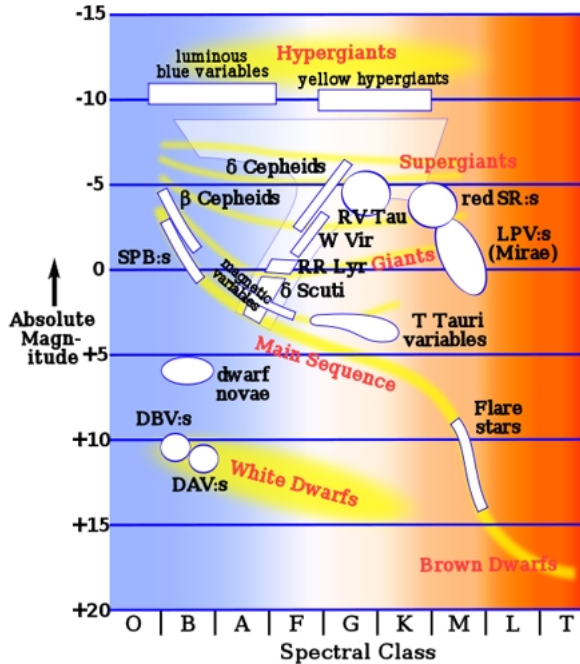


Figure 2.2.1: Types of variable stars in the H-R diagram.

evolutionary stage in a star's life. Stars start to pulsate when their evolutionary tracks cross the instability strip and they stop oscillating upon leaving the area. The radial motion is a constant back-and-forth of the stellar envelope, which is due to the rise and fall of the temperature of the material within the star.

2.2.2 Pulsations

Pulsation is one of the most interesting stellar variability mechanisms, and one of the most understood. In this section I will briefly discuss the two main types of stellar oscillations, namely radial and non-radial pulsations.

Every object has its natural modes of oscillation. In the music domain differences in the frequency of vibrations are heard as different pitches or overtones. The frequency of those modes depends on the length on the vibrating string. Figures 2.2.2 and 2.2.3 show the fundamental and the first overtones in a one-dimensional string and a two-dimensional drum head [19]. This is a useful mental image before entering the world of three-dimensional stellar pulsations.

All oscillation patterns have points which do not move during the process, these points are called *nodes*. The oscillation modes are characterized by some sort of "quantum numbers". The format is $(n_{rad}, n_{non-rad})$, where n_{rad} is the number of radial nodes and $n_{non-rad}$ is the number of non-radial nodes. In the case of three-dimensional stars there exist three numbers to characterize a specific mode of oscillations. The first number is n , the number of radial nodes present, the *overtone* of the mode. Number ℓ is the *degree* of the mode and designates the number of surface nodes, while m is called the *azimuthal order* of the mode and $|m|$ specifies the number of the surface nodes that are also lines of longitude. That means that the number of surface modes that are lines of latitude is $\ell - |m|$. The range of m is from $-\ell$ to $+\ell$ so there are $2\ell + 1$ m-modes for each degree m . The principle of numbering is known from quantum mechanics.

According to present observations with mmag photometric and $m^{-1}s$ radial velocity precision, the majority of stars do not pulsate; and those that do, they pulsate in their natural modes. Since there are stars (e.g Mira) that pulsate in the same way for hundreds

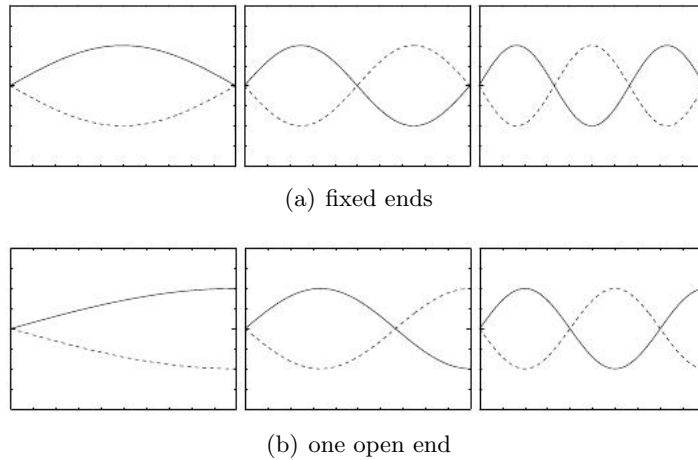


Figure 2.2.2: The fundamental and the first two overtones of a vibrating string. The first overtone has one node while the second overtone has two, in both cases.

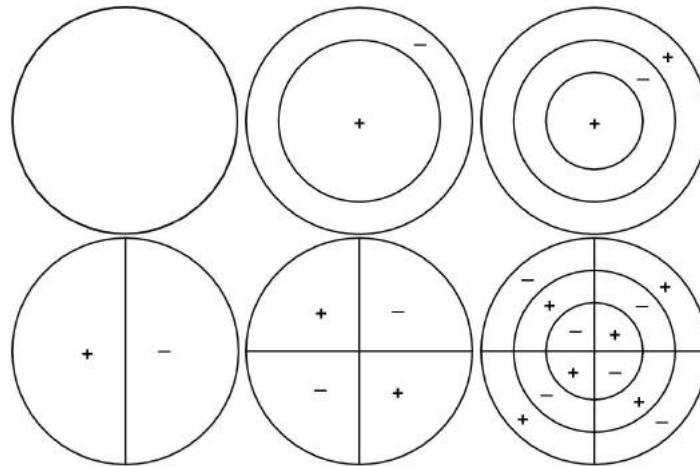


Figure 2.2.3: The two-dimensional pattern of pulsation on a drum head. The edge of the drum is considered in all cases a node. The top left case represents the fundamental mode. The top middle is the first radial overtone, which means that the inner circumference is a node and it does not move. The top right is the second overtone with two nodes. At the bottom the non-radial modes are shown. The bottom left is the simplest non-radial mode, the dipole mode, in which a line that crosses the center of the drum is not moving. The logic behind the other two modes is the same. The middle bottom is the quadrupole mode. At the right bottom panel there is a mixing of oscillation modes. The signs indicate the parts that move towards the reader (+) and away from him (-). Reading from top left to bottom right the modes are (0,0), (1,0), (2,0), (0,1), (0,2) and (2,2).

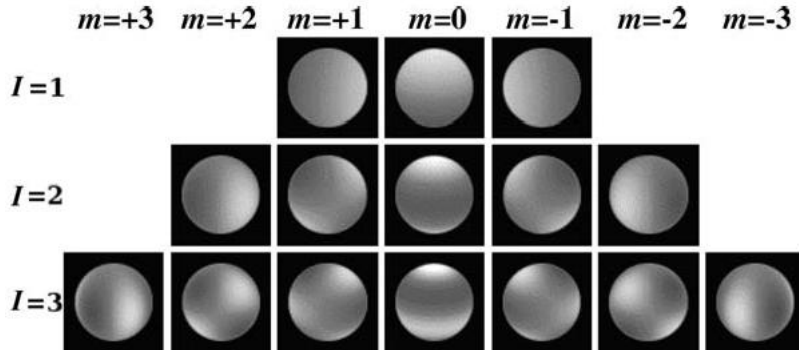


Figure 2.2.4: Non-radial pulsation modes for certain values of ℓ and m . The regions of the star that move outwards are color coded white, while the regions that move towards the center are darker.

of years one can say that stellar pulsation is a relatively stable phenomenon. During a pulsation cycle the star loses energy via continuous contractions and expansions, so there must exist a mechanism to drive the oscillations. Usually a shell that contracts and therefore heats up gains energy, which is then damped by the bulk motion of the star.

For the most cases of pulsating variables the driving mechanism is opacity. And since a "lot of opacity" is needed for a whole star to oscillate, H and He are the primary opacity contributors, as are the most abundant stellar materials. A qualitative approach is as follows. H and He within the ionization zones of the star block radiation and as a result pressure and temperature of the gas increase. The expansion starts at the point where the equilibrium is overwhelmed. In the next stage the ionization of the gas reduces the opacity and radiation is free to flow. Pressure is reduced and the gas is cooled. The expansion stops and the contraction starts. Upon contraction, H and He recombine and flux of radiation is blocked once more. When the critical point is reached the cycle starts again. The large heat capacity of the H and He ionization zones is responsible for the delay of about 90° between the phase of maximum luminosity and the phase of minimum radius. The whole process is known as the *k-mechanism*. The mechanism can rely on other chemical elements also. The pulsations of β Cephei stars are driven by the k-mechanism acting on elements of the Fe-group. The mechanism resembles the operation of a heat engine.

Stochastic driving is the mechanism responsible for solar-like and red giant pulsations. This is the case where a great deal of acoustic energy is stocked within the ionization zone, thus there is resonance and the star oscillates in one of its natural modes. Stochastic noise can be translated into global oscillations.

The other proposed driving mechanism for stellar pulsation is the *ϵ -mechanism*. The symbol originates from the well-known stellar structure equation

$$dL(r) = 4\pi r^2 \rho(r) \epsilon(r) dr \quad (2.2.1)$$

and is the energy generation rate in the stellar core. Fluctuations of this rate can possibly drive global oscillations especially in evolved and very massive stars. However there exist no observational evidence to support the theoretical work to date.

To determine whether a star is pulsationally unstable, one first has to determine the structure of the given star. The stellar structure equations

$$r = r(M_r), \quad (2.2.2)$$

$$P = P(M_r), \quad (2.2.3)$$

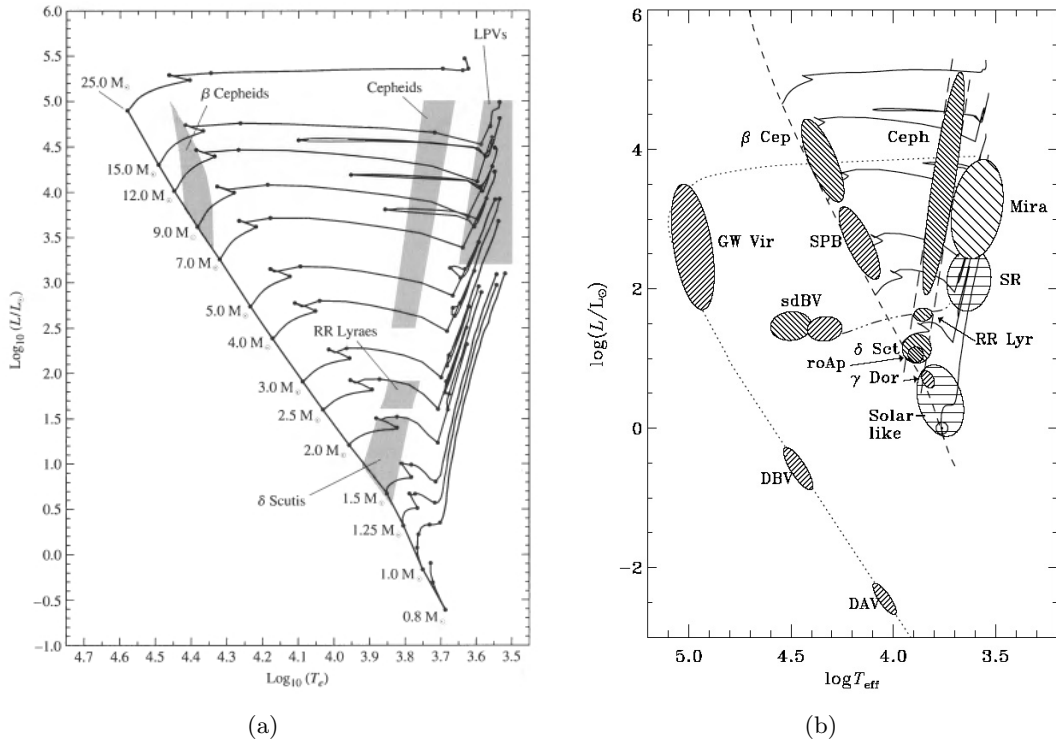


Figure 2.2.5: Two versions of the H-R diagram containing well-known types of pulsating variables. Evolutionary tracks are also visible.

$$\rho = \rho(M_r), \quad (2.2.4)$$

$$L_r = L_r(M_r) \quad (2.2.5)$$

have to be solved. Then one has to solve the linearized equations for the oscillation modes. Adiabaticity for stellar oscillations is usually assumed. Then a stability integral can be introduced and the sign of this integral determines whether the stellar modes are stable to self-excited oscillations at a particular frequency (eigenmode).

Pulsating stars display a $P\sqrt{\rho}$ behavior, namely the product of period P and the square root of density ρ , is constant for a particular group of pulsating stars,

$$P\sqrt{\rho} = \sqrt{\frac{1}{\kappa G}} \quad (2.2.6)$$

where κ is a dimensionless constant and G is the gravitational constant. Thus the shorter period stars are more dense than longer period ones.

Radial Pulsations

The radial oscillation of stellar material is the simplest case of pulsation. In this case the number of surface modes is $\ell = 0$; the fundamental radial mode is also characterized by the absence of surface nodes as lines of latitude, $m = 0$. The star in this configuration contracts and expands radially while the core acts as a node and the surface acts as an open end (fig. 2.2.2(b)). Along with the surface of the star, temperature and pressure also fluctuate. During the contraction phase their values build up and in the expansion phase the star cools and the pressure drops. This is the mechanism that drives the pulsation of classical Cepheids and RR Lyrae variables.

In the first overtone $n = 1$, the star oscillates radially while one shell remains at rest in the stellar interior. The motions above and below that shell are not in phase. The external layer of the star acts again as an open end. In roAp stars which pulsate non-radially, the first overtone can be directly observed in their atmospheres [20].

Observations suggest that there are certain cases of Cepheid, RR Lyrae and δ Scuti variables which pulsate in the fundamental and the first overtone at the same time [19]. Those double-mode Cepheids have a ratio of the first overtone period to the fundamental period of ≈ 0.71 . For the δ Scuti stars this is ≈ 0.77 . Using asteroseismology tools these periods can be explained. Gradients of sound speed, hence temperature and chemical composition inhomogeneities are responsible. As for the small difference of the ratios between the above two types of variables, it is due to the properties of those types. Cepheid variables are giant stars hence they are more condensed in the central region than the hydrogen burning δ Scuti stars.

Non-radial Pulsations

While radial oscillations are described by a second order linear differential equation or two coupled first order differential equations, non-radial oscillations are introduced with an angular dependence proportional to the spherical harmonic $Y_{\ell m}$ and have periodicities close to those that correspond to radial modes.

As it can be seen in Figure 2.2.4 the simplest of the non-radial modes is the case with $\ell = 1$ and $m = 0$. In this case the "northern" hemisphere of the star expands while the "southern" contracts. The heating of the star follows the pattern. The expanding volume cools down and the contracting, heats up. This mode is known as the *dipole* mode. The star's center of mass does not follow the oscillation. Dipole mode is the primary pulsation mode for rapidly oscillating Ap stars.

Pulsation modes with $\ell = 2$ are commonly referred to as *quadrupole* modes. They are characterized by two surface nodes. In Figure 2.2.4 all possible oscillation modes up to $\ell = 3$ are shown, known as the *octupole* modes.

2.2.3 Eruptions

The eruptive variable stars are usually faint stars that eject mass. They are more than often, members of binary systems in which mass is transferred from one component to the other. This class of variables shows no regular behavior. The light variations are due to sudden outbursts. Stellar material is ejected to space in a non-periodic manner. These stars may also be surrounded by a shell of material. Stellar wind can interact with this material and produce sudden brightness changes. Examples of this category are *flare stars*, various kinds of *nebular variables* and *R Coronae Borealis stars*. The transient events can span a wide range of energies, from small flares and chromospheric events on main sequence stars to nominal flare stars (with energy 10^3 times higher); more energetic events are possible to occur also.

Cataclysmic variables is another subdivision of eruptive variable stars. Although in the classic case of eruptive variables the phenomena that cause the light variation are mainly concentrated in the chromosphere or the coronae of those stars, cataclysmic (or explosive) variables vary due to nuclear reactions on the stellar surface or interior. Explosions can be so energetic that can even destroy the whole star. This group includes *novae*, *nova-like stars*, *dwarf novae* and *supernovae*.

The term cataclysmic variable refers to another kind of variable star also. They are binary star systems which consist of a white dwarf (WD) and a cooler, less-evolved star (e.g a red giant) that has filled its Roche lobe. Thus mass flows from the stellar companion onto the WD. The whole phenomenon is a nova or a supernova in preparation.

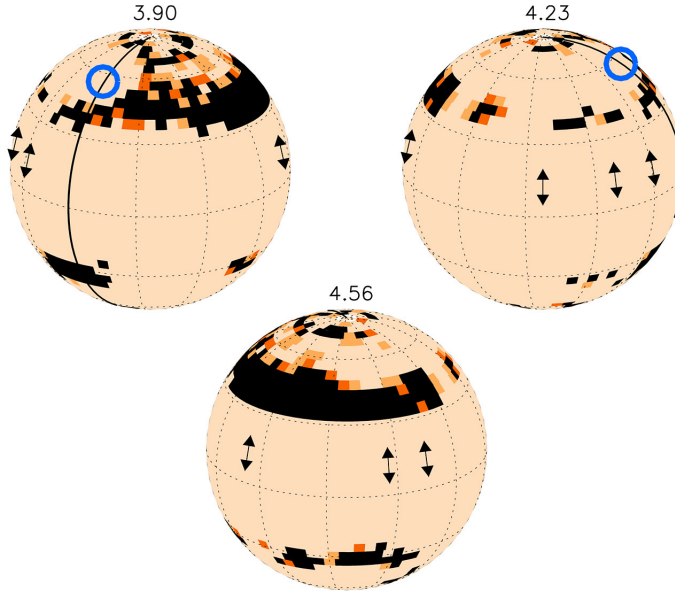


Figure 2.2.6: Reconstruction of the surface of the star BO Microscopii. A series of starspots is visible and a flare was also detected. The source of the flare is interestingly enough, not one of the spots.

2.3 Extrinsic Variability

In this case the variability is due to processes external to the star. The interpretation of light variations can give rise to interesting results concerning the environment of the star under investigation. Eclipsing binaries can be identified and studied, masses can be determined and even fundamental physics can be put to the test using radio observations (e.g gravitational wave detection). The study is facilitated even more if spectroscopic data are available.

2.3.1 Eclipses and Binary Stars

Binary and multiple stars are a common place in the Universe. Binary stars are a great astrophysical laboratory because stellar masses and other parameters can be determined with increased accuracy. Eclipsing variables are systems that have components which periodically produce eclipses to each other. Historically eclipsing binaries were classified according to phenomenological criteria, namely the appearance of the light curve. Nowadays binary stars are understood in a deeper and more physical way on the basis of Roche geometry and equipotential surfaces.

In contemporary astronomy there are four identified types of binaries, namely visual, astrometric, spectroscopic and eclipsing binaries.

Visual binaries are double systems with both components resolvable with a telescope. Masses of both components can be directly deduced using Kepler's third law

$$\omega^2 = \frac{4\pi^2}{P^2} = G \frac{M_1 + M_2}{d^3} \quad (2.3.1)$$

and equation

$$a_1 M_1 = a_2 M_2 \quad (2.3.2)$$

where a_1 and a_2 are the semi-major axes of the absolute orbits of the first and second component about the common center of mass. Unfortunately the case when both absolute

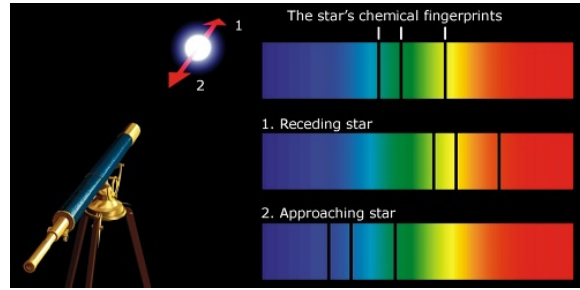


Figure 2.3.1: The principle behind radial velocity determination.

semi-major axes can be measured is extremely rare; in order to compensate for this problem the semi-major axis of the relative orbit is used

$$a = a_1 + a_2 \quad (2.3.3)$$

Inclination and eccentricity are other crucial orbital elements that can also be deduced using observations of eclipsing binaries.

The resolving power of a telescope is given in arcseconds by

$$RP = 206265 \times 1.22 \frac{\lambda}{D} \quad (2.3.4)$$

where λ is the wavelength in which the observation is carried out and D is the diameter of the instrument (primary mirror, objective lens or antenna aperture). Of course the theoretical limit is never achieved due to atmospheric phenomena, as seeing. When one of the components is not resolvable or is much less bright than the other, astrometric measurements are used. This is the case of astrometric binaries, in which both components orbit the common center of mass. The observational signature of this effect is the motion of the visible component which can be measured. In many cases (e.g planet-star system) the center of mass of the system is within the visible (and more massive) component which makes the motion extremely difficult to catch, so high precision astrometry is needed of the order of milli-arcseconds.

Spectroscopic binaries are the third type of binary stars. Identification of such stars is done using spectra. Thus the investigation of those systems is not subject to geometric limitations (e.g line-of-sight etc.). Given enough telescope aperture, exposure time or both, spectroscopic binaries can be identified and studied even in nearby galaxies. The mass ratio of the components can be determined using radial velocity data.

Finally, *eclipsing binaries* are the type of stellar system that have the appropriate geometrical configuration for eclipses to occur. In this case the phased light curves (light curves folded to display one period) display certain patterns that are characteristic of the system under investigation. Keeping in mind some geometrical considerations there can be a classification of light curves according to these patterns. Primary and secondary eclipses can be identified and any deviation from the "ideal" light curve can be attributed to other effects related to mass transfer between the components, the existence of a hot spot and so on.

A very didactic classification of binary stars is in terms of their *Roche geometry*. There exist three categories, namely detached, semi-detached and contact binaries. The inner point where gravitational forces balance is the inner lagrangian point, L_1 . Many contact binary systems undergo mass transfer through this point. The equipotential surface that passes through L_1 , consists of two intersecting surfaces called the *Roche lobes* of each component. The classification is as follows:

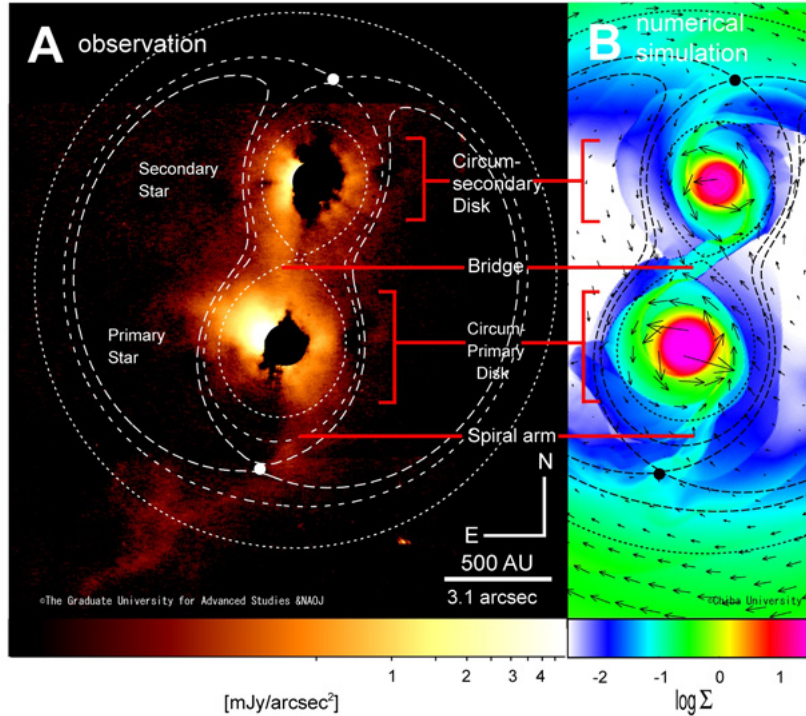


Figure 2.3.2: Direct imaging of the binary star SR24 as captured by the Coronagraphic Imager with Adaptive Optics (CIAO) mounted on the Subaru Telescope. Roche lobes are overplotted. A numerical simulation model is also visible.

1. *Detached systems* are binaries with neither of the components filling its Roche lobe.
2. A *Semi-detached binary* is a system whose one component is over-filling its Roche lobe and mass transfer is highly probable.
3. *Contact binaries* are the systems whose both components fill their Roche lobes. In this case the components share their common atmosphere. Other commonly used terms for such systems are *over-contact binaries* or *common envelope binaries*.

A very interesting aspect of eclipsing binaries is the potential of distance determination. Large telescopes and advanced instruments enable the study of eclipsing binaries even in Local Group galaxies, such as the Small and Large Magellanic Clouds, M33 and M31. Eclipsing binaries are not considered standard candles as RR lyrae, Cepheid variables or Supernovae do. But as long as one has enough observational data, namely radial velocity and light curves, then a careful selection of the model will yield important and accurate results. Atmospheric eclipses can also help deduce important astrophysical results. An atmospheric eclipse is the case when one component is eclipsed not only by the other star but from its atmosphere also. Such eclipses occur in binaries when at least one component has an extended atmosphere. One classical example is ζ Aurigae. In this star, the eclipse is wider in the ultraviolet than in longer wavelengths. Another such system is EB V444 Cygni. Atmospheric eclipses are important as they can give insights to the composition of stellar atmospheres. When pushed to the limit, observations could even investigate and characterize extra-solar planetary atmospheres.

An interesting terminology issue arises at this point. It is the designation of which component is the primary and which is the secondary. This issue has implications due to the different and contrasting ways photometrists and spectroscopists use the terms. The term *zero phase* is also ill-defined. While light curve specialists define zero phase as the

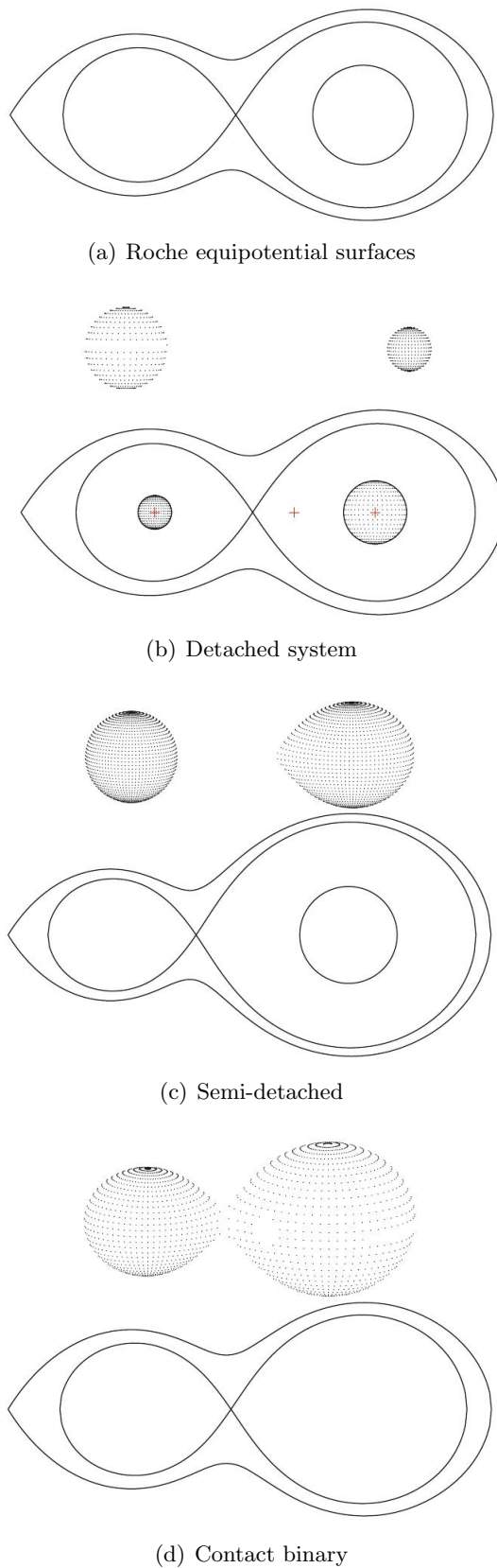


Figure 2.3.3: Classification of binary stars according to Roche geometry.

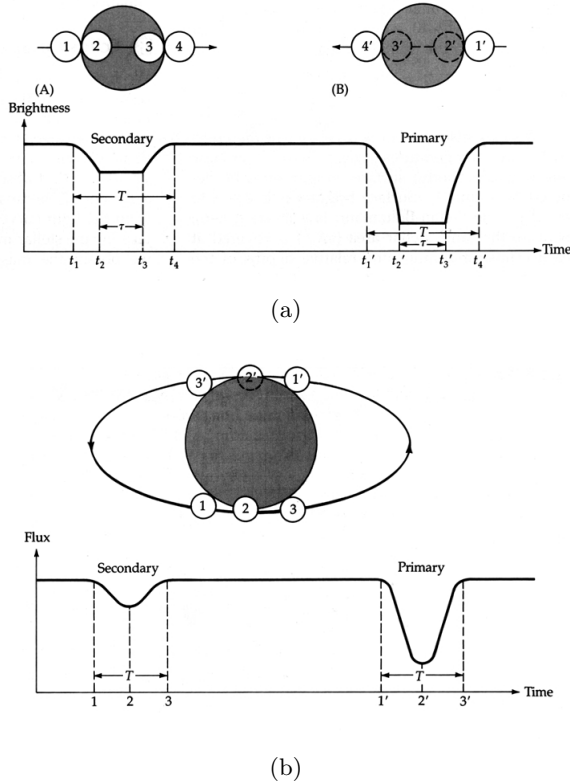


Figure 2.3.4: Eclipse geometry and associated light curves.

primary minimum, radial velocity experts use the same term associated with the time of periastron passage. For photometrists the primary minimum is the deeper minimum, when the difference in depths is clear enough, but the selection could be arbitrary when the depths appear to be equal.

The issue of designation of the primary component in a binary, is difficult to tackle. Photometrists use the term to refer to *the star being eclipsed during the primary minimum*. The designation does not directly point to the more massive or bigger star but rather to the star with the highest temperature. In the case of circular orbits the star being eclipsed during the primary minimum is the brighter one per unit area. The above definition does not resolve the case of equal minima either. In this case the selection is arbitrary unless other data are available.

In spectroscopy and especially in the study of spectral line features, the component with *the strongest spectral features, the more luminous one*, is considered as the primary. In radial velocity studies the primary member is *the one with the lowest radial velocity amplitude, namely the more massive one*. Again, in the case of equal radial velocity characteristics the selection is arbitrary.

In other disciplines of astronomy, as in stellar evolution investigations, the primary component is *the originally more massive one which has the potential to become the less massive due to mass transfer*. In celestial mechanics the situation is more complicated. In the context of the restricted three-body problem, *both components are considered as primaries with respect to the third massles body*. However in the general three-body problem the *massive components is the primary*.

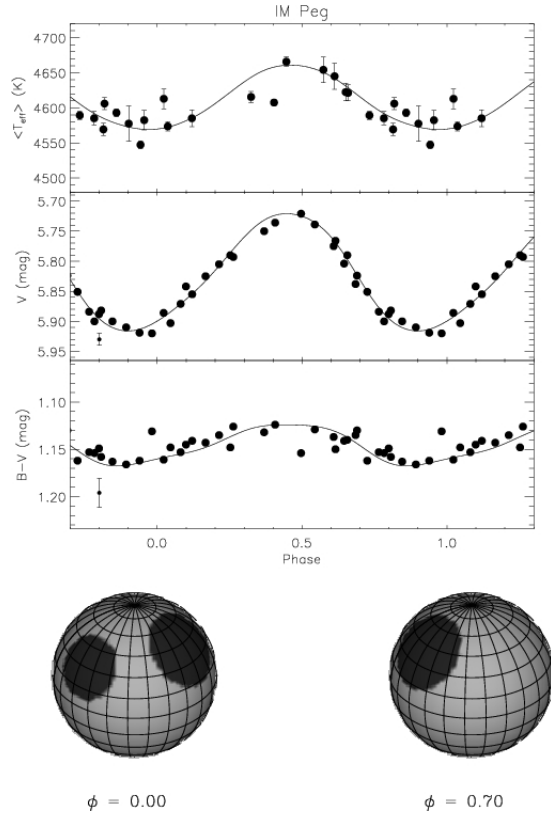


Figure 2.3.5: The effect of starspots on a rotating star. The upper curve is the effective temperature, the middle curve is the magnitude in the V band and in the lower panel the B-V magnitude is shown (from Frasca et al. 2005).

2.3.2 Stellar Rotation

Among the fundamental physics postulates, the conservation of angular momentum is of great importance and dictates the motion of all objects including stars. Modern stellar formation theory suggests that stars form within clouds or discs with an intrinsic amount of angular momentum. This "primordial" momentum is then inherited to the newly formed star.

Stellar rotation as a contributor to stellar variability has many faces. As stars rotate they deform. Fast rotating stars assume the shape of an *elongated* figure just like the earth's equatorial bulge. This effect can have a significant observational signature, especially when the star is spotted. Many variable star types owe their variability to star spots. Star spots are regions cooler than the rest of the stellar surface. As a result a spotted rotating star varies due to non-uniform surface brightness. This is the case for FK Comae stars as well as for the BY Draconis variables. Stars rotate *differentially* in general. This means that the speed of rotation is a function of the stellar latitude, meaning that spots in the equator rotate faster than spots in other latitudes. There are extreme cases of star spotting, where almost all of the stellar surface is spotted. Using latest optical interferometry data, spots can be directly observed on the surface of other stars like Betelgeuse (Haubois et al. 2009). In other cases observational data point to the existence of spots, namely phases of minima agree in V and in V-I but not in U-B, color amplitudes increase when going to V → R → I as expected for cool spots and V-I, V-K, U-B excess.

An important aspect of stellar rotation is chemical mixing. There are certain types of variables that show a severe depletion in He on their surface while in the same time they are overabundant in heavier metals like Fe, Si and Cr especially in their spots. All

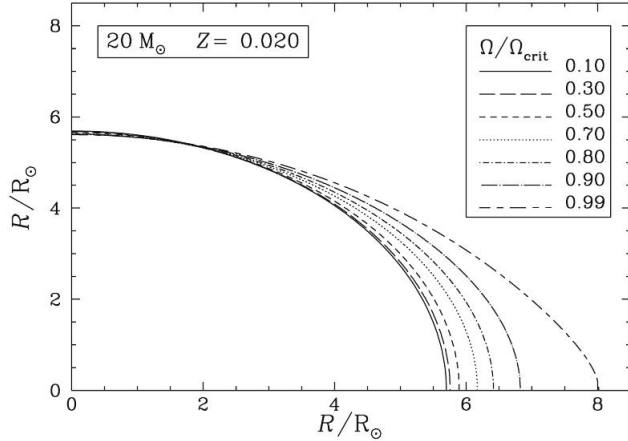


Figure 2.3.7: The effect of rotation to a $20M_{\odot}$ star with a $Z=0.02$ at ZAMS. The shape is clearly distorted

those stars are referred to as *chemically peculiar (CP)* or Ap stars and they are known to astronomers since the early days of spectral classification. It is believed that rotation is responsible for the mixing of stellar material.

Except for chemical mixing a mechanism related to stellar rotation is meridional circulation. In the case of our Sun, it is a large-scale flow of solar material which is observed in both hemispheres. The material flows from the equator to the poles and as there is no observational evidence of accumulation at the polar regions, it is suspected that there is an associated flow from the poles to the equator deeper within the solar interior. The observed amplitude of the flow is of the order of 15 ms^{-1} . Meridional circulation is probably responsible for the solar 11 year cycle because it carries magnetic flux. Meridional circulation is an effect that is observed in other stars also with helioseismic studies.

Pulsars are another observational manifestation of stellar rotation. They are fast rotating and highly magnetized neutron stars. Their distinguishing characteristic is that they emit very regular pulses with periods from 1.558 ms to 4.308 s . Most pulsars are discovered due to their radio emission but some of them also emit in the optical regime. The explanation of the emission mechanism is based on the rapid rotation and the strong magnetic field. The magnetic axis and the rotation axis of the star are tilted with respect to each other and strong magnetic fields are induced to the environment around the star. The electric field accelerates free electrons present on the surface of the neutron star in relativistic speeds. The outcome of this process is a jet flow of electrons which gives rise to an energetic and highly collimated synchrotron beam. Whenever such a beam crosses the earth it is recorded as a pulse. A more detailed picture of the emission mechanism will be presented in a subsequent section dedicated to pulsars.

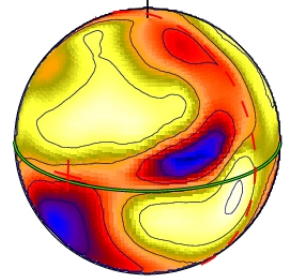


Figure 2.3.6: Distribution of calcium on the surface of the Ap star HR 3831.

2.4 The Solar Case

For centuries the Sun was considered to be a quiet celestial body. As more advanced instruments were introduced, the wealth of observational data showed that our star is far from being quiet. In fact the Sun incorporates most of the above variability mechanisms.

Many theories were proposed to explain the brightness variations of the Sun but decisive contribution was made by Richard Carrington and Gustav Spörer. After long lasting

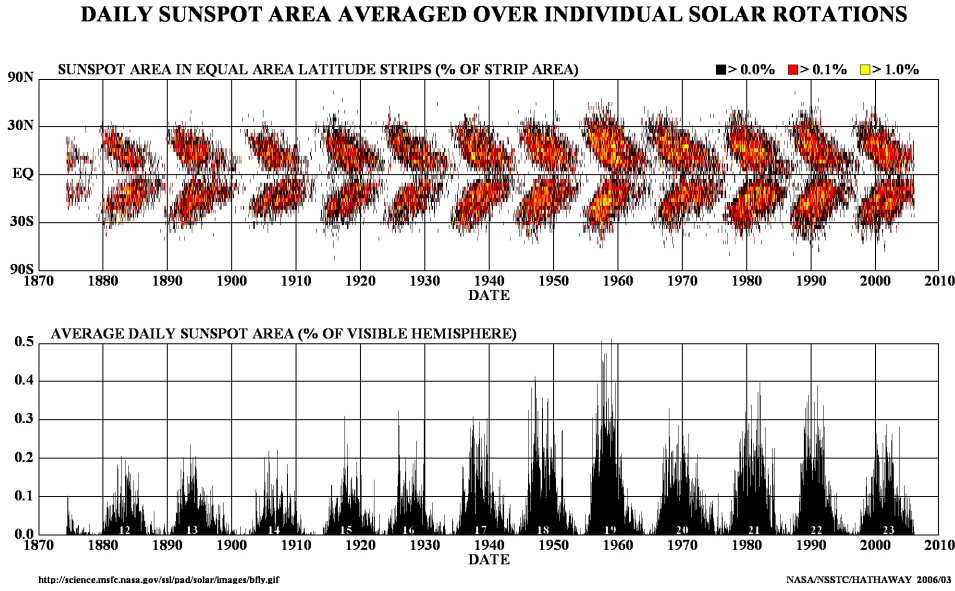


Figure 2.4.1: The well-known butterfly diagram. The association between the spot number and the heliocentric latitude is shown.

observations of the behavior of sun spots, in the 1850s they independently showed that the solar atmosphere does not rotate as a solid body. From his observations between 1853 and 1861 Carrington deduced the expression

$$\Omega(\text{deg}/\text{day}) = 14^\circ 42 - 2^\circ 75 \sin^{7/4} \phi \quad (2.4.1)$$

to represent the Sun's rotation rate, where ϕ is the heliocentric latitude. Later Hervé Faye found that the formula

$$\Omega(\text{deg}/\text{day}) = 14^\circ 37 - 3^\circ 10 \sin^2 \phi \quad (2.4.2)$$

better suits the observations and explains the dependence of the angular velocity from the heliocentric latitude. In 1942 Jaakko Tuominen established the tendency of spots in latitudes lower than 20° to migrate towards the equator and for spots in latitudes greater than 20° to migrate towards the solar poles.

Solar rotation was established using spectroscopic means in 1871. Hermann Vogel measured the Doppler shift of the spectral lines in the two opposite solar hemispheres. Doppler measurements showed clearly that one hemisphere was approaching while the other was receding. The Doppler rotation rate was similar to the one deduced by the solar spot method. The first scientist to propose that axial stellar rotation could be determined by the broadening of spectral lines was William de Wiveleslie Abney in 1877.

The Sun exhibits variability due to motions in many different scales. Except for the large scale axisymmetric motions which are associated to differential rotation and meridional circulation, velocity fields have been observed that correspond to turbulent convection and also oscillations with a period of about five minutes. These oscillations have drawn much attention since for the first time we have the chance to probe the solar interior. Chromospheric phenomena like prominences and torches are also present.

Solar activity has serious implications on the Earth environment. The so-called space weather is associated with eruptions on the solar surface, coronal mass ejections and particle acceleration that can have impressive effects, like the aurora, on Earth or can pose serious dangers to satellites or astronauts. Some very interesting physical mechanisms are responsible for all these phenomena. Thus many missions constantly observe the

changing Sun and many work groups are interested in the interactions within the Sun–Earth environment.

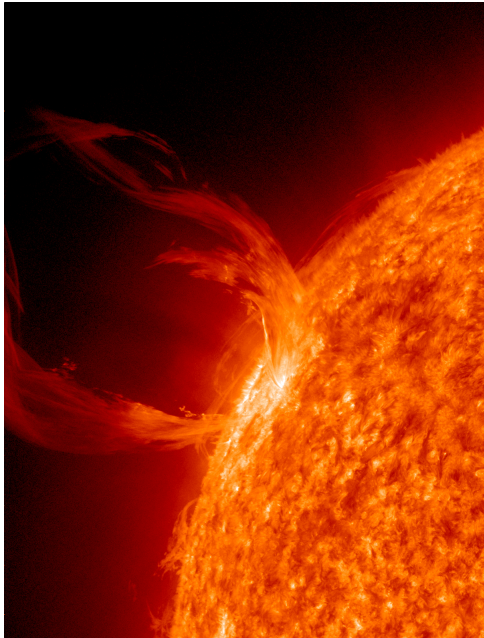
2.4.1 Helioseismology

The study of solar oscillations gave rise to a new field in astronomy. Helioseismology using state-of-the-art instrumentation and also computational tools, is able to monitor the solar oscillations and build models of the solar interior.

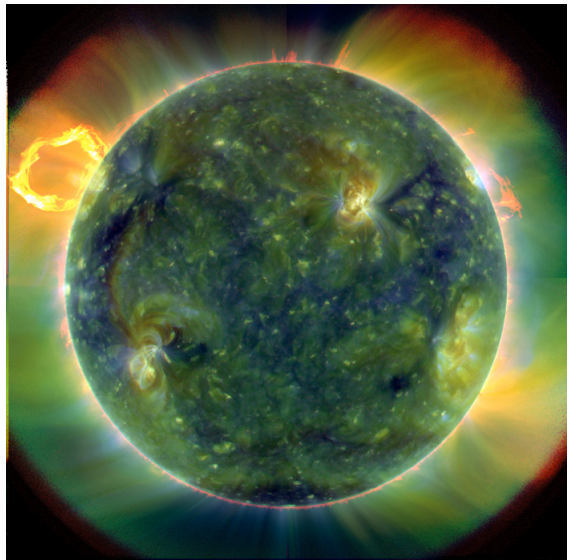
The Sun is to a certain extend a low-amplitude variable star. Leighton, Noyes and Simon in 1962 first observed a Doppler shift in absorption lines and argued that it is due to vertical motions of the solar material with a five-minute period and velocities of the order of 1Kms^{-1} . Somewhat later, Urlich (1970) and Leibacher and Stein (1971) proposed individually that the Sun undergoes global non-radial oscillations. These five-minute oscillations, which have frequencies between about 2 mHz and 4 mHz, have been extensively studied ever since. They are associated with standing acoustic waves that are tapped beneath the solar surface, with each of the modes travelling within a shell in the solar interior. The data suggest that the sun rotates internally in a complex manner.

Several studies indicate that the rotation rate in the solar convection zone is similar to that at the surface, with the polar regions rotating more slowly than the equatorial belt. At the base of the convection zone, there exists a transition to uniform rotation at a rate corresponding to some average of the rate in the convection zone. This layer, which is known as the solar tachocline, is centered near $r = 0.7R_{\odot}$. Recent studies indicate that it is quite thin, about $0.06R_{\odot}$.

The actual rotation rate in the radiative zone is uncertain due to the lack of accurate measurements of acoustic modes. From the base of the convection zone down to $r \approx 0.1\text{--}0.2R_{\odot}$ the measurements are consistent with uniform rotation at a rate somewhat lower than the surface equatorial rate. The rotation rate inside that radius is even more uncertain. There are studies that suggest that the rotation rate of this inner core might be between 2 and 4 times larger than that at the surface. According to others, however, it is more likely that this inner core rotates with almost the same period as the outer parts of the radiative core. Asteroseismology and helioseismology is a vivid domain of research full of potential towards the understanding of stellar structure and evolution.



(a)



(b)



(c)

Figure 2.4.2: Latest images of the solar surface acquired by the Solar Dynamics Observatory (SDO) mission.

3

An Overview of Variable Stars

”A walk through the biggest zoo of all!”

3.1 Introduction

VARIABLE sources in the night sky have always intrigued the observers, whether the observations were carried out by naked eye or with a telescope. After centuries of earth-bound and space exploration, still a blinking star that is bright enough will catch everybody's eye and of course the astronomer's telescope.

In this chapter I will give the definition the GCVS uses for each one of the variability types mentioned. An exact reproduction of the original GCVS classification is beyond the scope of this diploma thesis. I will not stick to the exact definition and I will include as many variables as possible in the same category using logical criteria, for reasons of simplicity and to help others use this diploma thesis as a gateway to the realm of variable stars.

3.2 Eclipsing Variable Stars

We adopt a triple system of classifying eclipsing binary systems: according to the shape of the combined light curve, as well as to physical and evolutionary characteristics of their components. The classification based on light curves is simple, traditional, and suits the observers; the second and third classification methods take into account positions of the binary-system components in the (MV ,B-V) diagram and the degree of inner Roche lobe filling. Estimates are made by applying the simple criteria proposed by Svechnikov and Istomin (1979).

3.2.1 Algol Type Stars

Initially eclipsing binary star systems were classified according to their light curves. Three standard types were identified that are designated EA, EB and EW after their prototype stars Algol, β Lyrae and W Ursae Majoris (W UMa) respectively. The differentiation between Algol type (EA) and other eclipsing variable stars is based on the shape of the light curve, which is dominated by two minima. The flux remains relatively constant between the eclipses, which vary in depth according to the evolutionary stage of the two components, forming the system.

Light curves of this form are the result of an eclipsing binary in which both components are nearly spherical, or slightly distorted. There is also the case where one of the

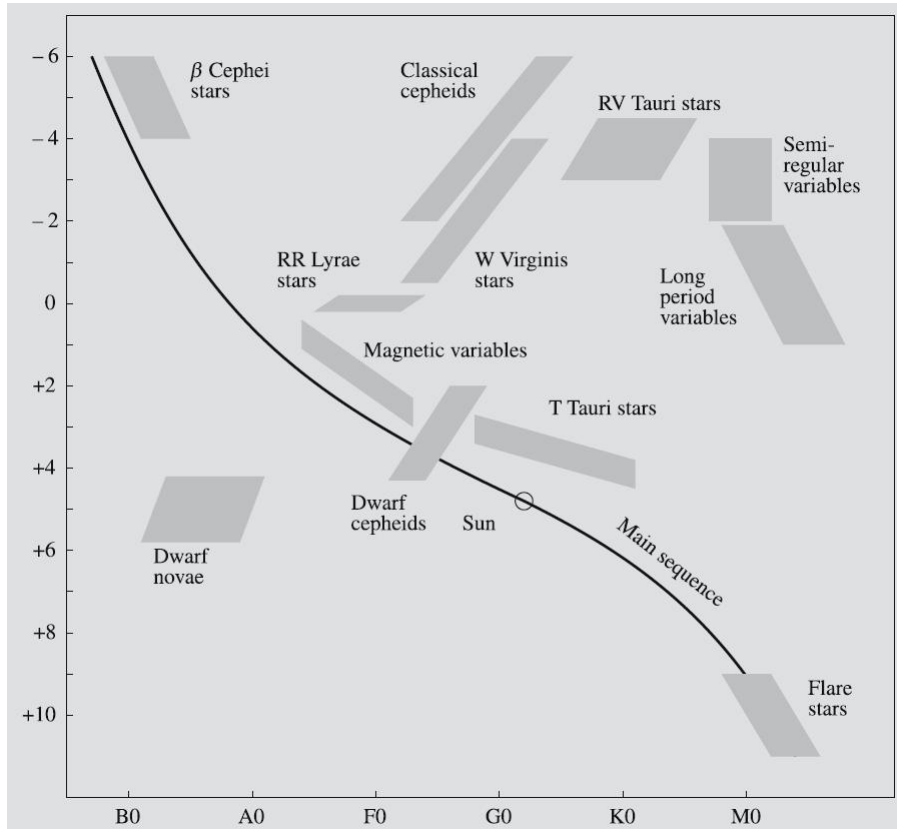


Figure 3.1.1: The position of variable stars on the H-R diagram. Adopted from [16].

components is highly ellipsoidal, even filling its Roche lobe, provided that its contribution to the total flux is minimal.

Among the Algol type binaries, one can find systems having components in different evolutionary stages,

- binaries containing two main sequence stars of any spectral type from O to M (CM Lac)
- systems whose components are evolved (one or both of them) but have not yet overflowed their Roche lobes (AR Lac)
- binaries having one star evolved, filling its Roche lobe and undergoing mass transfer (RZ Cas)
- binaries with one component highly evolved, at the stage of hot subdwarf or white dwarf (V 1379 Aql)
- or systems with a component not being evolved at all (V 471 Tau)

Orbital periods for such systems vary from extremely short (a fraction of a day) to very long (27 years for ϵ Aurigae). Orbital periods can be calculated by timing the eclipses. Period variations have been found and many physical mechanisms can produce such an effect. Some of them are apsidal motion, mass transfer between components, solar-type magnetic fields or the presence of a third body.

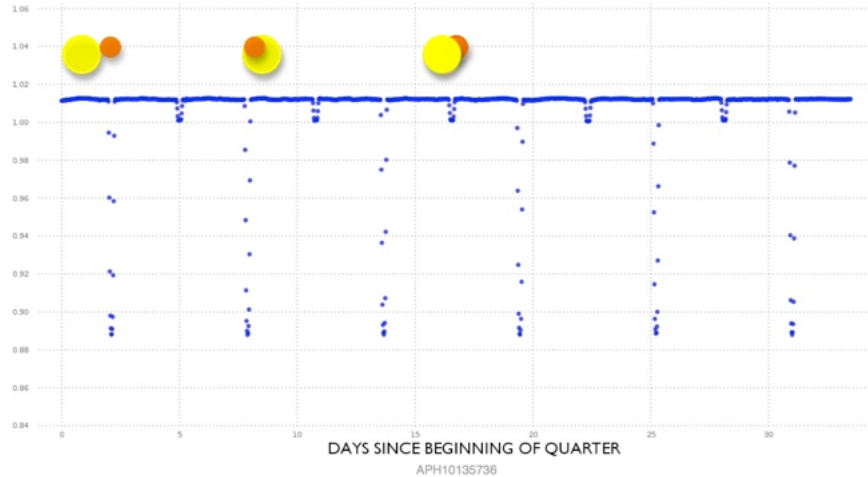


Figure 3.2.1: Characteristic light curve of an Algol type variable.

3.2.2 β Lyrae Stars

This subgroup (EB) of eclipsing variables is also identified by its light curve shape. In the case of β Lyrae type stars the exact times of minima cannot be deduced accurately as the light curve varies continuously between the eclipses. Light curves of such shape are produced by an eclipsing binary in which one or both components is highly ellipsoidal, even filling its Roche lobe. The presence of a primary and a secondary eclipse is prominent with significantly different depths, orbital periods longer than a day and spectral types B or A.

EB variables can consist of components at different evolutionary phases:

- binaries consisting of main sequence stars with short orbital periods (XY UMa)
- systems with one or both components evolved but not filling their Roche lobes (ζ And)
- semi-detached binaries subject to mass transfer originated from the evolved star to the unevolved (β Lyr)
- systems consisting of a highly evolved star at the stage of hot subdwarf or white dwarf and an evolved component, which produce an ellipticity effect (AP Psc)

3.2.3 RS Canum Venaticorum

These stars can also be classified as rotating variables due to the starspots which introduce characteristic patterns to their light curves. In particular this (RS) classification appears twice in the GCVS. It appears as one type of 'eruptive variable stars' and also as "close binary eclipsing systems". In the first case the actual variability mechanism is rotational modulation, as the surface brightness is non-uniform due to cool spots distributed unevenly in longitude, yet those systems do not fall in the category of "rotating variable stars". The second is the case of RS CVn type stars which are binary systems with the hotter of two being an F or G and showing strong emission reversals during all phases, and not only during eclipses (definition by Hall, 1976). These systems generally have one component evolved off the main sequence but not yet filling its Roche lobe, radiating in X-rays and radio waves, also have strong emission lines in the far ultraviolet and lose mass via stellar wind. Furthermore RS CVn systems have variable orbital periods, between 1

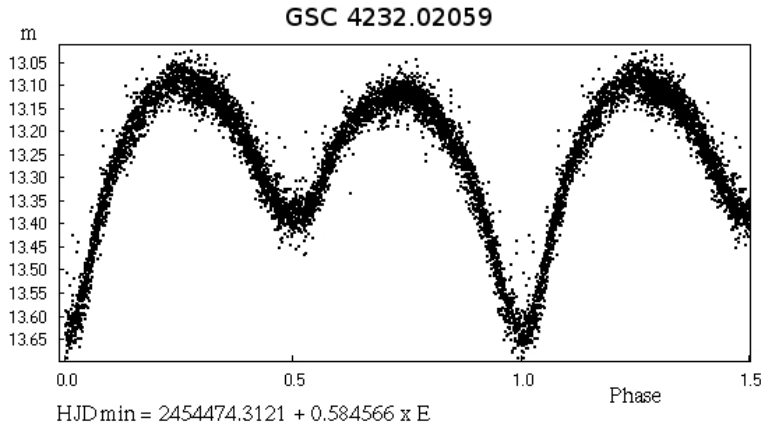


Figure 3.2.2: Characteristic light curve of a β Lyrae type variable. It is clear that the exact times of minima are difficult to deduce. (<http://www.astronet.ru/db/varstars/msg/1226023>)

and 14 days. They display a starspot wave behavior, and undergo more intense changes in the mean brightness, which can be evidence of a magnetic cycle like our own Sun's 11-year cycle. There is also another group of similar stars that have orbital periods less than a day (the short-period group) and greater than 14 days (the long-period group). It is valid to consider those two types as one class, the "stars showing the RS Canum Venaticorum behavior".

The RS CVn systems show variability other than that attributed to eclipses. The *starspot wave (or distortion) wave* is sometimes the actual cause of variability. This is obvious by the sinusoidal modulation in the light curve of such systems. This distortion wave is caused by the starspots that, due to the rotation of the star, are turned to and away from the observer. The amplitude of the distortion wave is linked to the change of the starspot area on the star. This constitutes a measure of stellar activity, and changes in long-term periods. The change of phase of the distortion wave is attributed to the differential rotation of the star that affects the position of the starspot region relative to the orbital phase and to the companion star.

The obvious mechanism that causes all the above activity is, as in the most cases, the magnetic field which is caused by the rotation of the a star. RS CVn stars rotate rapidly, in fact several times the normal rate, so they have a really strong magnetic field. This is because of tidal interactions with their companion star which have a 'spin-up' effect on the primary star.

3.2.4 Contact Binaries – W Ursae Majoris Variables (W UMa)

W UMa-type variables, or EW stars, are over-contact eclipsing binaries with orbital periods ranging between 0.2 and 1 day. Both components are main sequence stars (viz. burning hydrogen in their cores) with spectral types between A and K. None of the spectral type or colour of a W UMa star changes during the orbital cycle. This fact implies that the common envelope is optically thick and has a largely constant temperature. There are indications of temperature differences of a few hundred Kelvin between the components. The mass ratio q lies between 0.08 and 0.8. Spectral features for these stars include rotationally broadened and blended absorption lines. There are also emission lines in the ultraviolet spectrum which is an indication that these stars are chromospherically active.

Two subclasses (A-type and W-type systems) can be identified based on whether the

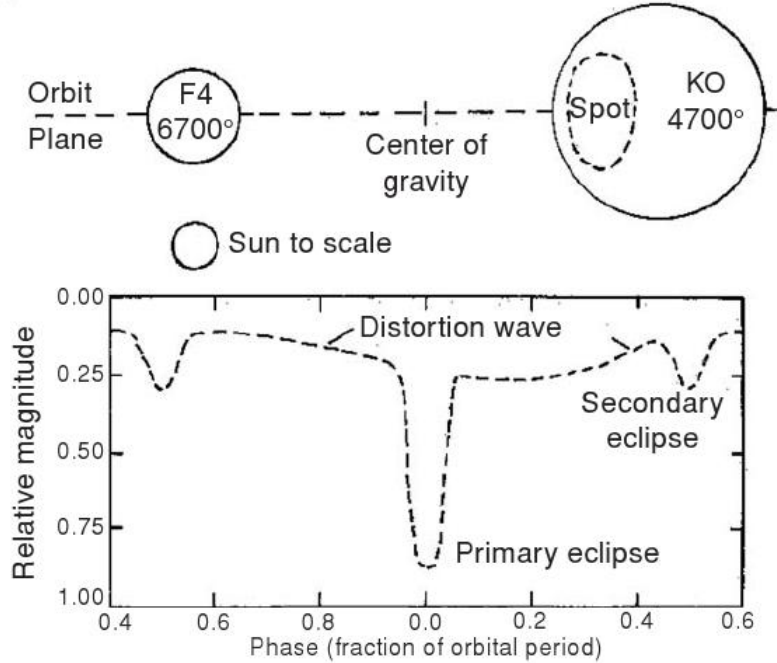


Figure 3.2.3: Light curve and model of RS CVn system. Below: the light curve of the system, the primary and secondary eclipses are shown as is the distortion or starspot wave. Starspots can migrate in longitude causing the wave to move along the light curve.

larger or smaller component has the higher temperature. In the case of A-type systems (spectral type A to F) the more massive component possesses the higher temperature, whereas for W-type systems (spectral type G to K) the smaller component has higher temperature.

All EW systems display period changes. This is attributed to mass transfer which is also connected to luminosity transportation from the primary (more massive) to the secondary component. The behavior of period changes is rather complex with period jumps of alternating sign interrupted by phases of constant period. Positive and negative jumps are randomly distributed, which is difficult to explain. The low luminosity of such systems is a major drawback as it prohibits us from having a large sample of W UMa stars. The GCVS only lists 542 EW systems. Light curves are available for a minor fraction of those, while radial velocity measurements are available for even less systems.

3.2.5 Transiting Extra-Solar Planets

I have arbitrarily placed transiting extra-solar planets under the category of eclipsing variables, because transits (eclipses) is one of the most successful planet-finding techniques. Although the detection of planets around other stars is beyond the scope of the thesis in hand, I shall discuss briefly this phenomenon.

The advances in observational techniques, technology and CCD imaging have enabled astronomers to search and detect very faint deeps in light curves which imply the presence of a body orbiting or transiting a star. Transits is not the only technique used to survey the sky for extra-solar planets. Radial velocity measurements, gravitational microlensing, astrometry, direct imaging and timing form the astronomer's arsenal in this difficult quest.

The fundamental requirement for the detection of a planet with the transit method, is

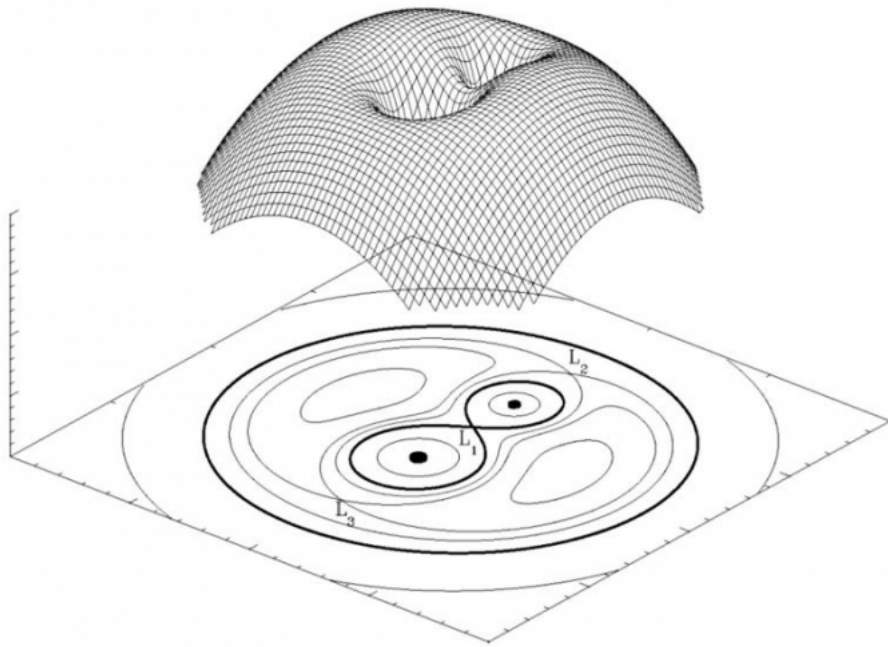


Figure 3.2.4: The Roche potential which dictates the physical behavior along with the observational manifestation of eclipsing binaries and other variable stars.

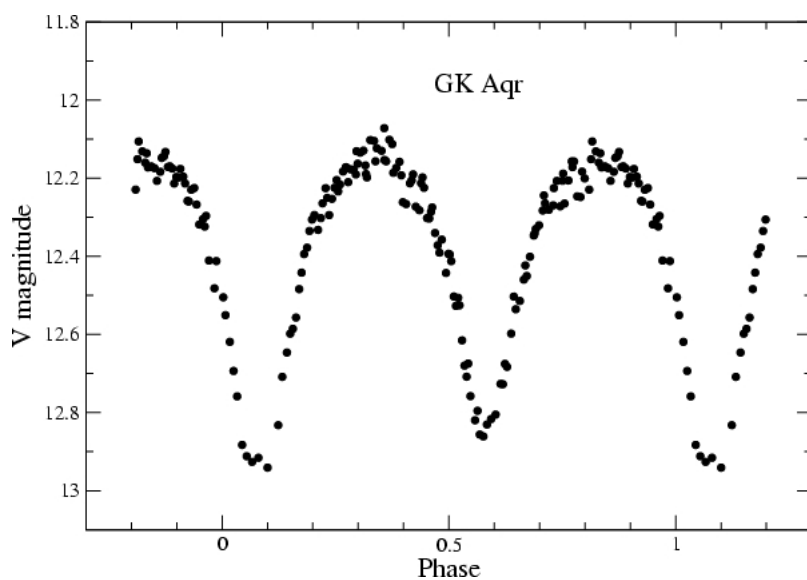


Figure 3.2.5: Light curve of an EW (or W UMa) system, GK Aqr

the planet to pass in front of the host star along the observer's line of sight. This produces a light curve with a shallow minimum of the order of 1% in general. This calls for high photometric precision and challenges the current noise removal techniques. Hot-Jupiters and super-Earths have been discovered already while Earth-like planets await to be found by the new generation of earth-bound and space-based instruments. Extra-solar planet detection and characterization is an open field of study with lots of potential for discovery.

Other types of eclipsing variables: Ellipsoidal variables – detached eclipsing binaries – Semi-detached eclipsing binaries – VV Cephei stars.

3.3 Rotating Variable Stars

Variable stars with nonuniform surface brightness and/or ellipsoidal shapes, whose variability is caused by axial rotation with respect to the observer. The nonuniformity of surface brightness distributions may be caused by the presence of spots or by some thermal or chemical inhomogeneity of the atmosphere caused by a magnetic field whose axis is not coincident with the rotation axis.

3.3.1 FK Comae Stars

The FK Comae stars are very fast rotating giant stars. The variability is attributed to inhomogeneous surface brightness modulated by rotation. The GCVS lists under this category binary and single stars. These stars are so fast rotators that it is believed that they are the product of merging of a W UMa binary system, rather than being young stars with high angular momentum. This is probably the case for FK Comae Berenices, but there are other stars of this class that do not rotate so rapidly. Such stars could be evolved single A type stars that have not yet lost their original rapid main sequence rotation.

The mean rotational period of the prototype for this class, FK Comae Berenices, is 2.4 days. Light variations range from a few hundredths to a few tenths of a magnitude.

3.3.2 BY Draconis Stars

This subgroup of rotating variables owes its variability to non-uniform surface brightness (localized starspots) and rotation. BY Draconis stars are of type K and M (i.e. cool stars) compared to G type sunlike stars. These stars also display noticeable chromospheric activity which gives rise to emission lines in their spectrum. BY Draconis stars can either be single or binary and the high rotational velocity is either inherited or induced by a close orbiting companion. Many BY Dra variables also show flares, which perplexes the differentiation between BY Dra and UC Ceti stars.

Typical periods for such stars are between 1 and 10 days. The prototype of this class BY Dra is a binary consisting of a K4V and a K7.5 star and has an orbital period of 5.975 days. Its variability was discovered by P.F. Chugainov in 1966. YY *Geminorum* (Castor C) is a well-known representative of BY Dra class variables. It was discovered in 1926 as an eclipsing binary. However, YY Gem is clearly a BY Dra variable. The spectral type of YY Gem is dM1e + dM2e and the variability between the eclipses is due to the presence of starspots.

3.3.3 Pulsars

Pulsars are highly magnetized and fast rotating neutron stars that emit a beam of electromagnetic radiation. The existence of the beam gives rise to the so-called "lighthouse

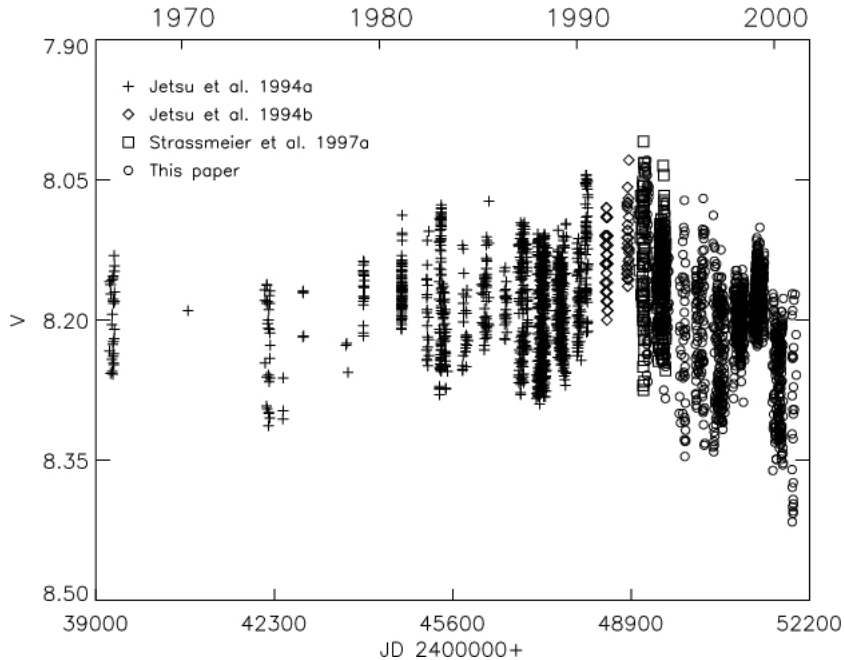


Figure 3.3.1: Activity of FK Comae Berenices (Korhonen et al. 2001).

effect”, namely the detection of the pulse only if the beam happens to be face-on to the observer’s line of sight. Most pulsars are found due to this very emission and only a small fraction of them also emits in the optical regime. The emission of radiation is highly canonical with periods between 1.558 ms and 8.5 s.

Pulsars were first discovered in 1967 by Jocelyn Bell Burnell and Antony Hewish. They form after the gravitational collapse of intermediate mass stars and the subsequent supernova explosion. The conservation of angular momentum forces the neutron star, which retains a small fraction of the initial stellar radius, to rotate with high velocity. The beam of radiation is formed along the magnetic axis of the neutron star which is not necessarily aligned to the rotation axis.

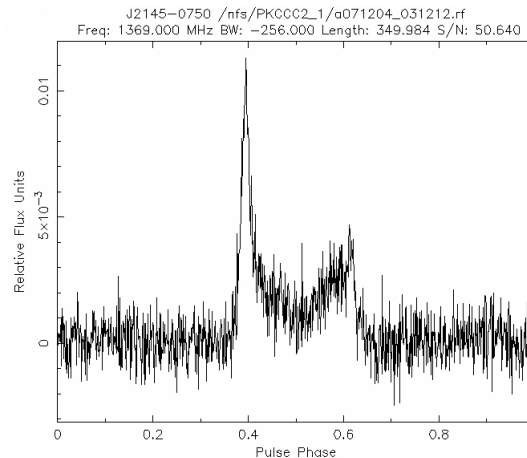


Figure 3.3.2: Typical pulse profile of a radiopulsar. The main pulse and the subpulse are visible.

3.4 Pulsating Variable Stars

Pulsating variables are stars showing periodic expansion and contraction of their surface layers. The pulsations may be radial or nonradial. A radially pulsating star remains spherical in shape, while in the case of nonradial pulsations the star's shape periodically deviates from a sphere, and even neighboring zones of its surface may have opposite pulsation phases.

3.4.1 Classical Cepheids

Early in the previous century Henrietta Leavitt discovered one of the most well-known and useful relations in the history of astronomy. She noticed that the magnitude of Cepheid variables in the Small Magellanic Cloud are linearly related to $\log P$, where P is the period of the variability. This magnificent discovery led to the capability of accurately measuring distances using Cepheids. In fact, using the Hubble Space Telescope distances up to the Virgo cluster have been determined.

Classical Cepheids are supergiant, pulsating and relatively young variable stars that "rest" in a narrow strip almost in the middle of the H-R diagram. Their periods range between 1 and 100 days along with some exception which reach periods of 200 days. Their surface temperatures are 6000K to 8000K. Cepheids that display 2 days period have a mass of $5M_{\odot}$ and an age of about 10^8 years, while Cepheids with 40 days period have a mass of $15M_{\odot}$ and an age of 10^7 years. Most Cepheids pulsate in the fundamental mode (see chapter 2) while some pulsate in the first overtone. These overtone pulsators are characterized by their lower light variations and the sinusoidal light curve. Their periods are between 1.5 and 4 days.

There exists a small group of Cepheid variables with periods from 2 to 6 days that show considerable differences from cycle to cycle [39]. This effect is attributed to the existence of two periods and points to the direction that there are two distinct categories of Cepheid variables, the fundamental and first overtone pulsators and the fundamental and second overtone pulsators. The full analysis and classification of Cepheid variables is performed with Fourier decomposition.

3.4.2 Population II Cepheids (W Virginis Stars)

W Virginis stars are the low mass and aged counterparts to classical Cepheids. These variables have masses of the order $0.6M_{\odot}$ and periods between 0.75 to 40 days. They can be found in the halo of the Milky Way galaxy but also the old disc population. Population II Cepheids pulsate for the same reason classical Cepheids do. They are radial pulsators and studies suggest that shock waves propagate through the star's atmosphere in every pulsation cycle.

One cannot distinguish population I from population II Cepheids only on the basis of the light curve shape, Fourier decomposition is needed. However the period–luminosity (P-L) relation is different due to the difference in masses. Walter Baade was the first to introduce the concept of two populations among Cepheid variables. Prior to that, astronomers used to measure distances using classical Cepheids and population II Cepheids altogether. The correction of this mistake led to the increase of the distance scale of the Universe by a factor of two.

3.4.3 RR Lyrae Stars

Due to the presence, in hundreds, of these stars in globular clusters they are often referred to as cluster-type variables. Such variables also occur outside clusters in the general "field". In the H-R diagram, RR Lyrae stars populate the horizontal branch region, a

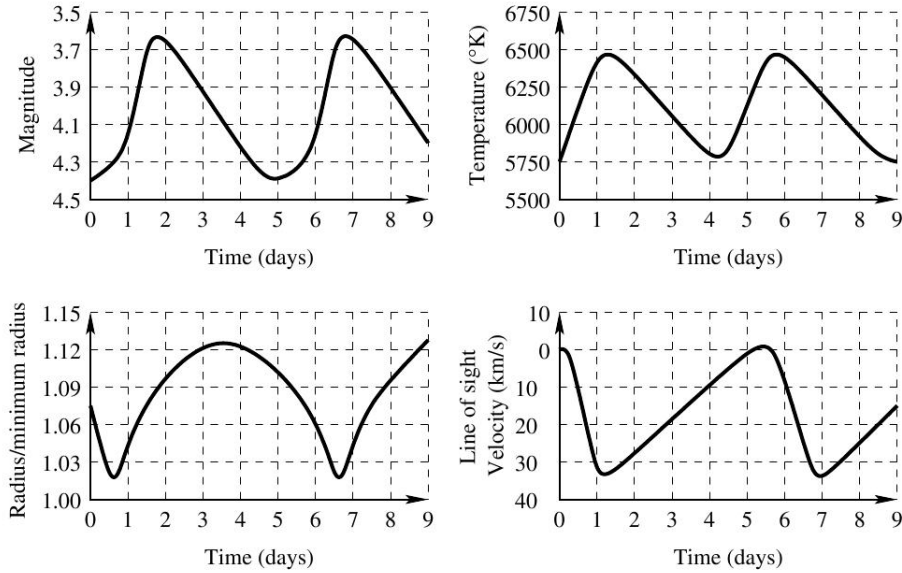


Figure 3.4.1: Light curve, temperature, radius and radial velocity of δ Cephei, the prototype of population I Cepheids [29].

stellar evolution stage that occurs between a star's first and second ascent of the giant branch.

RR Lyraes are radial pulsators with periods from 0.1 to 1 day, light variations in V band of the order 1.5 mag and masses of the order $0.5M_{\odot}$. According to their evolutionary stage the metallicity ranges from that of the Sun to one hundred times less. Their absolute magnitude is of the order $M_V = +1.0$ for stars with solar-like metallicity and $M_V = +0.5$ for stars with metallicity one hundredth of the Sun's. Their spectral types range from A5 to F5.

Based on the shape of the light curve, one can categorize RR Lyraes in two classes, RRab and RRc stars. RRab variables show high light variations, typically 1 mag and asymmetric light curve shape with a steep ascending branch. Their pulsation mode is probably the fundamental. RRc stars display lower light variations (0.5 mag) and more symmetric, nearly sinusoidal, profiles. RRc stars probably pulsate in the their first overtone. Their periods are in the range 0.2 to 0.5 days, while RRab variables fall in the range from 0.4 to 1 day. The period of RR Lyrae stars increases and decreases with time. In 1916, Richard Prager and Harlow Shapley have independently observed that the light curve of the RR Lyrae (the prototype star) is modulated in shape and amplitude within a period of 41 days. The effect is called *Blazhko effect* and until now remains to be further investigated.

Outside our Galaxy, RR Lyrae type variables have been discovered in the Magellanic clouds, Andromeda galaxy and other dwarf galaxies, members of our local group.

3.4.4 δ Scuti Variables

Variable stars of this class pulsate radially with periods less than 0.3 days, light variations in the visual regime in the range of few millimags to 0.8 mag and spectral types A to F. The group of δ Scuti variables lies in the instability strip of the H-R diagram. The absolute visual magnitude of these stars ranges from $M_V = +3.0$ to $M_V = 0.0$. These stars are often referred to as *dwarf Cepheids*, *RRs variables*, *AI Vel stars*, *SX Phe stars* and *ultra-short period Cepheids*.

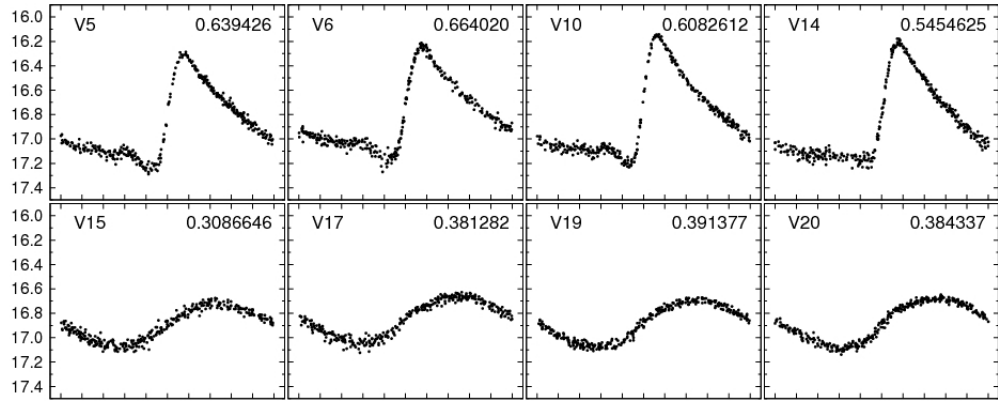


Figure 3.4.2: Light curves of RR Lyrae stars. On the top panel RRab light curves are visible, while on the bottom RRc curves. (A&A 507, 803-815 (2009))

δ Scuti variables may exhibit very complex patterns of variability since some may pulsate in one radial mode only, while others may pulsate simultaneously in radial and non-radial pulsational modes. Mode switching is also a possibility. Many asteroseismology projects have δ Scuti stars at their epicenter, since the observational manifestation of such a behavior can probe the internal structure of these stars.

3.4.5 Rapidly Oscillating Peculiar Ap (roAp) Stars

Before proceeding to the discussion of roAp stars, an introduction to the properties of *Ap stars* is useful. Since the birth of spectral classification, many star with peculiar spectra were known. These *chemically peculiar stars (CP)* display a severe depletion of He on their surface and an overabundance of Fe, Si and Cr in certain regions of the stellar surface, usually their starspots [39]. CP stars are of spectral type B2 to F and their spectra reveal the presence of Fe and rare-earth elements. Ap stars have global magnetic fields ranging from 0.3 KG to 30 KG (thousands of times stronger than the solar magnetic field). The magnetic field strength displays variations with rotation which led to the introduction of the *oblique-rotator model* in order to interpret the observational data. In this model the magnetic axis is tilted with respect to the rotation axis; as such spectrum, color and brightness vary slowly. The time scales of light variations for the Ap stars range from minutes to decades. Ap stars are intrinsically slow rotators and they are considered to be rotating variables.

Rapidly oscillating Ap (roAp) Stars are hydrogen burning stars with mass of the order of $2M_{\odot}$ having global dipole magnetic fields with effective strength from a few hundred to few thousand Gauss. They pulsate in high-overtone, low-degree, non-radial p-modes in time scales from 4 min to 15 min. These stars also display chemical peculiarities. The amplitude of light variations is less than a few millimags. The amplitude of pulsations is modulated with rotation in phase with the magnetic field modulation. Two models have been proposed to address this issue, the *oblique pulsator-model* (Kurtz 1982) which assumes that the pulsation and magnetic axes are aligned, but oblique to the rotation axis. The varying appearance of non-radial pulsations causes the rotational variation of brightness. The *spotted-pulsator model* assumes that the pulsation axis is aligned with the star's rotation axis so the pulsation modes are always seen under the same angle, but the ratio of flux to radius variations and the phase difference between the flux and radius variations are variable over the star's surface as a function of the magnetic field strength (Mathys 1985).

Recent observations of a cyclic-frequency variability, suggest that a magnetic cycle

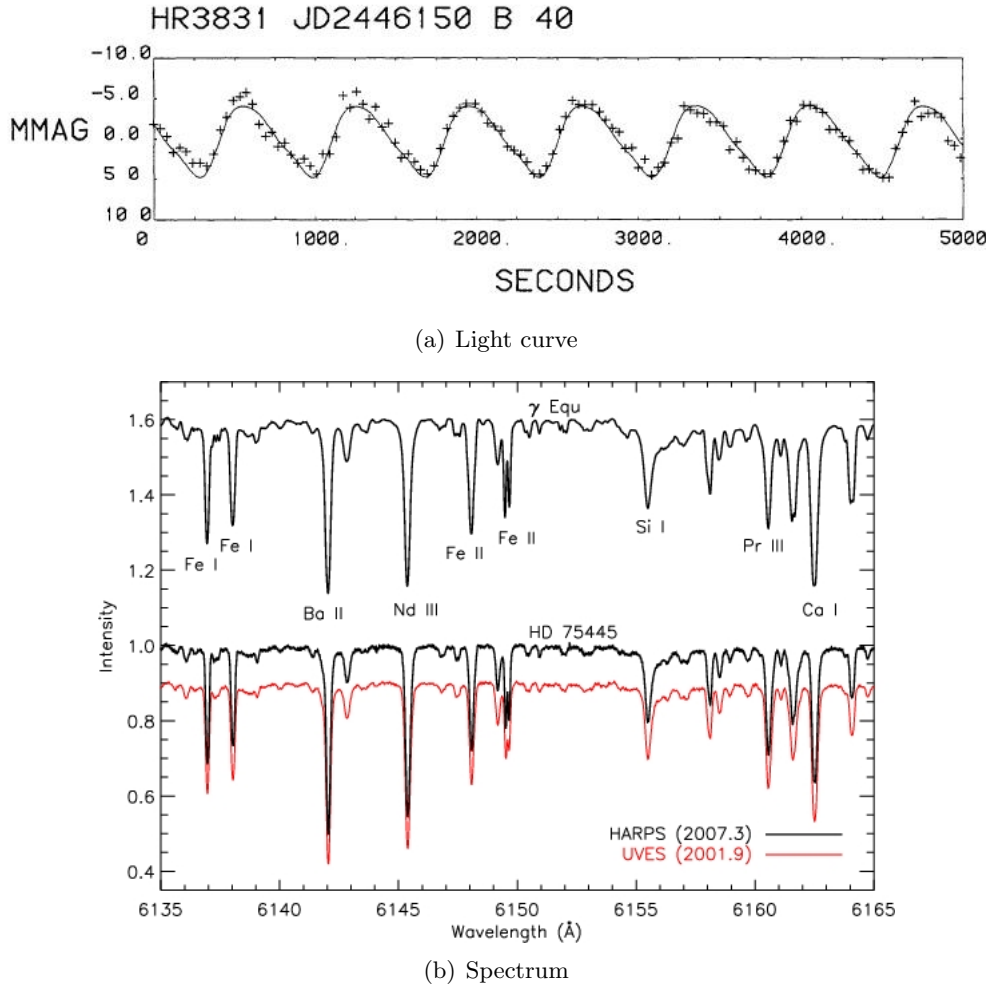


Figure 3.4.3: Spectrum and light curve of a roAp star. Chemical peculiarities are visible in the spectrum.

may be operating in these stars. The variability ranges from hundreds of days to years.

3.4.6 β Cephei (β Canis Majoris) Stars

This class of variables has puzzled theorists for many years, as the driving mechanism for the pulsations was not known. The variability of β Cephei was established very early in the last century. β Cephei exhibited short period light and radial velocity variations which were difficult to be explained on the basis of geometric effects (i.e. eclipses), as such stellar pulsation was the key.

β Cephei variables are normal, early B type giant and subgiant stars. The range of their light variations is less than 0.1 mag and display radial velocities less than $50Kms^{-1}$. The variability pattern is monoperiodic with quasi-sinusoidal light curves, but some harmonics of the fundamental period are present in certain cases.

In 1966 Christy observed that the ionization zones of He^+ which drives the pulsations of classical Cepheids, δ Scuti, RV Tauri and RR Lyrae variables cannot destabilize β Cephei stars. Recently it was pointed out that the κ -mechanism, acting on a zone of 200000K temperature, could drive β Cephei-type pulsations.

In the past β Cephei variables were also referred to as β Canis Majoris stars.

Other types of pulsating variables: Mira variables – α Cygni stars – RV Tauri – Pulsating degenerate stars – Pulsating Red Giants – Red Supergiant variables.

3.5 Eruptive Variable Stars

Eruptive variables are stars varying in brightness because of violent processes and flares occurring in their chromospheres and coronae. The light changes are usually accompanied by shell events or mass outflow in the form of stellar winds of variable intensity and/or by interaction with the surrounding interstellar medium.

3.5.1 Flare Stars

Flare stars are late-type dwarf stars that exhibit sudden brightness increases at irregular time intervals. This behavior is of the same type as solar activity, only much more energetic. They belong to K or M spectral types, but most of them are Me stars, namely emission lines are visible in their spectra. The light output variation can be greater than 6 magnitudes. Flares are more prominent in shorter wavelengths i.e., they are stronger in the U band rather than in V band. The time intervals between flares can range from hours to days and the energy output is of the order of $10^{34} \text{ erg} = 10^{27} \text{ J}$, one thousand times more than that of a typical solar flare.

X-ray observations have proven to be a very interesting tool for the study of stellar activity. Flares, energetic as they are, emit a significant amount of their energy in the X-ray domain. In fact according to X-ray observations another type of activity is recognized. The so-called *micro flares* have energies 10 to 100 times lower than those of a typical flare and are visible in X-rays. Micro-flaring is a common phenomenon and the total energy output is significant. The physical mechanism to produce flares remains an open problem. Magnetic fields and stellar rotation are largely responsible for flares and the physics of reconnection of magnetic field lines has to be understood and applied to such active stars.

3.5.2 Cataclysmic Variables (CVs) and Nova-like Stars

Cataclysmic variables are binary stellar systems that contain a low-mass main sequence secondary and a white dwarf (WD) primary component. Mass transfer through Roche lobe overfilling is continuous due to the low physical separation of the system. The mass flow originates from the main sequence secondary towards the white dwarf. An accretion disk forms around the white dwarf and after the material spins several times, it falls onto the compact object. The overall configuration of the system makes it highly dynamic. Some systems often undergo outburst phases. CVs include non-magnetic systems such as novae and dwarf novae and magnetic systems such as polars and intermediate polars.

Novae occur in white dwarfs that are binary systems. The driving mechanism of the outbursts is mass transfer between the WD and the cooler companion after Roche lobe overfilling by the latter. Most novae have occurred in close binary systems having orbital periods as low as 4 hours. The inflowing material has a high angular momentum to mass ratio, therefore an accretion disk is formed about the WD. Viscous forces cause material within the accretion disk to fall spirally onto the surface of the WD. Novae light curves show a relatively rapid increase (≈ 1 day) and a consequent gradual decline in brightness. In some cases nova light curves exhibit a pre-maximum halt followed by an approximately 1 to 2 mag rise until the final maximum. Early decline follows, that is the time interval from maximum brightness to 3-4 mag below the maximum. An even more "quiet" fall comes afterwards that lasts for 1 to 10 years. The pre-maximum spectra are characterized by broad absorption lines that change to later spectral types (A or F) as the nova passes

from the maximum. As decline proceeds emission lines that require higher excitation temperatures arise, due to ultra-violet radiation from the central WD [35].

Dwarf novae are systems that contain the same components as classical novae but are associated with lower accretion rates. These systems brighten by 2 to 6 magnitudes during outbursts that last between 5 to 20 days. The eruptions are separated by quiescent phases that last from 30 to 300 days. During the long quiescent intervals mass accretion rate is of the order $\dot{M} \approx 10^{12} - 10^{13} \text{ Kgs}^{-1} \approx 10^{-11} - 10^{-10} M_{\odot} \text{ yr}^{-1}$, while during the pre-outburst phase there is an increase to $\dot{M} \approx 10^{14} - 10^{15} \text{ Kgs}^{-1} \approx 10^{-9} - 10^{-8} M_{\odot} \text{ yr}^{-1}$ [6].

Polars contain a synchronously rotating magnetized white dwarf, with a magnetic moment of the order of 10^{34} Gcm^3 , and a cool companion near the main sequence. The strong magnetic field prohibits the formation of an accretion disk. The infalling material forms an accretion stream instead, that follows the field lines of the white dwarf's dipole magnetic field, so that the accretion occurs towards the magnetic poles. These systems show polarized optical radiation, strong X-ray emission, short period modulations due to orbital effects and finally periods of bright and low phases. Orbital periods are in the range of hours. Typical example of polars is the AM Herculis system.

Intermediate polars contain a non-synchronously rotating, magnetized white dwarf but with magnetic moment nearly 0.1 times the magnetic moment of an AM Her system and a cool near-main-sequence companion. In the case of intermediate polars the formation of an accretion disk is viable up to a point that the disk is disrupted by the white dwarf's magnetic field. The accretion continues via an *accretion column* towards the magnetic poles of the primary star (i.e. the WD). Variability is due to eclipses and rotationally modulated accretion effects. Typical example of intermediate polars is the DQ Herculis system. Cataclysmic variables are among the most interesting stellar objects one can study.

Post-common-envelope binaries (PCEBs) constitute a relatively new category of variable stars. These systems started their lives containing two main sequence components. Given certain conditions mass transfer is possible occur. The evolution of one of the components (the more massive) to the giant stage, results in its Roche lobe overfilling. As mass transfer continues the secondary component also reaches the phase of overfilling its own Roche lobe. This signifies the *common-envelope (CE)* phase of the system, where the two stars share a common stellar "atmosphere". Dynamical effects, such as viscosity, inside this common envelope drive the stars to orbit each other, with ever decreasing separation. The system enters its post-common-envelope stage when it ejects its common envelope to form a planetary nebula, due to energy and angular momentum constant "decay" [33], [34]. The nebula quickly diffuses (within thousands of years) and the system can be observed as a PCEB.

3.5.3 Symbiotic Binaries

Symbiotic stars are binary systems consisting of a cool giant usually of spectral type M and a hot main sequence star or a white dwarf with an accretion disk. As a result the spectrum of symbiotic stars displays simultaneously features from a cool star (i.e. absorption lines from molecules) and a hot companion, such as high excitation emission lines. The observational paradox about such stars is the fact that observed at short wavelengths they appear as hot, while observed at longer wavelengths they appear as cool stars. The class may contain any interacting binary with a hot and a cool component.

Variable symbiotic stars are named, after the prototype, *Z Andromedae*. Such stars display the "*symbiotic phenomenon*", this variability is due to mass transfer from the giant to the cool component. The majority of Z And stars contain either a main sequence star, which accretes mass by direct Roche lobe overfilling, or a white dwarf which accretes from the giant's stellar wind. There is also the case of *flickering* or eruptions from the accretion

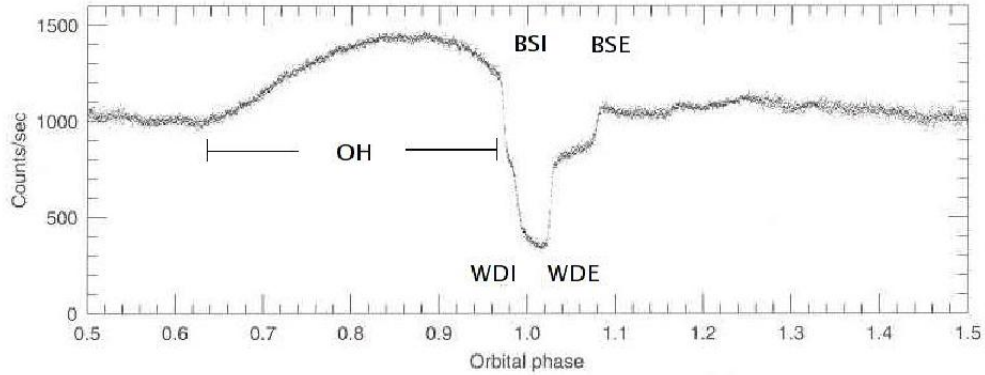


Figure 3.5.1: Light curve of a cataclysmic variable (CV) star. Image taken from [32]

disk especially when the mass transfer is originated from the cool star and stops at the hot object.

The level of activity and therefore variability depends strongly on the separation and evolutionary stages of the symbiotic components. The variability time scale ranges from seconds to decades, with the well-studied systems displaying activity in the time domain from days to tens of days. Variations due to orbital modulation are sometimes prominent in light curves of Z And systems. Orbital periods vary from 100 days to many years. There is a confusion here due to the fact that many systems are eclipsing. The behavior of Z And systems is a complex combination of the binary characteristics and eruptive nature of these stars. Well-known Z And systems include HM Saggitae, FG Serpentis, RR Telescopii and V1016 Cygni.

3.5.4 Wolf-Rayet Stars

Wolf-Rayet (WR) stars are luminous and hot population I¹ stars. Their luminosity reaches $10^6 L_\odot$ and their temperature is between 30 000K and 50 000K. WR stars show peculiar features in their spectra which are characterized by the presence of C, N, O, He and Si emission lines and absorption lines that correspond to O or B spectral types. They are characterized by their high mass-loss rate ($10^{-5} M_\odot \text{yr}^{-1}$) and mark an important evolutionary phase through which all massive stars above a certain limit are bound to pass, when going from the main sequence towards the end of their lives. WR stars appear to be the He-burning cores of stars with initial masses of $30M_\odot$ to $40M_\odot$, whose outer layers have been "radiated away" via the stellar wind process.

The time scales of light variations range from milliseconds to seconds, from minutes to hours and from hours to several days and years. Each variability is closely packed with a different process which the star undergoes. Multiple periods and variable amplitudes are often present.

3.5.5 Supernovæ

A supernova (SN) is an explosive stellar effect which dramatically and irreversibly changes the structure of a star. The SN are the stars with the largest brightness variation. In a few days they can vary more than 20 magnitudes, the luminosity may increase by a factor of 10^8 . After the initial and rapid ascent a decline that lasts for several years follows.

¹these stars tend to be hot and luminous. They populate the disk and especially the arms of spiral galaxies. They are young and exhibit higher metal content.

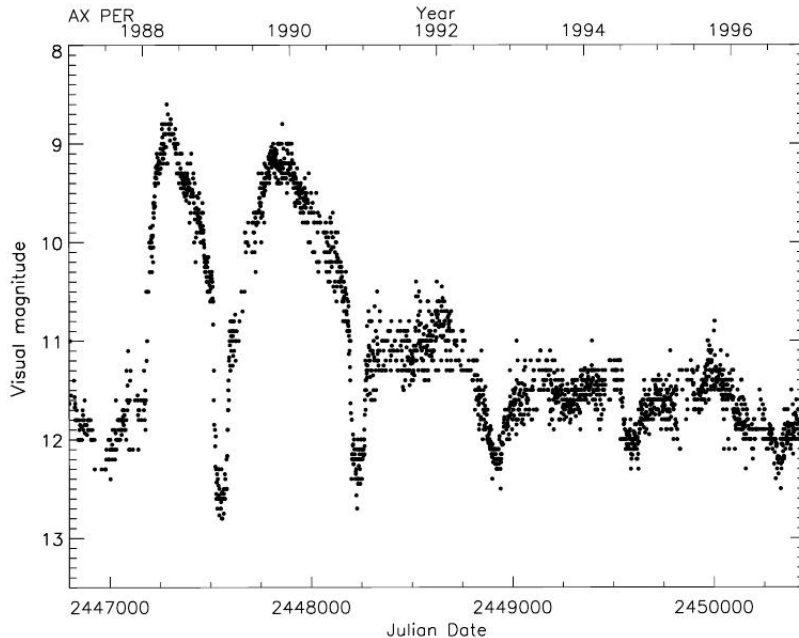


Figure 3.5.2: Light curve of the symbiotic system AX Persei. Eruptions are visible in the left-hand side of the curve while eclipses follow in the right-hand side.

During a SN explosion the shell of the star expands with a velocity of the order of 10 000 Km/s. The ejecta form a shock wave that continues to expand until it comes to rest due to, mainly, friction with the interstellar medium. What remains is a nebulous remnant (supernova remnant, SRN) of material visible for several thousand years after the explosion.

The SN are classified on the basis of whether their spectra display hydrogen features. Type I supernovae lack lines of hydrogen and are further divided into the following categories

Type Ia SN where Silicon is present

Type Ib SN where no Silicon is visible but He is present and

Type Ic SN where again no Silicon is present but there exist small amounts of Helium

SN are also differentiated based on their light curves. Type I supernovae fade away in a rather regular, almost exponential manner, while type II SN light curves show greater diversity in shape and absolute magnitude. A type II SN is the endpoint of a single star's life. Massive stars that have depleted their nuclear fuel are also progenitors of type Ib and Ic SN. Type II, Ib and Ic SN are collectively referred to as *core-collapse supernovae*.

Type Ia SN, however are very interesting objects. They occur in binary systems where a white dwarf accretes material from a higher-mass companion. As the accretion continues the system may undergo several nova outbursts. Some of the accreted material will turn into He or Carbon and Oxygen and will be collected by the compact object. The mass may reach the Chandrasekhar limit or exceed it. The compact object collapses and a SN type Ia explosion follows. This accretion induced collapse is a fundamental phenomenon with high impact on cosmology. As Ia SN occur at a given, well determined mass limit, the energy output is well defined, so as the absolute magnitude. As such, having a single measurement of the apparent magnitude of a SN, one can deduce the distance. Type Ia SN serve as "standard candles", providing us with the cosmic distance scale.

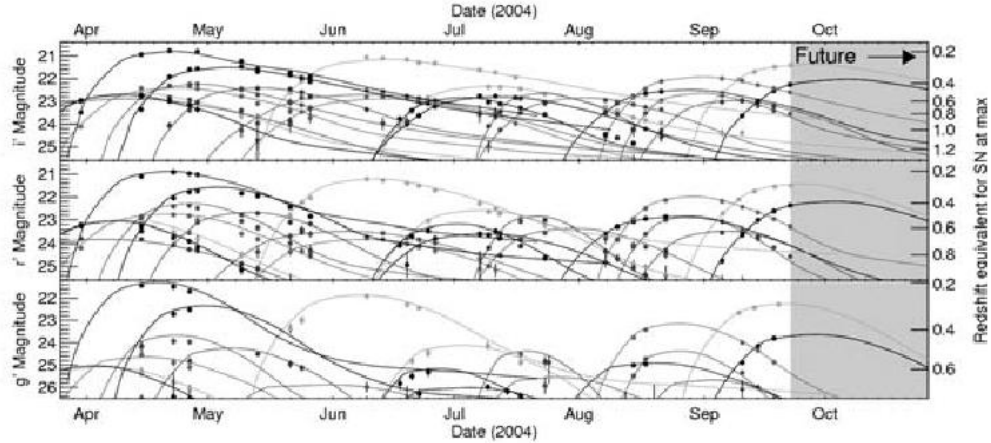


Figure 3.5.3: A Large sample of supernovae light curves in the gri photometric system, obtained by the SuperNova Legacy Survey. Figure adopted by [29].

Other types of eruptive variables: Luminous Blue Variables (S Doradus) stars.

3.6 Pre-Main Sequence Variable Stars

Pre-main sequence (PMS) variable stars are newly born stars that have not yet reached a sufficient central temperature to ignite core-hydrogen burning and thus enter the realm of "normal" stars. During their formation stage the PMS stars gain their energy from the Kelvin–Helmholtz contraction mechanism. PMS stars are usually classified as eruptive variables. The GCVS divides them in many subgroups (FU, IN, INA, INT, INYY and others) but this scheme is based only on morphological characteristics of the light curves. Since a more physically-oriented classification is more useful, one has to classify such stars according to intrinsic properties.

Currently a division according to mass is followed. PMS stars with masses $M \leq 3M_{\odot}$ are designated T Tauri stars. Intermediate mass PMS having masses between $4M_{\odot} \leq M \leq 8M_{\odot}$ are called Herbig Ae/Be stars. The division has no distinct border, as the case is for most of astronomy.

3.6.1 T Tauri Stars

Joy in 1942 was the first to observe T Tauri stars in the Taurus-Auriga dark cloud. T Tauri stars are characterized by late spectral types (G to M) and emission lines that resemble those of the solar chromosphere. These stars are very young stellar objects, having typical masses of $\approx 1M_{\odot}$, that have not yet reached the main-sequence, thus still being in the gravitational contraction phase. The continuous emission is sometimes so strong that almost covers the superimposed absorption spectrum. The strongest lines are the Balmer hydrogen lines. Other emission lines are those of slightly excited metals, such as CaII, FeII and lines of neutral He and Li $\lambda 6707$. Forbidden emission lines are also present, which suggest the presence of flowing circumstellar material. These forbidden lines arise from atomic transitions that require time scales of the order of 1s rather than the usual time of $10^{-8}s$ for normal transitions. The presence of Li is indicative of their youth. Li absorbs H and forms He, in fusion reactions, that can take place in an environment of only 1 million K.

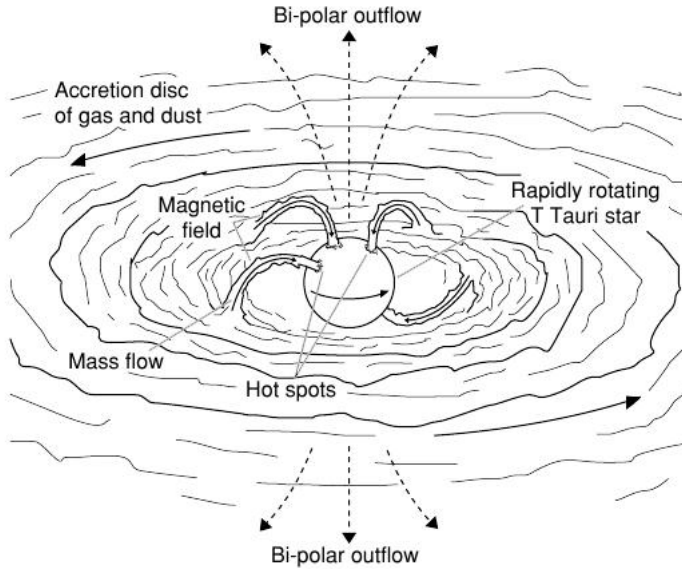


Figure 3.6.1: A schematic of the T Tauri phenomenon. Figure adopted by [29].

Multi-wavelength observations have shown that each type of variability arises from different areas of the star. IR variability comes from cool material in an accretion disk, UV variability comes from a hot spot as matter accretes onto the star. Visible and further IR variability may arise from the rotation of cool and hot spots of the star [29]. The observational manifestation of PMS stars is described on the basis of the interaction between the star itself and the accretion or circumstellar disk. For example, variability of FU Orionis stars is due to instabilities in the accretion disk. The variability of T Tauri stars displays a wide range of time scales, amplitudes and spectral "differences".

3.6.2 Herbig Ae and Be Stars

Herbig Ae and Be stars are the massive (2 to $10 M_{\odot}$) analogues to classical T Tauri stars. They are young ($\leq 100 My$) A and B stars that show emission lines, whose natural environment are dark obscured regions, and they are connected to reflection nebulae. They are embedded in gas and dust envelopes and may be surrounded by circumstellar disks. Classical Be stars are variable in many time scales. At least two Ae/Be stars are known to be eclipsing; V628 Cassiopeiae and T Orionis.

The criteria for Ae/Be classification are spectral type earlier than F0, Balmer emission lines in the stellar spectrum and infrared radiation excess due to the presence of the circumstellar disk.

3.6.3 Herbig–Haro Objects

Another mechanism than enables mass loss during the pre-main sequence stellar evolution, except for the expanding envelopes, are jets.² Jets² are narrow beams of gas ejected by the star in opposite directions. The first astronomers to observe Herbig–Haro (HH) objects, as the name denotes, were George Herbig and Guillermo Haro in the 1950s. HH objects are related to jets produced by young protostars, still at their formation stage. As the gas

²Astrophysical jets occur not only in cases such as HH objects. They are among the cornerstones of modern astrophysics and exist in all scales and in all energy regimes.

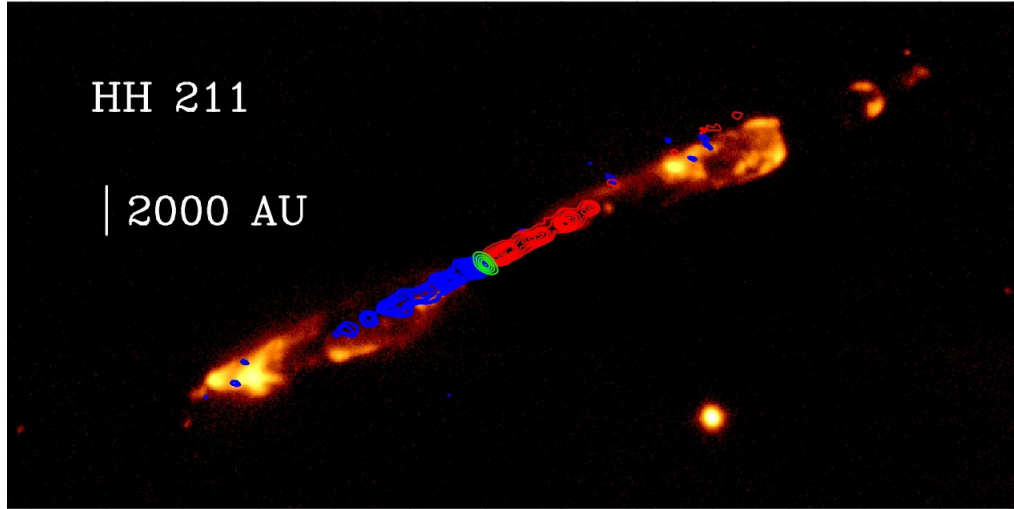


Figure 3.6.2: Herbig–Haro object number 211. The bipolar protostellar jet is prominent.

from the jet progresses into the ISM, collisions excite the gas. The result is the emergence of bright objects with emission line features in their spectra.

HH objects can be variable, with brightness that can vary up to several magnitudes in time scales of tens of years. Reflection of the light of the parent star is responsible for the continuous emission in the spectra of young stellar objects (YSOs). Regions of the circumstellar disk may also be illuminated by the central star.

Other types of PMS stars: FU Orionis.

3.7 X-ray Binaries

X-rays are high-energy photons. They are second only to γ -rays in energy. X-ray binaries are the neutron star counterparts to cataclysmic variables, namely they are interacting close binaries with a neutron star (or a black hole, BH). The difference between CVs and X-ray binaries is reflected on the amounts of energy they emit. CVs have an X-ray luminosity of $L_X \leq 10^{34} \text{erg/s} = (10^{27} \text{W})$ while X-ray binaries have typical luminosities of $10^{35} \text{erg/s} (= 10^{28} \text{W})$ to $10^{38} \text{erg/s} (= 10^{31} \text{W})$, these figures correspond to values from $25L_\odot$ to $25000L_\odot$. As a result X-ray binaries are discovered on the basis of their strong X-ray emission. The mechanism behind such luminosities is the conversion of gravitational energy into kinetic energy.

The simplest model of X-ray binaries includes a neutron star (NS) along with a, secondary, main sequence star or giant (or a second compact object in few cases) gravitationally bound together. The non-degenerate component is over-filling its Roche lobe and matter is being transferred from it to the neutron star (or BH). The angular momentum "content" of the material prevents it from falling right onto the compact object and an accretion disk is formed around it. Eventually and as viscous flow consumes the material's angular momentum it falls spirally onto the neutron star. The magnetic field of the neutron star is vital to the existence of the accretion disk. The existence of a large magnetic field disrupts the accretion disk and matter flows along the field lines towards the poles of the NS. Temperatures in regions close to the accretion disk reach values up to tens of 10^6 K. As a result, black-body radiation emitted peaks in the X-ray domain of the electro-magnetic spectrum. The central role of the accretion rate is more than obvious.

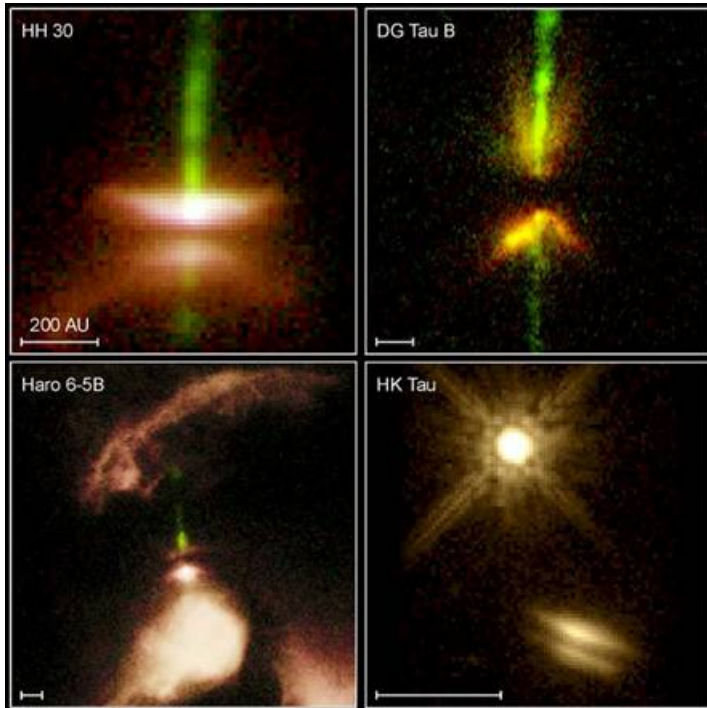


Figure 3.6.3: A collection of HH objects. Circumstellar disk and jet features are visible.

The first X-ray binary, Sco X-1, was discovered accidentally by Giacconi on 12 June 1962. The nature of this object was a mystery for many years, largely due to positioning errors. Eventually an optical counterpart to Sco X-1 was discovered and identified as a $V \approx 13$ mag variable star. This optical counterpart was displaying a very high X-ray over optical luminosity, namely $L_X/L_{opt} \approx 1000$, a fact that amazed the astronomical community. The connection between X-ray binaries and close binary systems was proposed by I. Shklovski in 1967.

X-ray binaries are divided into two categories primarily according to their ratio of X-ray over optical emission L_X/L_{opt} and secondly according to the mass of the secondary component. The categories are high mass X-ray binaries (HMXRBs) and low mass X-ray binaries (LMXRBs). HMXRBs have, an X-ray over optical, ratio between 10^{-3} and 10, most of them emit larger radiation amounts in the optical regime. LMXRBs have a ratio of 10 to 10^4 and they are very faint objects in optical wavelengths.

3.7.1 High-Mass X-ray Binaries

In HMXRBs the secondary companion, the mass donor, is a bright O to B giant or supergiant star. The concentration of HMXRBs near the galactic plane shows that they are very young objects. An interesting aspect of HMXBs is the emission of X-ray pulses in very short and regular time intervals, due to "*lighthouse effect*". Such X-ray pulses have periods of 0.061s to 835s . Matter is accreted by the NS along the strong-magnetic-field lines, towards the polar regions. If the rotation and magnetic axis are not aligned then the HMXRB will be visible to an observer only when the magnetic axis is faced towards him. As such the pulse period reflects the rotation period of the NS.

HMXRBs mostly vary in X-rays but in optical wavelengths the emission is due to the light of the bright companion. In the optical range, brightness variation is of the order of $0.1 - 0.2\text{mag}$. Photometric variability originates from the orbital motion of the system. The light curve is largely sinusoidal with two maxima and two minima of different depths.

This is due to *gravity darkening*, namely the heating of the companion's parts that face the compact object, due to extreme gravity. In some cases, when an accretion disk surrounds the primary component, there exists a minor optical contribution from the disk. Accretion could also be served via strong stellar wind.

3.7.2 Low-Mass X-ray Binaries

The configuration of a LMXRB system is equivalent to that of a HMXRB except from the mass of the secondary component which is generally $\leq 1 - 2M_{\odot}$. In addition, here a late spectral type star carries the role of the secondary companion. In optical wavelengths LMXRBs are faint objects with absolute magnitude $\approx +1mag$. The accretion disk that surrounds the primary "star" has the major contribution to the optical light output, this is achieved through the absorption of X-rays by the disk and re-emission of photons in longer wavelengths (and lower energies), making the disk much more luminous in comparison with CVs. Their spectra show features of emission lines embedded on a flat continuum.

LMXRBs are old objects and can be found both in the galactic bulge and the galactic plane. Some of them also reside in globular clusters. Their weak magnetic fields, owing to their age, enable LMXRBs to accrete matter from the inner parts of the disk, thus showing no X-ray pulses. However LMXRBs generate X-ray bursts at irregular time intervals, from hours to days, during which the X-ray luminosity is increased, within seconds, by a factor of 10 or more. The phenomenon is attributed to the thermonuclear burning of He on the surface of the SN, should a sufficient mass accretion rate is achieved. Optical variability in LMXRBs originates from a number of different phenomena associated with orbital motion of the system's constituents, each of which is characterized by a different periodicity.

4

Observations

"Some nights the magic works. Some nights it doesn't."

4.1 Introduction

ASTRONOMICAL surveys have a great history full of discoveries and breakthroughs. A survey is the astronomer's tool to go beyond the standards and pinpoint targets for potentially interesting (follow-up) observations. Especially in the search for variable stars, using a small telescope (\approx 8-11 inches), it is an easy task to monitor stellar fields across a wide field of view ($\approx 3^\circ$). Such fields of view offer the advantage of a bigger statistical stellar sample that leads to increased chances for a discovery. The above advantages do not come without compromise. Small telescopes pose restrictions on the limiting magnitude of stars included in the sample, yet more than enough bright stars can be monitored for light variations at the same time. A very interesting side product of variability surveys is the possibility for discovering transiting extra-solar planets; the probability of such an event is not negligible, especially if a careful selection of fields is performed (see section 4.3). In our survey I undertook the variable stars part.

The instruments for an astronomical survey have to be situated in a place with optimal weather and seeing conditions. The Holomon Astronomical Station incorporates some very interesting characteristics that comply with the needs of a variability survey with high expectations. Those are established after many years of observations and seeing measurements.

Observing Run	Telescope	Detector	Data
7 to 30 July 2008	C11	FLI CCD	\sim 2800 frames
6 to 31 July 2009	Takahashi ε -180 ED	FLI CCD	\sim 3000 frames

Table 4.1.1: A summary of the observing runs. The number of frames includes the calibration frames acquired.

4.2 The Site of Observations

The idea of an astronomical station for the University of Thessaloniki was first conceived by Prof. John H. Seiradakis and Prof. Stavros I. Avgoloupis. A place for observations away from the light pollution of Thessaloniki was an immediate need, since an ever growing number of students wanted to get involved with observational astronomy. The construction was taken up by the observatory's technician, Vaggelis Tsorlinis.

The archive of meteorological data for the region is available for many years. The data reveal that the position favours the construction of an astronomical observatory. The minimum temperature is -15°C , the maximum is 30°C , while the average is about 10°C . The relative humidity is about 70% and the annual rainfall is about 750mm, with 754mm in 2009.

The first attempts to measure the astronomical seeing of the region took place in 2005 by D. Mislis [23] and in 2007 by J. Nestoras [26].

The Holomon Astronomical Station is situated in Chalkidiki, Greece, at an altitude of 800 meters above sea level. It is within driving distance of Thessaloniki but away enough for most of the lights to be blocked. The site has another advantage. The Department of Forestry and Natural Environment of our university already has infrastructure for environmental training as well as for housing of students. This fact has facilitated the construction of the astronomical station by the Department of Physics, saving both resources and time.

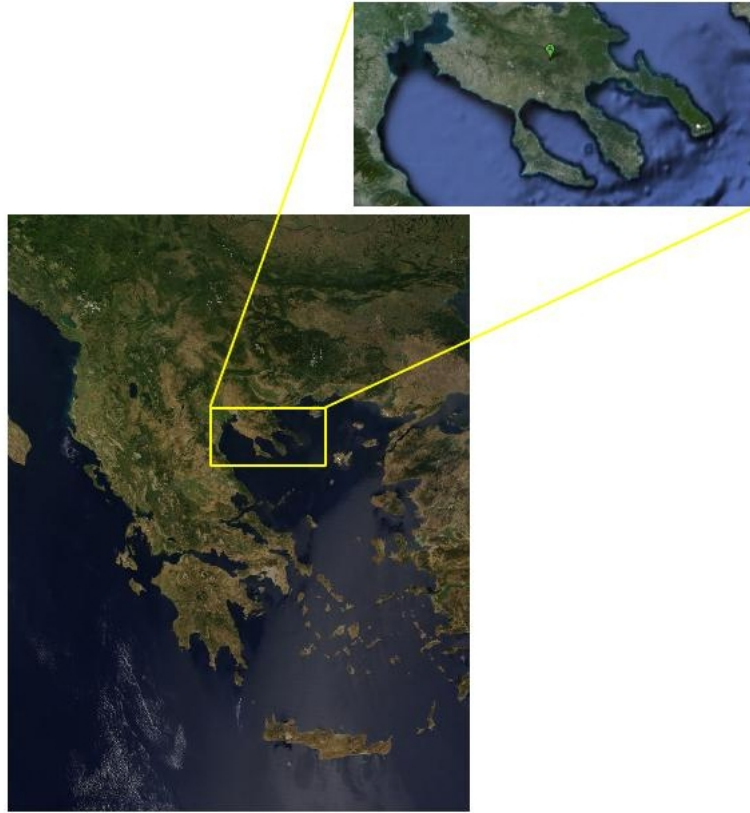


Figure 4.2.1: Map of the Chalkidiki region. The site of Holomon Astronomical Station is marked with an A.

4.2.1 Seeing Measurements

The calculation of astronomical seeing for the Holomon Astronomical Station is performed with the Differential Image Motion Monitor (DIMM) method. A variation of the method

Holomon Astronomical Station	
Latitude	40° 25' 35" N
Longitude	23° 29' 59" E
Elevation	800 m
Seeing (mean)	0.87 arcsec
Scintillation (mean)	0.049 mag
Isoplanatic angle (mean)	45.32 arcsec

Table 4.2.1: Holomon Astronomical Station geographical data.

ExoField #1 Data	
Right Ascension	22 ^h 53 ^m 53 ^s
Declination	+44° 30' 00"
Probability[%]	71.99

Table 4.3.1: ExoField #1 data, along with the transit detection probability.

is the ESO-DIMM introduced by Sarazin & Roddier (1990)[36]. We use the Seeing-GR software to obtain the raw seeing data. Seeing data analysis is performed afterwards using the Seeing-GR analysis code. Both software tools are written by I. Nestoras.

Over the time we have collected an amount of seeing data [27], [26] that can be used to characterize the region of mount Holomon as an exceptional site for astronomical research. The actual figures can be seen in Table 4.2.1 and Figures 4.4.2 through 4.2.5.

Seeing, Scintillation and Isoplanatic angle

The Earth's atmosphere causes a series of unwanted effects that degrade the quality of astronomical images. Positional changes along with image quality changes are referred to as *seeing*. The impact of seeing to data is inversely proportional to the telescope aperture. Smaller apertures are much more sensitive to seeing conditions than larger.

The amplitude variations of the stellar light caused by the Earth's atmosphere is known as *scintillation*. This effect can pose serious difficulties to high precision photometric studies. *Isoplanatic angle* is the angular separation between two stars at which the effect of atmospheric turbulence causes the light of the two sources to become uncorrelated.

4.3 Interesting Stellar Fields

A careful selection of fields has been performed according to the work done by Heller, Mislis & Antoniadis (2009) [12]. The primary aim of this work is to identify and pinpoint the promising spots for extra-solar planetary transits to occur. Hot Jupiters are within our observational capabilities.

Within this context we selected 5 promising spots. The main criteria were the instruments we had at our disposal and the probability for a transit to occur, since variable stars are more widespread in a given stellar field. The spots of interest were five, one of which we observed during July 2008 and 2009. The data for the given field (hereafter mentioned as ExoField #1) are summarized in Table 4.3.1.

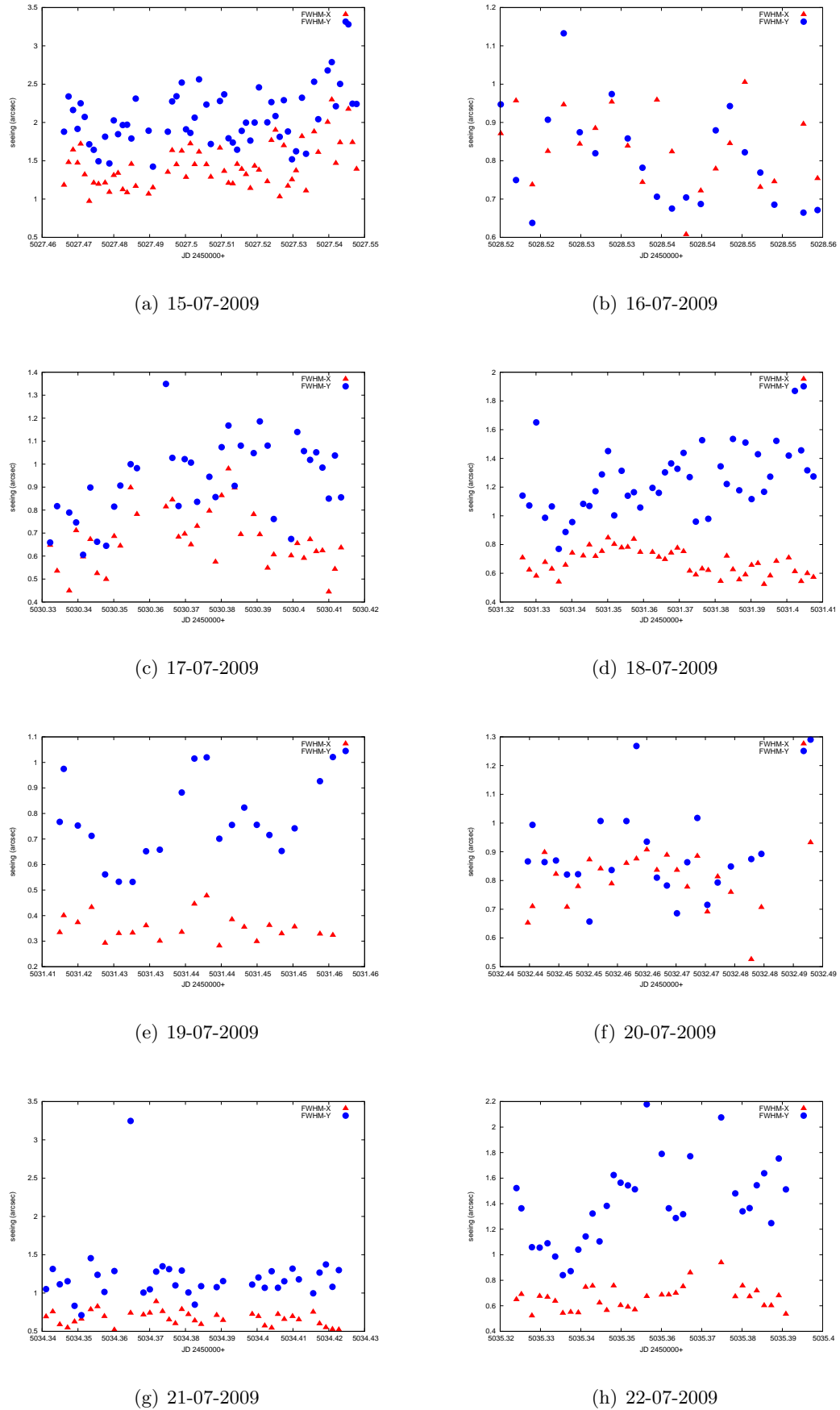


Figure 4.2.2: Seeing conditions at Mt. Holomon, during June 2009.

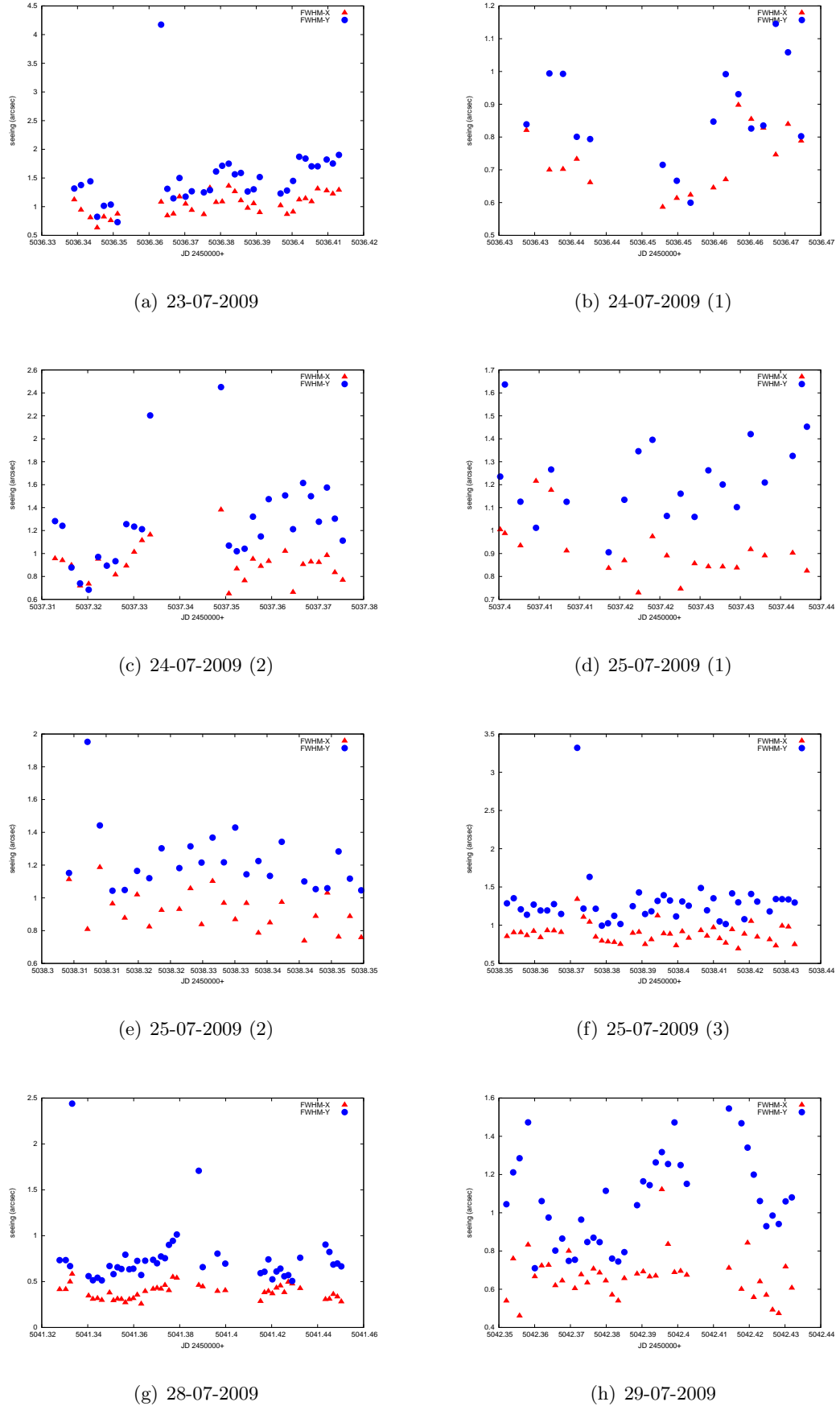


Figure 4.2.3: Seeing conditions at Mt. Holomon, June 2009
(cont.).

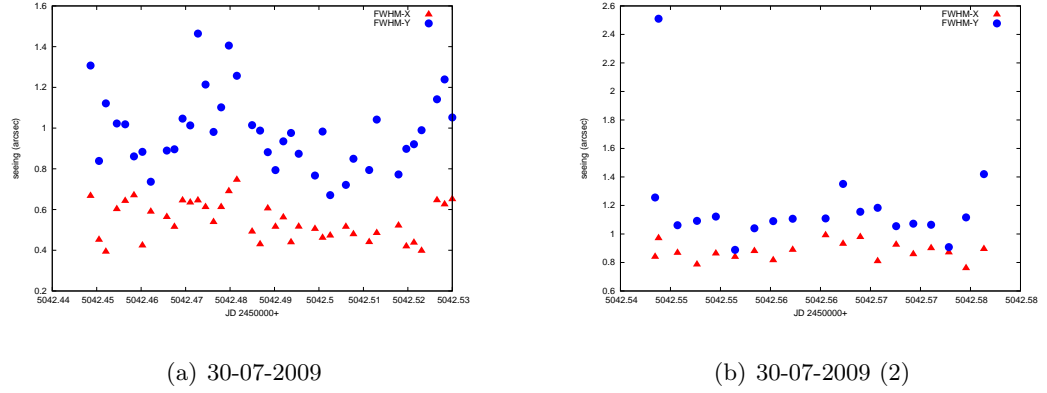


Figure 4.2.4: Seeing conditions at Mt. Holomon, June 2009
(cont.).

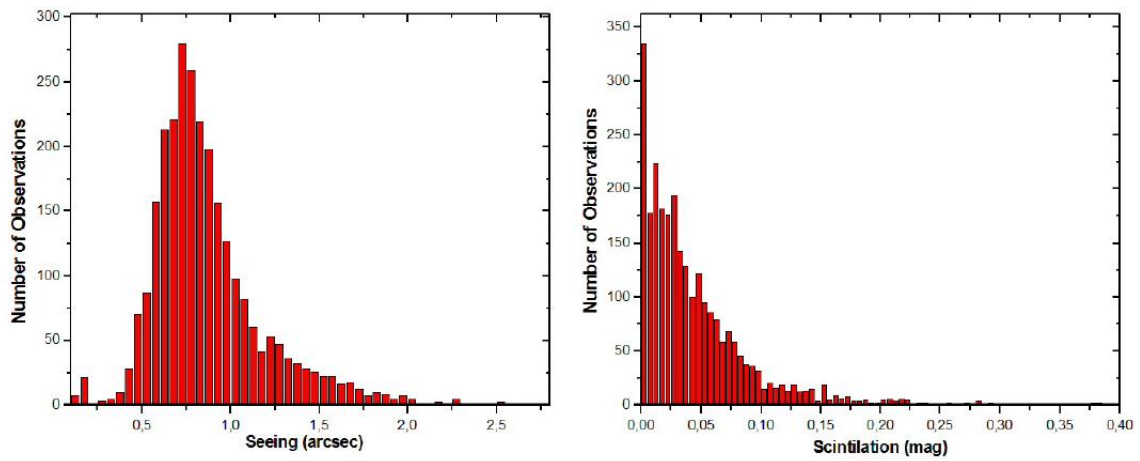


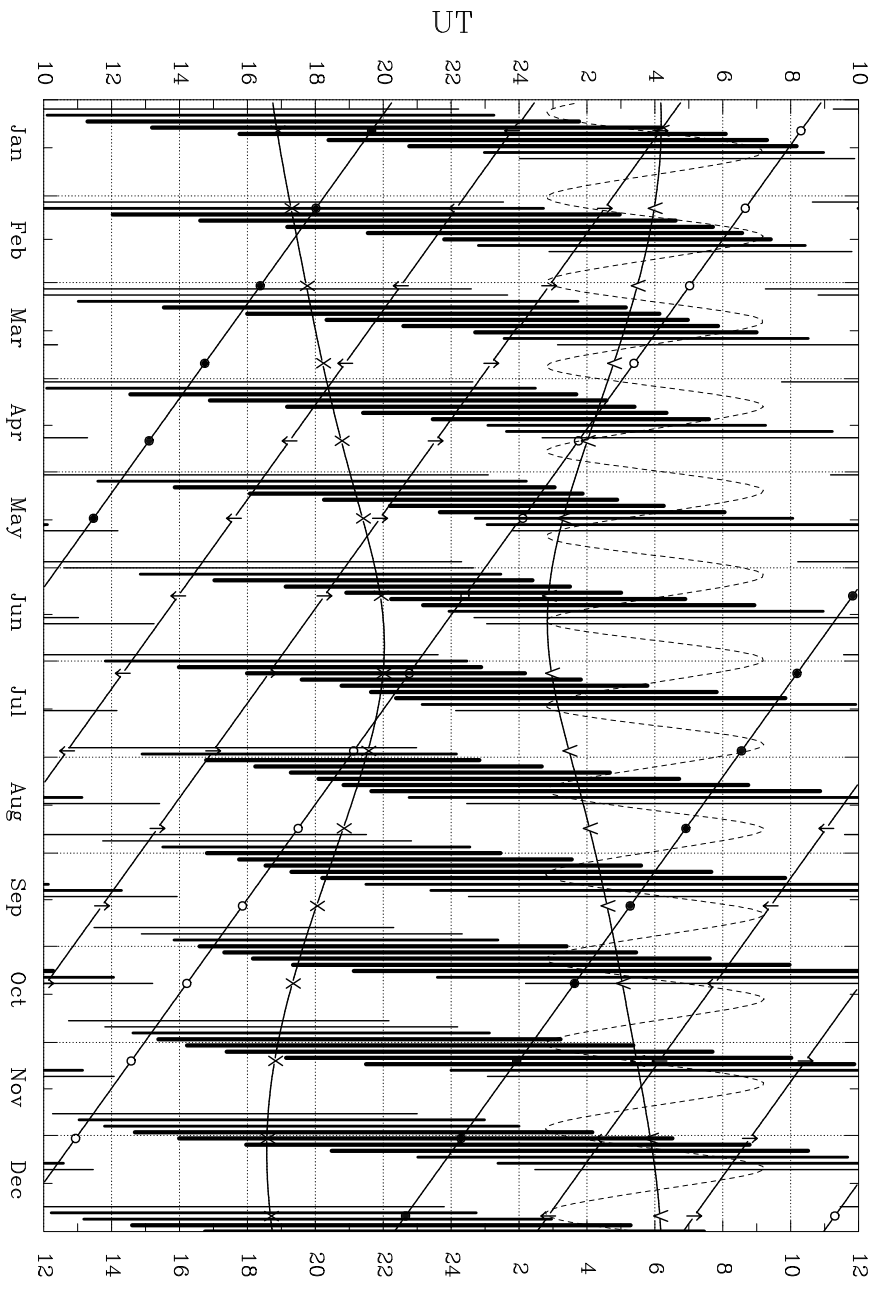
Figure 4.2.5: Overall Seeing and Isoplanatic angle measurements. Image taken from [26].

Visibility of ExoField #1

HOLOMON ASTRONOMICAL STATION

Year 2009

RA: 22h53m40.0 DEC: +44d44m55.0



↑ star rises ↓ star sets ○ star gets above 30° • star gets below 30°
 -x-twilight ends -v-twilight begins - - g.c. moon-star dist. (hrs)
 moon above horizon: thin line – moon 25%–50% illuminated
 medium line – moon 50%–75% illuminated
 thick line – moon 75%–100% illuminated

Figure 4.3.1: Visibility plot of the ExoField #1.

4.4 Instrumentation and Equipment

Charge-coupled devices (CCDs) are nowadays the most common imaging devices used in astronomy. They are used as counterparts to photographic plates and films, but there is hardly a comparison between them. CCDs have many advantages over old-fashioned techniques. Increased efficiency in photon collection and good spectral response across the optical spectrum are the highlights. CCDs are easy to operate and they are highly cost-effective. These characteristics enabled astronomers to design new instruments and to develop new observing techniques, like surveys.

A survey is the technique of observing a large portions of the sky with a single exposure and cover as much of the sky as possible. In the University of Thessaloniki we had the idea of designing a new survey in order to search for new variable stars and transiting extra-solar planets. The only equipment needed for such a survey is a commercial telescope and a high quality CCD camera, along with the computational infrastructure for data acquisition and analysis. Along with the above instruments Holomon Astronomical Station is also equipped with a DCF-77 radio unit for accurate timing and a weather station.

4.4.1 The Camera

In our survey we employed the ProLine PL6303E CCD camera model by Finger Lakes Instrumentation. This is a front illuminated, monochrome camera that uses the Kodak KAF-6303E chip. The specifications of the camera and the CCD detector chip are shown in Table 4.4.1. The majority of values shown, are the technical specifications provided by the manufacturer. In special cases, when the values are important for the reduction and analysis of the data, such critical parameters were calculated by us during our tests.

Array Size	3072×2048 pixels
CCD Type	Front illuminated
Pixel Size	$9\mu m \times 9\mu m$
Coating	None
Sensor Diagonal	33.3 mm
Full Well Capacity	$100000e^-$
Anti-Blooming	None
Peak Quantum Efficiency	68%
Dynamic Range (Saturation Signal/Dark Noise)	76 dB
Interface	USB 2.0
Digital Resolution	16-bit
Maximum Data Rate	8MHz
Typical System Noise	$9 e^-$ RMS @ 1MHz
Temperature Stability	$0.1^\circ C$
CCD Grade	2
Gain @ 2×2 binning (calculated)	2.108
Readout Noise (calculated)	12.920

Table 4.4.1: CCD camera and Sensor specifications.

4.4.2 Tests of our CCD Camera

The CCD camera is probably the most important instrument for a survey. Therefore one of the priorities was to establish the quality of the acquired data and the intrinsic

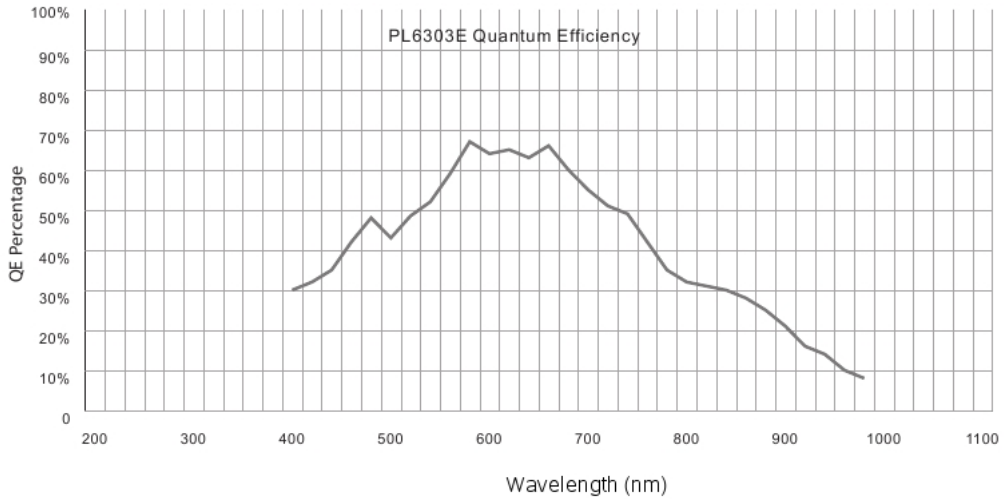


Figure 4.4.1: Spectral response of the KAF-6303 chip.

specifications of the camera itself. Certain tests were performed in order to check the integrity of all the above.

Linearity

A linearity test of the camera was performed in order to establish the good response of the system to incident photons. The test begins by repeated integrations with increasing exposure times. We chose a stellar field that is moderately crowded and has a wide distribution of magnitudes. The images were used to plot the counts of certain stars in the field against the exposure time. The results of the test are depicted in Figure 4.4.2. The slope of the linearity curve is equal to the gain of the detector.

Quantum Efficiency

This is another crucial parameter for CCD imaging. In CCD astronomy the primary scope is to count photons. This is done on a CCD array which has the property of turning incident photons into photoelectrons that are stored in the pixels potential wells. Quantum efficiency is the ability of the array to produce photoelectrons. The accurate definition is; *the ratio of incident photons to those that are detected and therefore turned into photoelectrons*. An ideal detector would have a QE of 100% and it would detect and count all incoming photons, but this is not the case for real detectors. There is also a strong dependence of the QE on the wavelength of incident photons. However modern CCD cameras house solid state arrays with high quantum efficiency (60% – 90%) that suit the needs of observational astronomy. The peak quantum efficiency of our FLI camera was 68%.

Gain

The gain of a CCD sensor is the conversion factor between the number of photoelectrons produced by incident photons and the amount of output digital units (ADU, analog-to-digital units or counts) that a pixel is going to produce. The usual way of expressing gain values is the number of photoelectrons needed to produce one ADU (e^-/ADU). For instance a gain of $3 e^-/ADU$, means that an ADU will be 'recorded' for every three photoelectrons the pixel accumulates. A major advantage of modern CCD imagers is the linear response over a wide range of data values. The maximum number of ADUs a pixel

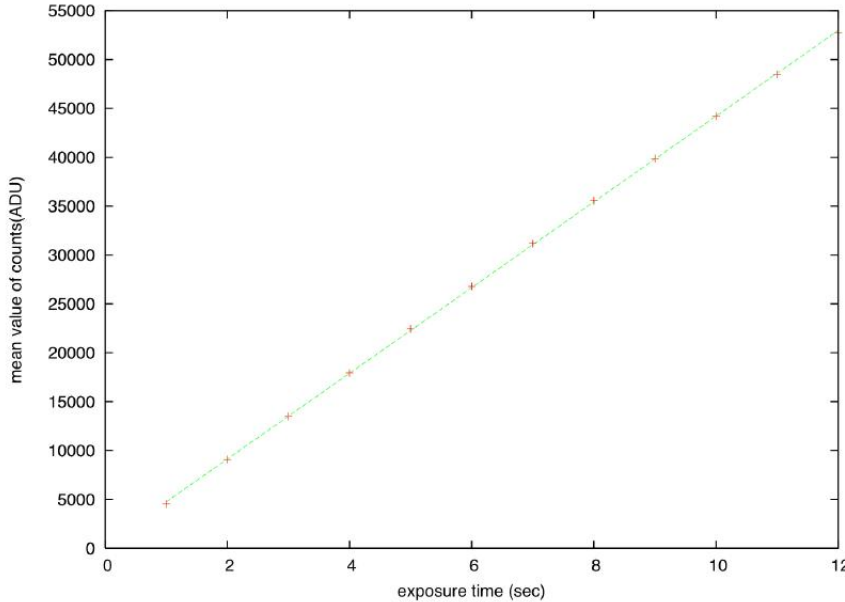


Figure 4.4.2: Linearity diagram of the KAF-6303 chip. Image taken from [1]

can produce is given by the bits, the analogue-to-digital converter utilizes. For example a 14-bit A/D converter can output numbers from 0 up to 16383, whereas a 16-bit A/D converter can produce numbers up to 65355.

Then we concentrated on measuring the true gain factor of the camera. This is a crucial parameter for accurate photometry using DAOPHOT II. The procedure we followed is described below:

1. Acquired a bias frame.
2. Acquired two flat fields of the same exposure time, Flat1 and Flat2.
3. Created the difference image by subtracting one flat-field from the other, $\text{diffflat} = \text{Flat1} - \text{Flat2}$.
4. Calculated the standard deviation of a region in the difference image that does not suffer from defects, e.g. cosmic ray hits.
5. Then the variance is calculated by squaring the standard deviation and dividing by 2, because variance adds per image so the variance of the difference image is the sum of the variance of Flat1 and Flat2.
6. One then has to bias correct one of the flat field, $\text{debiasflat} = \text{Flat1} - \text{bias}$.
7. From the statistics of the bias corrected flat, we obtained the mean counts of the image.
8. The gain is given by

$$\text{Gain} = \frac{\text{Mean}}{\text{Variance}} \quad (4.4.1)$$

The result is given in Table 4.4.1. A more accurate method for the calculation of the true gain of a CCD sensor is by acquiring a series of flat fields at certain illumination levels, that span throughout the range of the sensor until saturation. Then averaging the images at each level and repeating the same procedure, one comes to a result with increased precision. The idea is described in the work of Mortara and Fowler (1981) [25].

Readout Noise

Another very important parameter for reliable photometry is the readout noise of the camera. It is usually expressed in terms of extra electrons added to each pixel during the readout. Readout noise has two components. The first one is introduced during the digitization process, when a digital number is assigned to the analog signal. The output of the A/D circuit has a statistical character that cannot repeat itself. This means that there is a certain amount of randomness even if the same pixel is readout twice. The distribution around a mean value is not necessarily Gaussian. The second component is the electronics themselves. They will introduce "free-floating" electrons randomly, and consequently fluctuations into the output. The two components affect the output value of each pixel every time the array is readout.

A good way to determine the readout noise of a CCD is the 'two-bias' method [13]. According to this method, one has to calculate the standard deviation of a difference image of two bias frames. The relation is simple,

$$\text{Read Noise} = \frac{\text{Gain} \times \sigma_{B_1 - B_2}}{\sqrt{2}} \quad (4.4.2)$$

where B_1 is the first bias frame and B_2 is the second, see Table 4.4.1 for the results.

Signal-to-Noise Ratio

Signal-to-noise ratio, SNR or S/N, lays in the crux of every worthy data set in astronomy. A generic definition would be; the amount of interesting information compared to the irrelevant fluctuations, the signal displays for a number of reasons. The concept is simple,

$$S/N = \frac{\text{Signal} + \text{Noise}}{\text{Noise}} \quad (4.4.3)$$

A good SRN is considered to be 20-30 or more. At a more complex level our analysis has to take into account the various noise sources present in an observation. The complete quantitative expression to do that is,

$$S/N = \frac{N_\star}{\sqrt{N_\star + n_{pix}(N_{Sky} + N_{Dark} + N_{Read}^2)}} \quad (4.4.4)$$

known as the 'CCD Equation' (*Mortara & Fowler, 1981*)[25], where N_\star is the total number of photons or the signal. The noise terms at the denominator are again N_\star , N_{Sky} is total number of photons from the sky background per pixel, N_{Dark} is the number of dark current electrons per pixel and N_{Read}^2 is the number of electrons generated during readout per pixel. The coefficient n_{pix} is the number of pixels that are used during the analysis and it is used to scale the 'per pixel' values.

It is known that sources of noise that are described by Poisson statistics have an 1σ error of the order of \sqrt{N} for that signal level N (*Poisson noise*) [13]. Let us examine the situation of a CCD that is uniformly illuminated so that each pixel "counts" $10000e^-$ (quantum effects are not taken into consideration). An ideal CCD detector would detect $10000e^-$, while the real one counts on average $10000e^-$ per pixel with a standard deviation σ that shows how much fluctuation, about the mean value, is present. According to Poisson statistics, this standard deviation is equal to the square root of individual particles, so that if there are N particles in each CCD well, the mean value is equal to N , the standard deviation is \sqrt{N} and the S/N is $\frac{N}{\sqrt{N}}$. In this example the number of particles

is $N = 10000$ while the standard deviation is $\sigma = \sqrt{10000} = 100$ and the signal-to-noise ratio is $S/N = \frac{N}{\sqrt{N}} = \frac{10000}{100} = 100$.

The noise level drops as more photons arrive to the detector but never vanishes. Photon noise of all of the above kinds, from the sky and the source itself, obeys Poisson statistics. However the N_{Read} term behaves as shot noise, that is why it is squared in the expression above.

4.4.3 Telescopes and Mounts

In the course of our observations we used two different telescopes at different time periods. Both telescopes were mounted on SYNTA EQ-6 PRO german equatorial mounts with auto guiding capability. The first telescope we used is a Celestron C11. The other telescope of our survey is a Takahashi EPSILON-180ED astrograph. The reason behind this choice is the maximized field of view, which suits best the requirements of the survey.

Optical Design	Schmidt-Cassegrain
Aperture	279.4mm (11 inches)
Focal Length	2800mm (110.24 inches)
Focal Ratio	f/10
Focal Length with Reducer	1760.22mm
Focal ratio with Reducer	f/6.3
Field Flattener	yes

Table 4.4.2: The Celestron C11 Specifications.

Optical Design	Hyperbolical Newton
Aperture	180mm (7 inches)
Primary Mirror Diameter	190mm (7.5 inches)
Secondary Mirror (minor axis)	80mm
Focal Length	500mm
Focal ratio	f/2.8
Field Flattener	yes

Table 4.4.3: Takahashi EPSILON-180ED Astrograph Specifications.

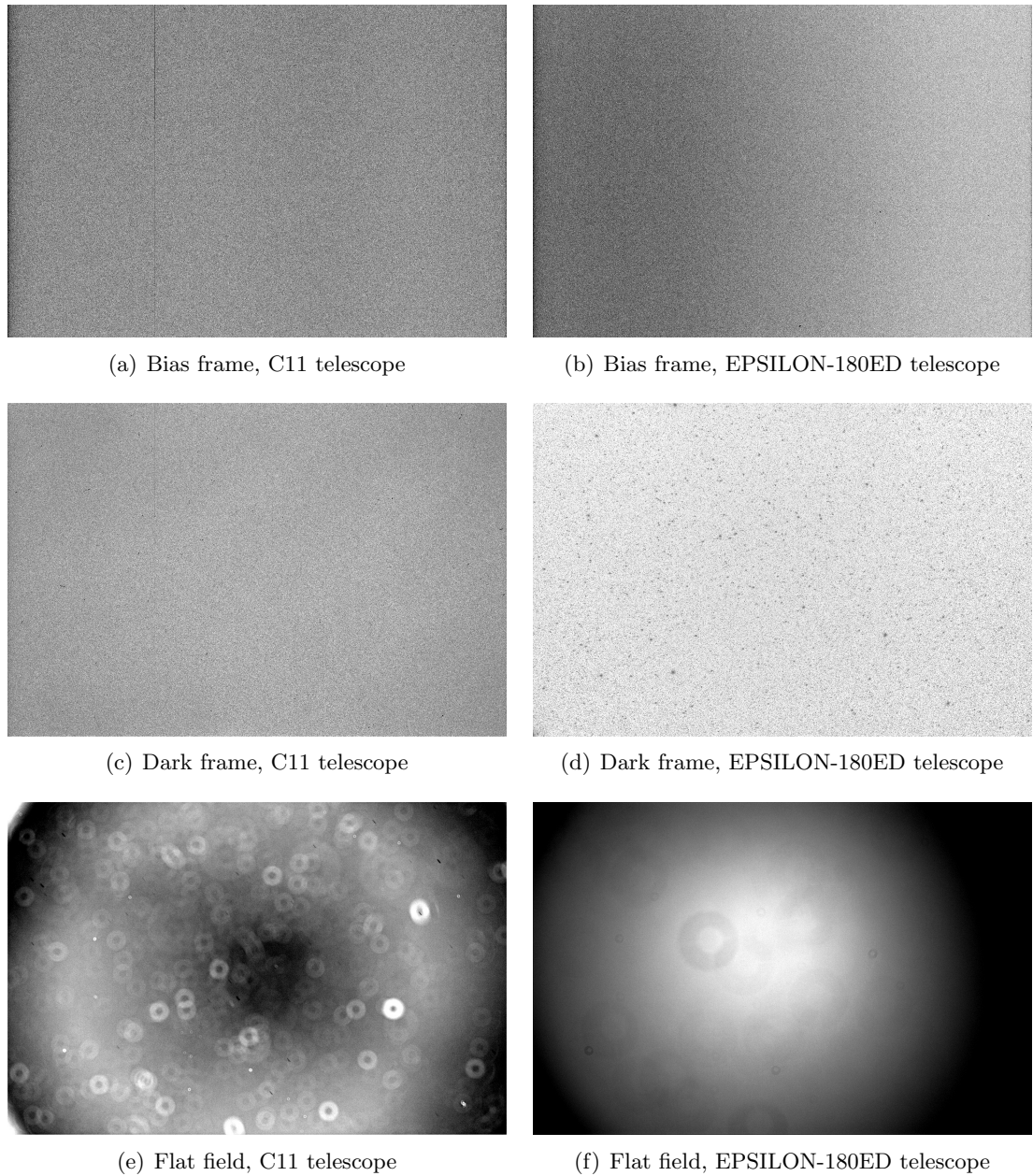
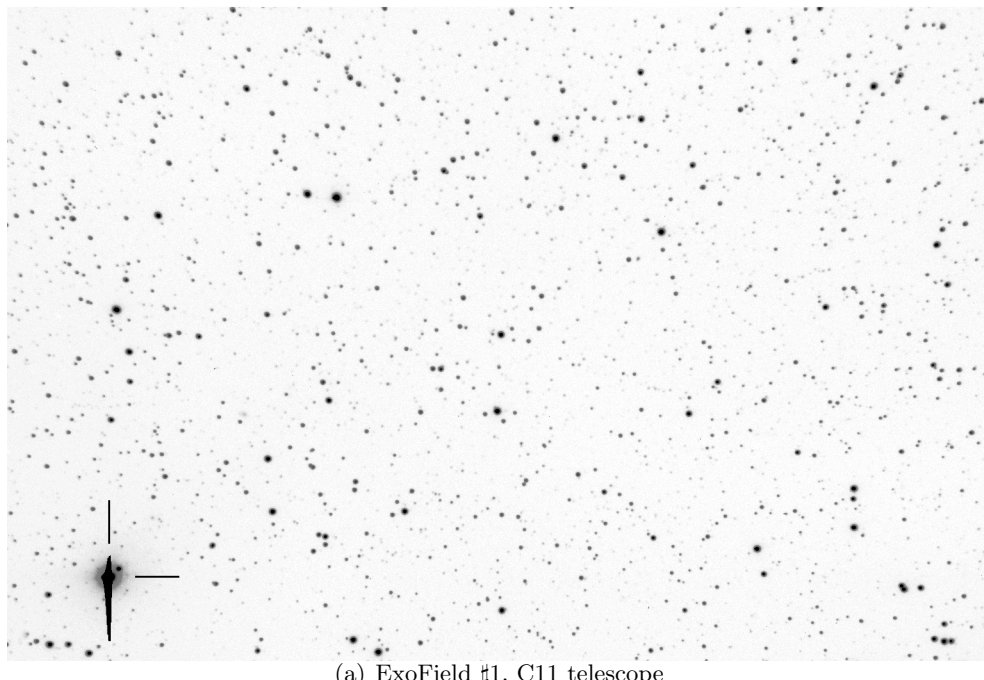
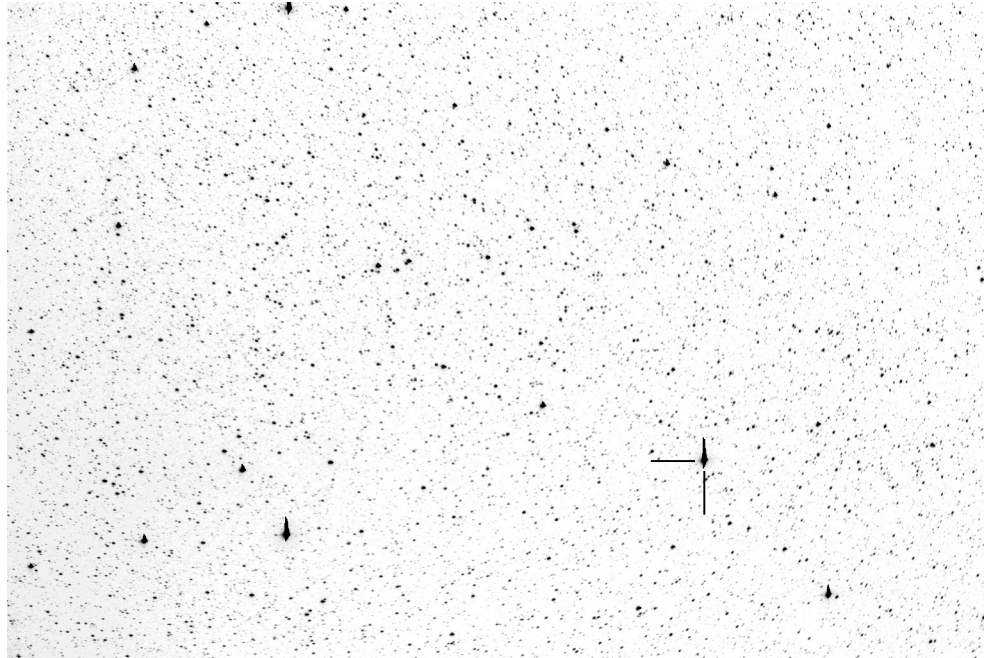


Figure 4.4.3: Typical calibration frames acquired with both telescopes. Obviously bias and dark frame parameters depend only on the camera configuration.

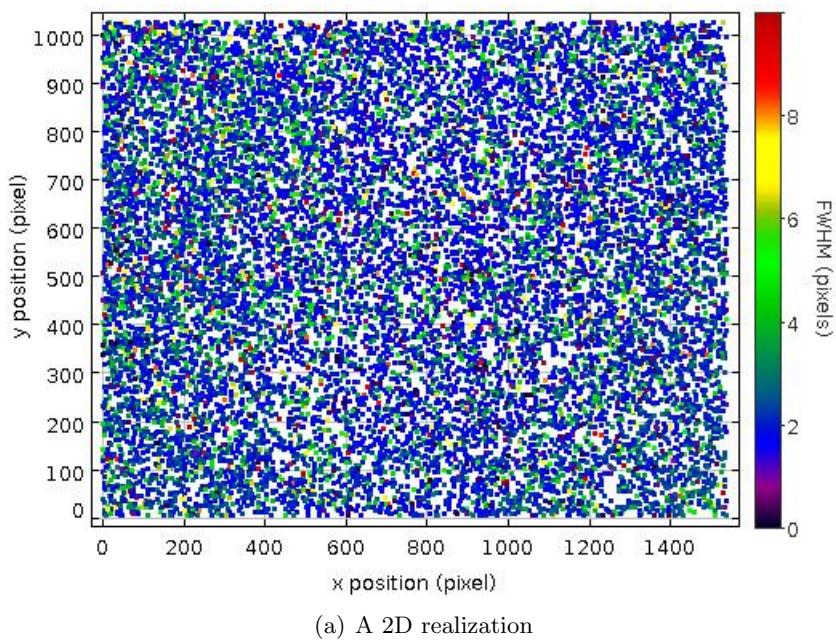


(a) ExoField #1, C11 telescope

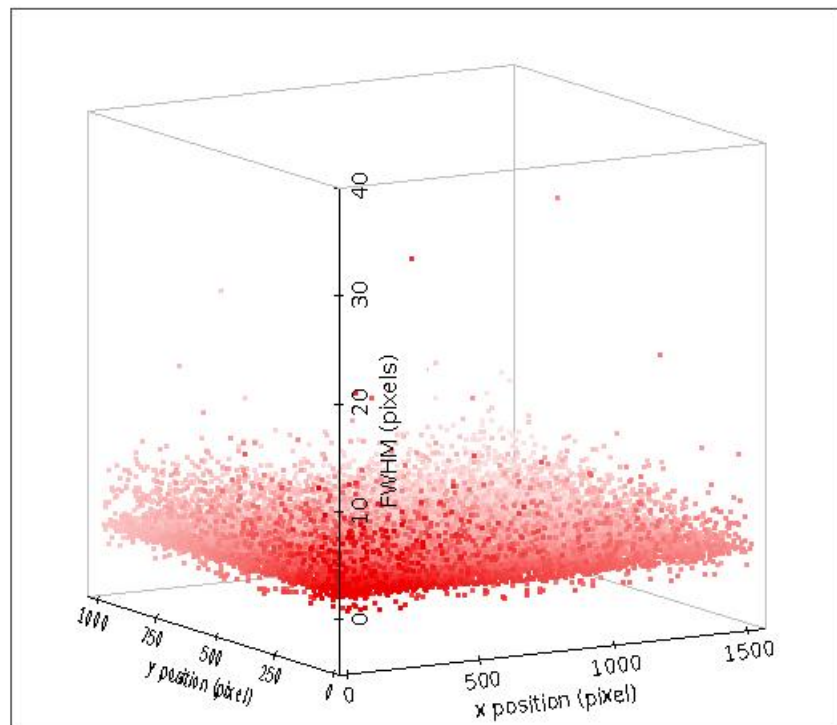


(b) ExoField #1, EPSILON-180ED telescope

Figure 4.4.4: Images of ExoField #1 using both telescopes.
The same star is marked for a comparison of the fields of view.



(a) A 2D realization



(b) A 3D realization

Figure 4.4.5: FWHM of the PSFs along the x and y axis of the CCD array, using the EPSILON-180ED telescope.

Data Reduction and Analysis

”No more fiction for us: we calculate; but that we may calculate, we had to make fiction first.”

-Friedrich Nietzsche
in *Number: The Language of Science*, Tobias Dantzig

5.1 Introduction

THE primary aim of CCD data reduction is to eliminate any effects that depend on the nature of the detector and telescope –’the instrumental signature’. These effects have to be accounted for, prior to any scientific interpretation of the images. Conventional image reduction is based on three types of calibration frames, namely bias, dark and flat frames, and of course the raw images of the object under investigation.

Then follows the analysis step. After the images are corrected for instrumental effects, the light curves are plotted and examined. The remaining errors are due to various noise sources that will be discussed below. High amplitude variability is easier, than low, to be spotted. The task of post-reduction analysis is aimed towards eliminating the remaining errors.

5.2 Outline of the Reduction Scheme

This section elaborates on generic CCD data reduction. Below are the basic steps that one needs to take in order to extract valid information from raw CCD images.

- Step 1 Raw image reduction
- Step 2 Photometry
- Step 3 Image centering
- Step 4 Light curve plotting
- Step 5 Post-reduction analysis and statistics

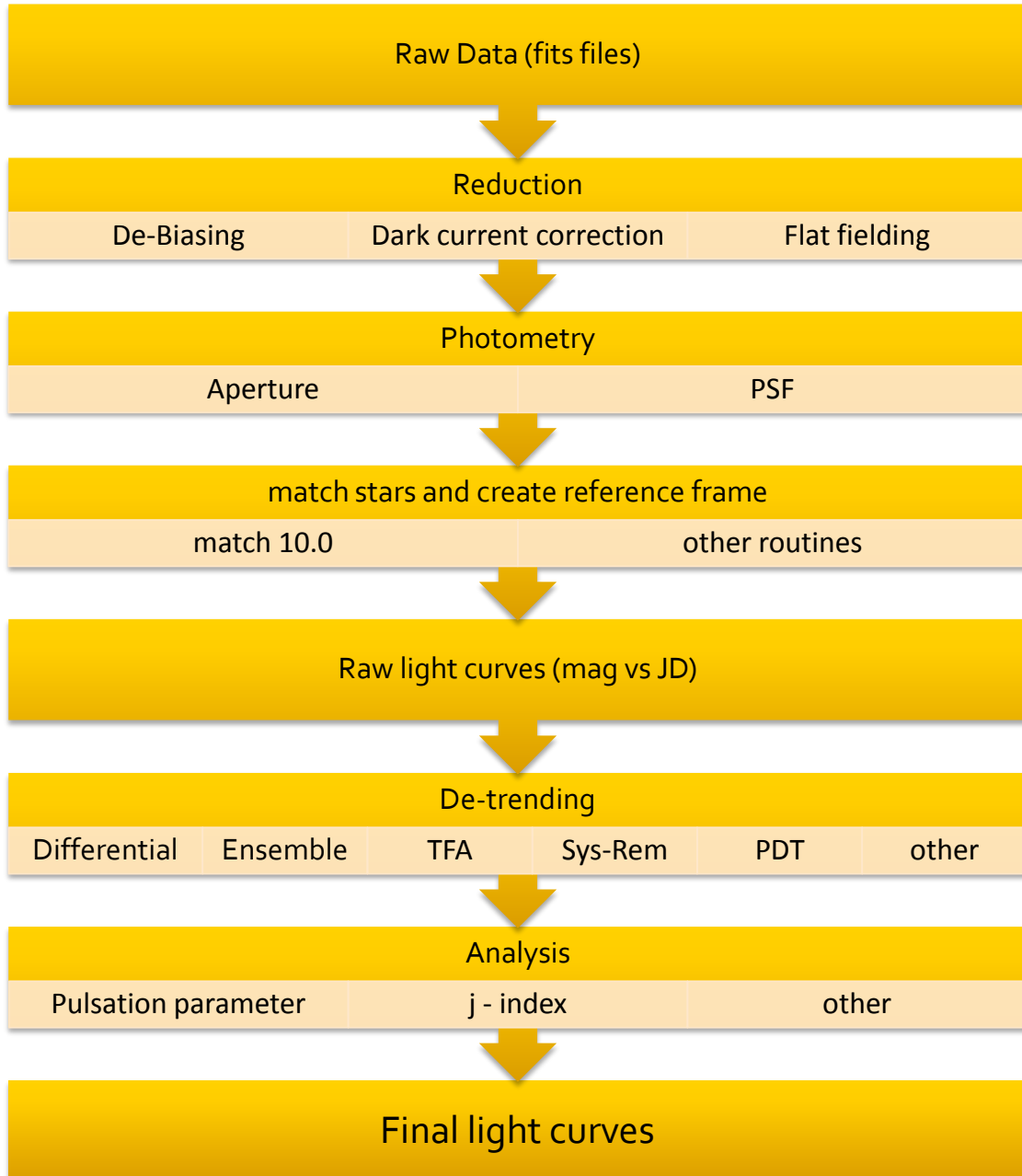


Figure 5.2.1: A road map of CCD photometry. Above are the steps one has to take in order to arrive to light curves of variable stars or any other object that will be of any astronomical interest.

5.2.1 De-Biasing

During the digitization process the A/D converter assigns a number of ADUs to each pixel proportional to the number of photoelectrons it accumulated in the integration phase. In a simple zero exposure time readout, there should be no photoelectrons present in any pixel except for those that are due to intrinsic noise. In a situation like this the A/D converter assigns a random number in a random manner that centers around zero. But negative numbers are not preferred due to practical problems, e.g memory consumption (a bit must play the role of a negative or positive sign). To address this problem the A/D converter, introduces a certain level of ADUs to each pixel even if there are no photoelectrons present. This number is the bias level of each pixel. It still remains random but it is never negative. A manifestation of this fact is presented in every linearity curve for CCD cameras. The curve never crosses the zero of the ADUs axis, it always has an offset. This is the bias level of the camera.

The bias level adds "extra luminosity" to our astronomical images, so stars appear brighter than they actually are. De-biasing is the procedure to remove this offset. By obtaining a certain number of bias frames, namely zero exposure images, and averaging them one can calculate the master bias frame. A master bias is used in order to have better statistical results. Then a simple subtraction from each target image will yield bias corrected images that do not suffer from this effect.

5.2.2 Dark Current Correction

According to semi-conductor physics, electrons have the tendency to escape from the valence band of the materials at temperatures above absolute zero. In case of that event these free electron will be collected into the potential wells of the pixels within the CCD array. Thermal electrons are indistinguishable from real photoelectrons coming from astronomical sources. The amount of that kind of free electrons strongly depends on temperature. Every 5-6 degrees (centigrade or Kelvin) the noise due to thermal electrons doubles. Therefore, some kind of cooling of the camera is needed. Widely used methods are thermoelectric cooling (Peltier cooling) or the use of liquid nitrogen.

The noise added to the signal due to thermal electrons is proportional to the square root of the dark current, this is because dark noise follows Poisson statistics (see section Signal-to-Noise Ratio).

Cooling the CCD camera can only reduce the dark noise level. For reliable photometric results one needs to correct the data frames for dark current. A technique to do that is to obtain a frame with exposure time equal or, bigger than that of the data frames (e.g 15-30min or more). This is done with the telescope sealed and the dome closed. After that the unitary dark frame is created by dividing the ADUs by the exposure time of the dark frame. For better statistics one can acquire a series of dark frames, create the unitary darks and combine them to create the master dark frame. Then the master dark is multiplied with the exposure time of the data frames and subtracted from them. If one chooses the exposure time of the dark frame to be equal to the exposure time of the data frames, then the creation of the unitary dark can be omitted. A simple subtraction will suffice. I have chosen the former technique that guarantees better results.

5.2.3 Flat-Fielding

The issue of flat-fielding can either end up as a happy, or as a really sad story. The pixels that consist an array do not respond to light with the same way. The aim of flat-fielding is to correct the data frames for this effect.

The basic concept behind flat-fielding is simple. Since neighboring pixels have slightly different values of QE and gain, one has to acquire an evenly illuminated image of a

”spectrally flat” target. The latter means that the target has to radiate evenly across the spectrum. After obtaining the flat-field, a simple division of the data frames with the flat-field will yield an image free of intra-pixel variations. Flat-fields can either be sky images just before sunrise or just after sunset, when no stars are visible called sky-flats or images of a light source inside the dome that has the above properties, in this case they are called dome-flats. All the above alternatives provide a calibration image with high signal-to-noise ratio. For even better results and better statistical distribution of errors, one should acquire a series of flat fields and average or median combine them to a master flat. If the observations are carried out using filters, the above process has to be repeated for each filter used separately. Dark current correction is applied to the flat-fields also.

After some practice and data reduction the user understands the importance of good flat-fields, he also sees that perfect flats is a utopia. In our survey we used a screen-type device, we constructed ourselves taking into account all the above considerations.

5.2.4 Photometry

This is eventually the goal of the process described above. The products of photometry are the raw light curves. Light variations can reveal many properties of the objects in study. Some processes though, are difficult to unveil due to the really small changes of intensity they introduce to the light curves e.g extra-solar planetary transits. This is where post-reduction analysis enters.

An extensive review of the reduction and analysis pipeline can be found in section 5.5.

5.3 De-Trending the Time Series

After the photometry step stars suffer from noise. In this work we have been using commercial telescopes of small aperture. This fact enables us to have a large field of view (FOV) but degrades the overall image quality by lowering the S/N ratio and introducing noise to the time series. Other effects as non-uniform illumination, differential extinction, vibrations, guiding errors and local weather changes that affect clusters of stars within the field also influence the data. Such noise sources that act on localized scale are collectively referred to as *trends*. In contrast to trends there is also *Poisson noise*, *shot* or *white noise* which behaves in a random manner (see section 4.4.2).

Improvement of the S/N ratio is of crucial importance to the success of a wide-field survey and therefore these noise sources have to be eliminated or at least minimized. A first strategy in order to tackle this problem is differential photometry. According to this a selection of template stars, has to be made. For large FOV surveys this selection poses limitations. Different parts of the image suffer from different trends of different ”magnitude”. The probability of selecting intrinsic variable stars as templates is high and this could undermine the detectability of real variable signals.

In this thesis I have chosen to use the Trend Filtering Algorithm (TFA) [18] in order to minimize noise within the time series. A coherent description of TFA is presented below.

5.3.1 The Trend Filtering Algorithm

The purpose of application of the TFA algorithm [18] is the removal of trends that affect the data series and decrease the possibility of detecting low-amplitude variability. The idea behind the TFA algorithm is that in a large data set there exist many stars that suffer from the same trends. Having this fact in mind, one has to select a representative template (base) set and create a linear combination of them. Then a subtraction of the linear combination from the non-template light curves (targets) has to be performed.

Let all time series in our data set be sampled in the same moments and contain the same number of data points N . The TFA algorithm creates a filter using a number of M template light curves. The filter $\{F(i); i = 1, 2, \dots, N\}$ is the linear combination of the template light curves $\{X_j(i); i = 1, 2, \dots, N; j = 1, 2, \dots, M\}$

$$F(i) = \sum_{j=1}^M c_j X_j(i) \quad (5.3.1)$$

Letting $\{Y(i); i = 1, 2, \dots, N\}$ be the target time series and after having all template light curves zero averaged, the coefficients c_j are deduced by minimizing the D parameter, defined as follows

$$D = \sum_{j=1}^N [Y(j) - A(j) - F(j)]^2 \quad (5.3.2)$$

where $\{A(i); i = 1, 2, \dots, N\}$ is the current best estimate of the de-trended light curve. In the current application of the TFA algorithm there is no *a priori* knowledge of any periodic or aperiodic signal that might be present in the light curve. Hence we take $A(i)$ to be constant and equal to the mean magnitude of the time series. Since target light curves are also zero averaged the value of $A(i)$ is zero.

The expression

$$\sigma^2 = \frac{D}{(N - M)} \quad (5.3.3)$$

yields the estimated variance of noise level of the filtered data.

The stages of TFA application are

1. Zero averaging of all target light curves
2. Selection of M template light curves with as wide distribution, within the field, as possible. In order to meet this requirement in this thesis, I have selected the 20 brightest stars with pulsation parameters below 0.4.
3. Zero averaging of all template light curves
4. Calculate normal matrix from the template time series

$$g_{j,k} = \sum_{i=1}^N X_j(i) X_k(i) \quad \text{where } j, k = 1, 2, \dots, M \quad (5.3.4)$$

and compute the inverse of it, $G_{j,k}$

5. Compute the scalar products of target and the template time series

$$h_j = \sum_{i=1}^N Y(i) X_j(i) \quad (5.3.5)$$

for every light curve in the data set

6. Calculation of the solution for c_j

$$c_j = \sum_{i=1}^M G_{j,k} h_k \quad (5.3.6)$$

7. Arrive to the corrected time series Υ_i by

$$\Upsilon_i = Y_i - \sum_{k=1}^M c_j X_j(i) \quad (5.3.7)$$

5.4 Variability Criteria

The relatively large number of detected stars (12 790, see section 6.2) in our field calls for a robust, efficient and reliable variability determination index. Such indices are the j-index introduced by P. Stetson in [40] and modified according to [44]. Another variability measure we used is the pulsation parameter [42]. Both variability indicators are discussed below.

5.4.1 The j-index

The j-index is introduced in [40]. According to it, every star in our sample is assigned with a j-index as defined by

$$j = \frac{\sum_{k=1}^n w_k sgn(P_k) \sqrt{|P_k|}}{\sum_{k=1}^n w_k} \quad (5.4.1)$$

where k denotes a pair of consecutive observations, each given a weight w_k and a

$$P_k = \begin{cases} \delta_{i(k)} \delta_{j(k)}, & \text{if } i_k \neq j_k \\ \delta_{i(k)}^2 - 1, & \text{if } i_k = j_k \end{cases} \quad (5.4.2)$$

where $\delta_{i(k)}$ and $\delta_{j(k)}$

$$\delta = \sqrt{\frac{n}{n-1}} \frac{v - \bar{v}}{\sigma_v} \quad (5.4.3)$$

are the residuals of normalized magnitudes from the mean magnitude of all data points for observations i and j within the pair k . The weights are defined by

$$w_k = e^{\frac{\Delta t_k}{\Delta t}} \quad (5.4.4)$$

where Δt_k is the time interval between the observations of a given pair and Δt is the mean value for the n pairs. In our work the weights were taken to be unity, since the time intervals between the data points are constant. Finally, the definition of the sgn function is

$$sgn(x) = \begin{cases} -1, & \text{if } x < 0 \\ 0, & \text{if } x = 0 \\ 1, & \text{if } x > 0 \end{cases} \quad (5.4.5)$$

In a time series that consists of magnitude pairs that are affected only by random noise, the expected value of $\langle \delta_{i(k)} \delta_{j(k)} \rangle$, within a given pair k , is zero. Hence j-index should tend to zero for a non-variable star while it should tend to a positive value for a variable one.

After the calculation and the assignment of a j-index to each star we plot a j-index against magnitude graph. By selecting a limiting value above which a star is considered a physical variable the light curves can be examined in order to establish the variability.

5.4.2 Pulsation parameter

The pulsation parameter is another method one can implement in order to search for variable star signals within a data set [42]. It is defined as the *standard deviation*, σ of a given time series

$$\sigma = \sqrt{\frac{1}{n} \sum_{i=1}^n (m_i - \bar{m})^2} \quad (5.4.6)$$

over the inner pulsation index, σ_{inner} which is defined as

$$\sigma_{inner} = \sqrt{\frac{1}{2(n-1)} \sum_{i=1}^{n-1} (m_i - \bar{m})^2} \quad (5.4.7)$$

In all the above expressions n is the number of data points (exposures), m_i is the magnitude of a star in a given exposure i and \bar{m} in the mean magnitude in n exposures. The inner pulsation index is a measure of point-to-point magnitude variation within the data set.

Finally we arrive to the definition of the pulsation parameter

$$P = \frac{\sigma}{\sigma_{inner}} \quad (5.4.8)$$

which is the measure of variability. Stars exhibiting high P values are likely to be physical variable stars.

5.5 ThReT Reduction & Analysis Pipeline

In this section I will give a complete description of the pipeline used during the course of this diploma thesis.

The ThReT (Thessaloniki Research for Transits) reduction pipeline is written by I. Antoniadis, former colleague and now PhD student at MPIfR. It consists of a series of C-shell scripts and FORTRAN routines that perform the calculations. The necessary changes have been done in order for the pipeline to run properly with the new data sets, obtained using different instruments. Changes have also been done as a new variability index has been implemented (j-index, see section 5.5.1).

The structure of the pipeline is sketched in Figure 5.6.2. The primary use of the first script, namely *threat.csh* is to initialize all necessary variables and STARLINK itself. All initial reduction steps are performed using the STARLINK routines CONVERT [7], EXTRACTOR (*Chipperfield & Draper 2004*), FIGARO [38] and KAPPA [8]. During this phase all images (.fit files) are converted to the STARLINK accepted format, the *sdf*. The second step is the combination and creation of the master frames, namely *master dark*, *master flat* and *master bias*. The calibration of science frames is done next according to the steps described in section 5.2.

After the calibration of data frames the *allstar.csh* script initiates DAOPHOT II: The next generation, written by Peter Stetson (DAO), for photometry. In order for the program to run properly a number of parameters has to be specified. Crucial parameters are the readout noise, gain and maximum and minimum good data values to determine the saturation level of the images, etc. The user selects whether aperture or PSF photometry will be performed. In this script photometric annuli are also selected. In the case of Holomon survey data, we have used aperture photometry due to the fact that ExoField #1 is moderately crowded and the PSF photometry is a much more CPU-time consuming procedure which, in our case, yields results comparable to those of aperture photometry.

Aperture photometry parameters

In July 2009 we have obtained approximately 2000 scientific frames during 15 nights of observation. The frames contain 12 790, at a 3.5σ detection level, stars and typically the FWHM of a stellar point spread function is 4 pixels. Therefore a series of apertures, ranging from 0.5 to 9 pixels, are used to determine the stellar flux by DAOPHOT II. Two more apertures, an inner of 10 pixels and an outer of 15 pixels, are used for the

determination of the sky background contribution. The apertures used are:

```
A1 =0.5
A2 =1.5
A3 =2
A4 =3
A5 =4
A6 =6
A7 =8
A8 =9
IS =10
OS =15
```

where the radii are given in pixels around the center of each stellar PSF.

The next step is light curve generation. The Julian Date (JD) and air mass are calculated by *timer.csh* given the data taken from the header of the original .fit files. The *ref.csh* script creates the reference frame, that is a list of all stars in the frame along with their X and Y positions, in pixels. Then *matcher.csh* uses the MATCH routine in order to identify and match all stars in each individual frame. Finally *curver.csh* creates the light curve files. An ASCII file is generated for each star containing the JD the instrumental magnitude along with its extracted error and the air mass. Light curve files have the extension .curve, and can easily be plotted using gnuplot or any other plotting program.

Initial statistics of our sample are calculated in *sigma.csh*. The output of this script is the file sigmaplot.txt that contains the mean instrumental magnitude, sigma, inner pulsation index, pulsation parameter, the rms error, the logarithm of the rms error, the j-index and the ID number of each light curve. This stage is important in order for the user to be able to select template stars for the de-trending stage as well as for having a first impression of the photometric quality of the data set.

The de-trending procedure follows with the application of the TFA algorithm. The script *tfa.csh* follows the steps described in a previous section (see 5.3.1). At this stage the user defines the criteria according to which the selection of template light curves will be done. One can chose among the brightest stars that display a pulsation parameter or a j-index value below a certain threshold, or any other desired combination. All the calculations are performed by the fortran routines shown in Figure 5.6.1.

The interested reader may refer to [1] for a concise introduction to the ThReT reduction & analysis pipeline.

5.6 Astrometric Calibration

This step is essential in order to deduce the positions of the stars in the image. The astrometric calibration was performed using the GAIA [10] program within the STAR-LINK suite. After loading the desired image I have chosen to automatically match the star positions. The path to this utility is, Image–Analysis → Astrometry Calibration → Automatic Position Matching → Simple. Then the program automatically obtains the RA and DEC of the image center from the header file and provided the image scale (5.0 worked best in our case) it calculates the positions of the stars within the image. The catalogue I have used is the USNO at ESO.

To test the quality of the astrometric solution, one can overplot the entries of a given catalogue on the original image. Another test is to compare the positions of characteristic stars within the field with those provided by the Digitized Sky Survey (DSS)¹. I have

¹<http://archive.eso.org/dss/dss>

performed both checks using the Aladin [4] software package to visualize the catalogue data and SIMBAD to overplot 1006 objects in a radius of 2.208° from the image center. After the above checks I found the accuracy obtained, using the method described, to be very reliable.

I have used the Virtual Observatory (VO) utilities, namely TOPCAT² and Aladin, to compile a catalogue of the stars in ExoField #1 and cross-matched the output files of EXTRACTOR and ref.csh, *test.cat* and *referance* respectively. The test.cat file contains the X and Y position of each star (in pixels) along with their Right Ascension and Declination in degrees. The referance file contains the ID and the X and Y position of each star as well. After the matching procedure the output catalogue contains the X and Y position of each star along with its RA and DEC. A table with the positions of variable stars within ExoField#1 can be found in section 6.2.1.

A sample .fit image header is shown below.

```
FITS headers in thret--1537.fit:
SIMPLE = T
BITPIX = 16 /8 unsigned int, 16 & 32 int, -32 & -64 real
NAXIS = 2 /number of axes
NAXIS1 = 1536 /fastest changing axis
NAXIS2 = 1024 /next to fastest changing axis
BSCALE = 1.0000000000000000 /physical = BZERO + BSCALE*array_value
BZERO = 32768.000000000000 /physical = BZERO + BSCALE*array_value
INSTRUME= 'Finger Lakes' / instrument or camera used
DATE-OBS= '2009-07-22' / YYYY-MM-DDThh:mm:ss observation start, UT
TIME-OBS= '21:13:18' / HH:MM:SS observation start time, UT
EXPTIME = 60.00000000000000 /Exposure time in seconds
EXPOSURE= 60.00000000000000 /Exposure time in seconds
SET-TEMP= -33.00000000000000 /CCD temperature setpoint in C
CCD-TEMP= -33.268891632556915 /CCD temperature at start of exposure in C
XPIXSZ = 18.00000000000000 /Pixel Width in microns (after binning)
YPIXSZ = 18.00000000000000 /Pixel Height in microns (after binning)
XBINNING= 2 /Binning factor in width
YBINNING= 2 /Binning factor in height
XORGSUBF= 0 /Subframe X position in binned pixels
YORGSUBF= 0 /Subframe Y position in binned pixels
IMAGETYP= 'Light Frame' / Type of image
OBJCTRA = '22 49 21' / Nominal Right Ascension of center of image
OBJCTDEC= '+45 11 13' / Nominal Declination of center of image
OBJCTALT= ' 47.1273' / Nominal altitude of center of image
OBJCTAZ = ' 63.1250' / Nominal azimuth of center of image
OBJCTHA = '-3.9626' / Nominal hour angle of center of image
SITELAT = '40 25 58' / Latitude of the imaging location
SITELONG= '23 30 20' / Longitude of the imaging location
TRAKTIME= 2.0000000000000000 /Exposure time used for autoguiding
FOCALLEN= 0.0000000000000000 /Focal length of telescope in mm
APTDIA = 0.0000000000000000 /Aperture diameter of telescope in mm
APTAREA = 0.0000000000000000 /Aperture area of telescope in mm^2
```

²<http://www.star.bris.ac.uk/~mbt/topcat/>

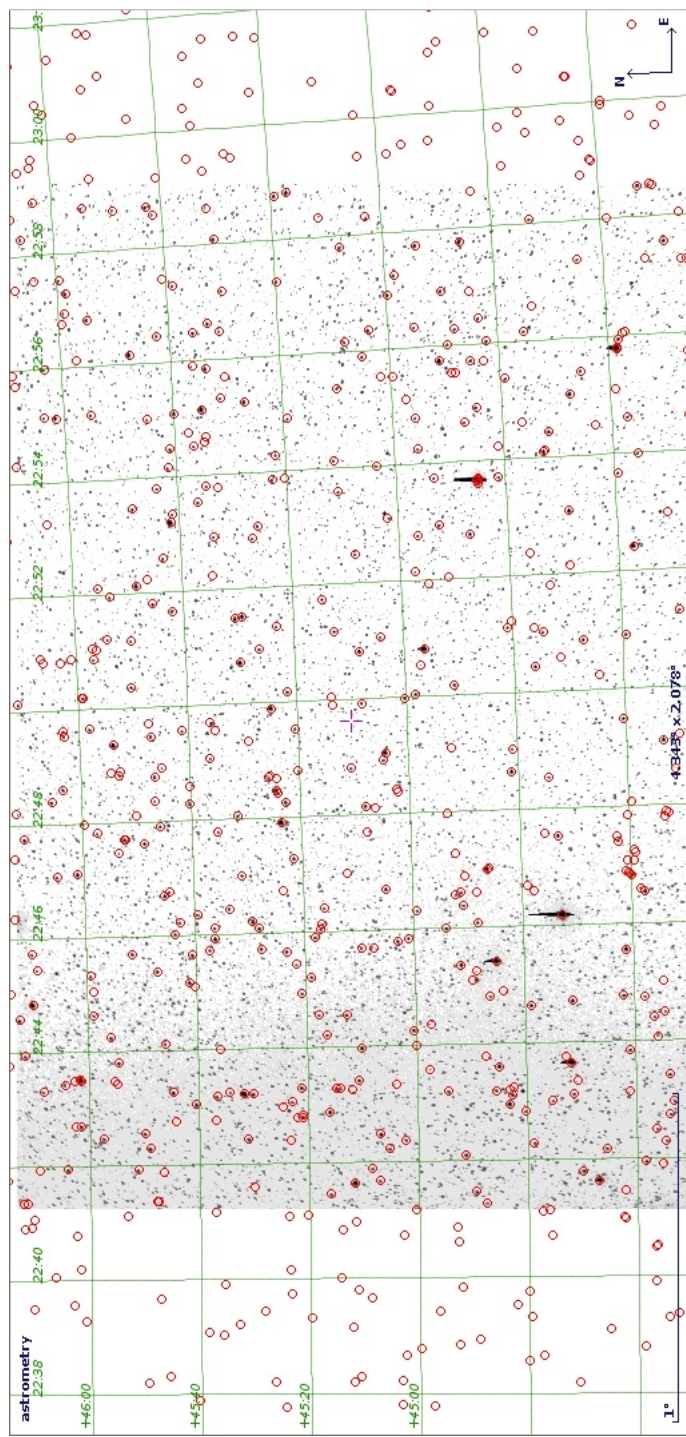


Figure 5.6.1: 1006 SIMBAD objects, within a radius of 2.208° from the image center, overplotted on ExoField #1.

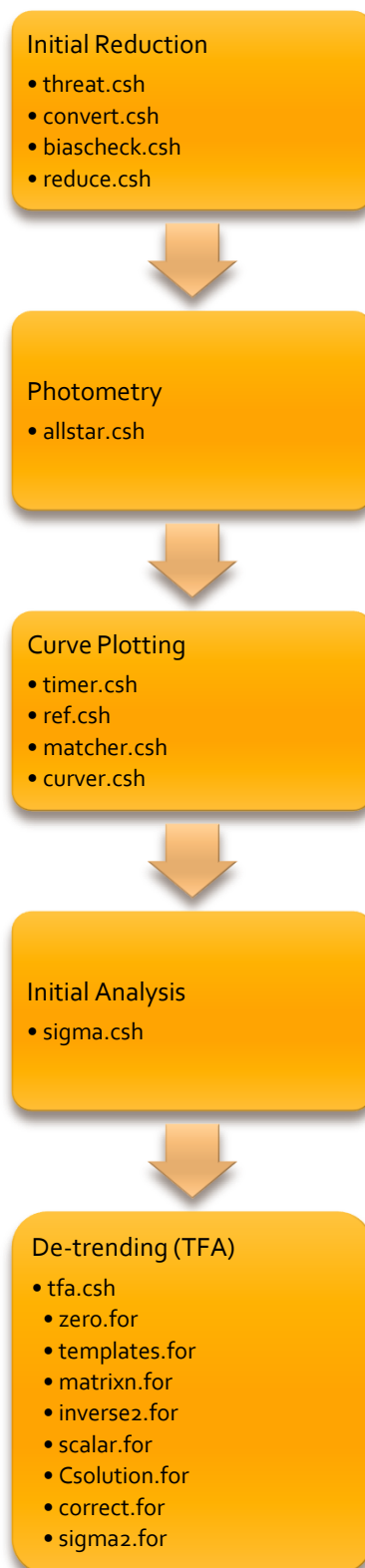


Figure 5.6.2: The structure of ThReT reduction and analysis pipeline.

6

Results and Discussion

”Data in isolation are meaningless, a collection of numbers. Only in context of a theory do they assume significance...”

-George Greenstein, *Frozen star*

6.1 Introduction

In this chapter I will present the results of our observations during July 2009. Due to guiding problems and mainly bad weather conditions only the observations of 24 July 2009 were analyzed yielding interesting results.

In the following pages I present the light curves of those stars that display the higher j-index and pulsation parameter values. Every light curve is associated with an ID number. A table with the each star's ID and its coordinates is also provided. Finally I present the results from a multi-object query to the SIMBAD Astronomical Database.

As an ending remark, I chose to discuss some thoughts and potential additions to the data reduction and analysis pipeline.

6.2 The observations of 24 July 2009

The data set of 24 July 2009 consists of 258 science frames of the ExoField #1 (image center $\alpha: 22^h 53^m 40^s$, $\delta: +44^\circ 44' 55''$) of binning 2, along with a set of calibration frames, namely 2 dark frames of 10 min and 30 min exposures, 60 bias frames and 7 flat frames obtained with a light box to avoid a shutter effect that is present in sky-flats of lower exposure times. Each science frame contains 12 790 stars, at a 3.5σ detection threshold, which we examine for indications of variability. In the process of identifying variables it is necessary to eliminate stars that are poorly sampled. This might be due to, cloud passing, blending, saturation etc. As a result only stars with more than 30 data points were accepted for further analysis.

The observations were carried out using the Finger Lakes KAF-6303 CCD camera and the Takahashi EPSILON-180ED astrograph. This combination offers a wide field of view ($3.122^\circ \times 2.083^\circ$) but has the disadvantage of delivering stars with very narrow PSFs, of the order of 4 pixels. This turned out to be a major drawback during photometry. Many consecutive analysis attempts were made, as such.

After the application of TFA algorithm the light curves were zero averaged, as a result the information of mean instrumental magnitude is lost (though not permanently) and the stars fluctuate about zero magnitude. Selection criteria have been implemented in order to flag potential variable stars, namely j-index above 0.6 and pulsation parameter above

2.5. For this reason two subgroups of 3.5σ and 7σ deviation have been defined for j-index and pulsation parameter values respectively (see Figures 6.2.4 and 6.2.6). These subgroups correspond to the threshold values and constitute an acceptable trade-off between the bulk of light curves and true variability.

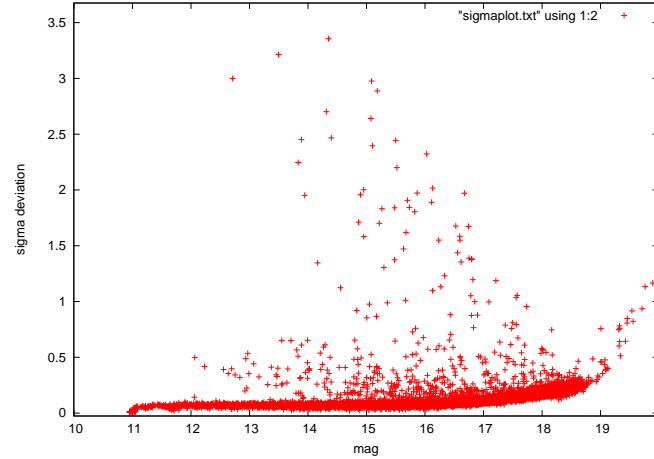


Figure 6.2.1: Standard deviation versus magnitude plot for the 24/07/2009 data prior to the application of the TFA algorithm.

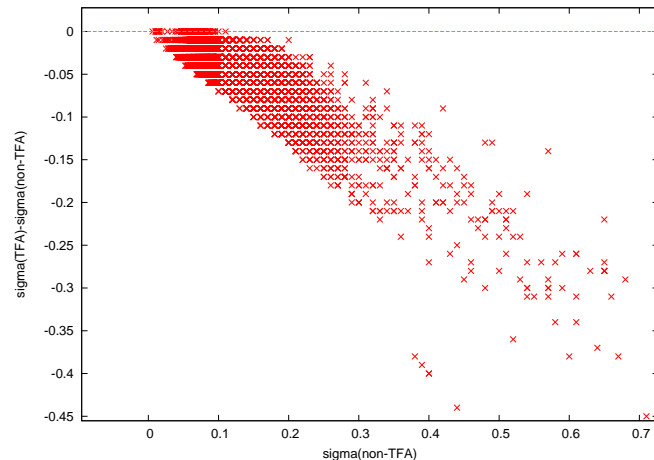


Figure 6.2.2: $\delta\sigma$ versus $\sigma_{\text{non-TFA}}$ plot for the 24/07/2009 data. The decrease of the standard deviation is prominent due to the application of the TFA algorithm. The zero correction level is visible using the horizontal line.

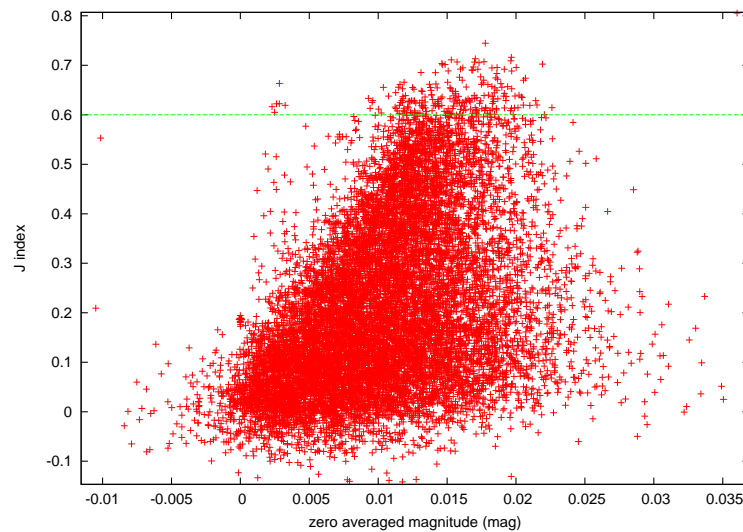


Figure 6.2.3: Distribution of variability index j for the stars in ExoField #1. A limiting value of 0.6 is selected.

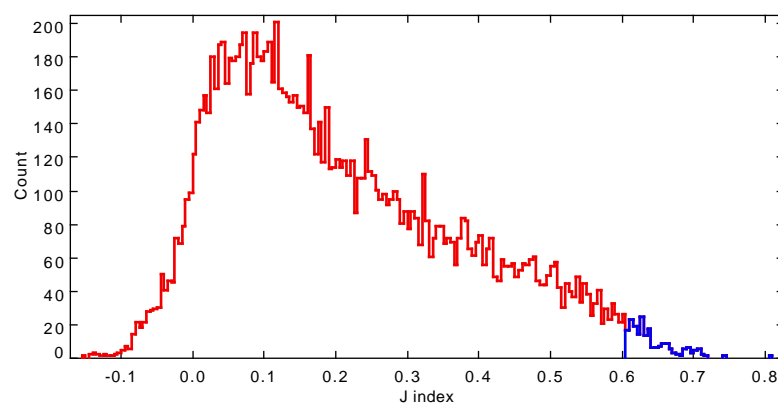


Figure 6.2.4: Histogram of j -index values of the stars within the field. A 3.5σ deviation subset is defined.

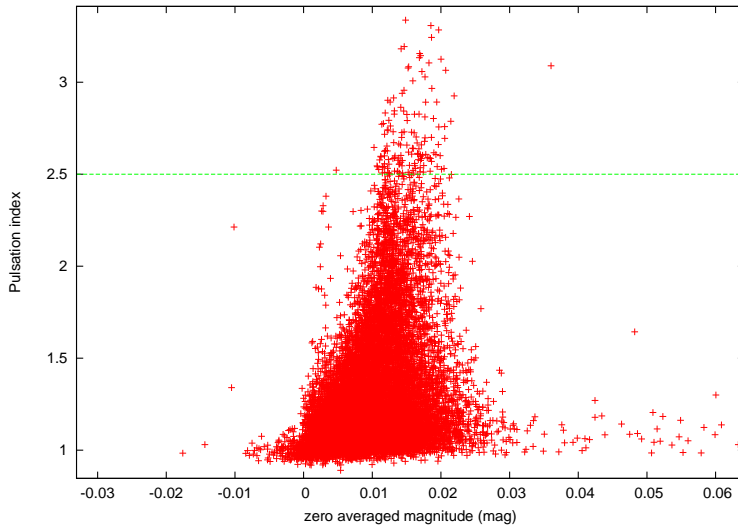


Figure 6.2.5: Distribution of the pulsation index in ExoField #1. A limiting value of 2.5 is selected.

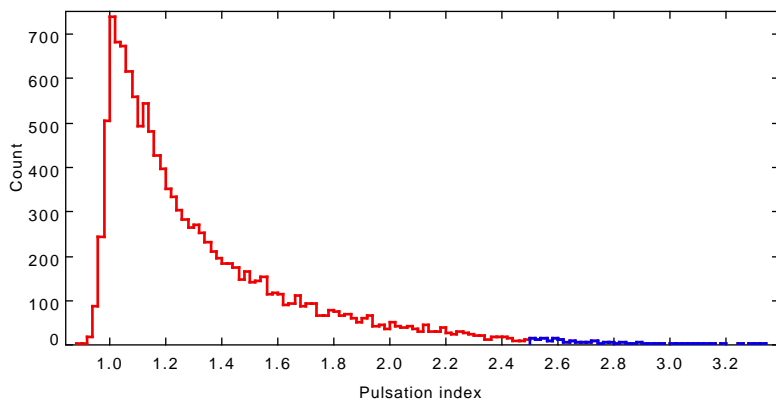
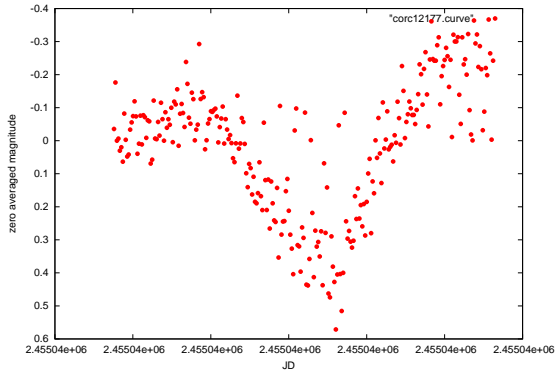


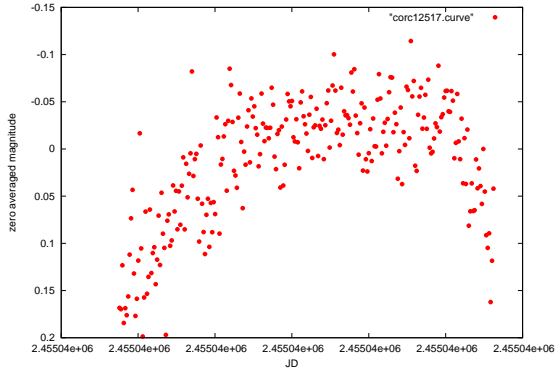
Figure 6.2.6: Histogram of pulsation parameter values of the stars within the field. A 7σ deviation subset is defined.

6.2.1 Light Curves of Variable Stars within ExoField #1

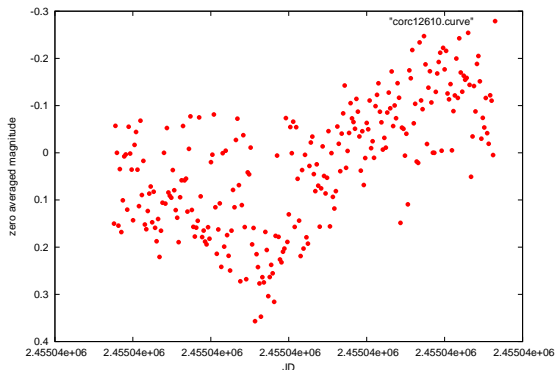
In this section I present the 21 light curves of the stars that can be considered variables according to the selection criteria discussed in previous sections. I have selected limiting values of 0.6 and 2.5, for the j-index and pulsation parameter respectively. Any light curve with j-index and pulsation parameter above the corresponding threshold was inspected visually.



(a) Star ID 12177

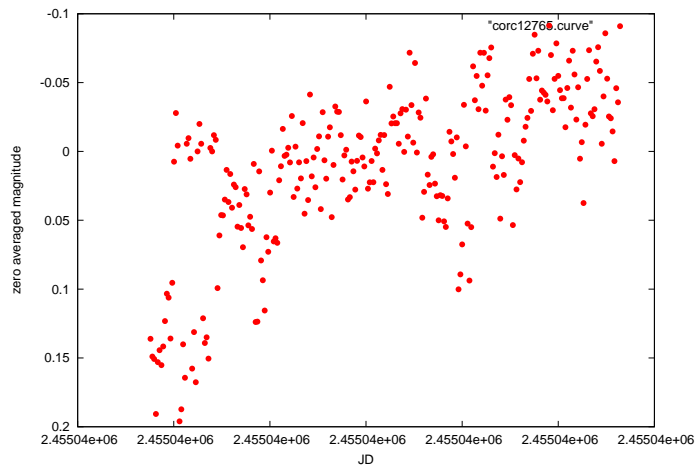


(b) Star ID 12517

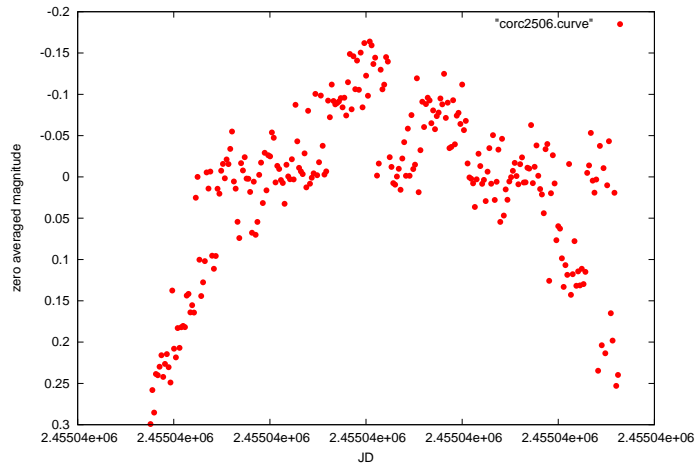


(c) Star ID 12610

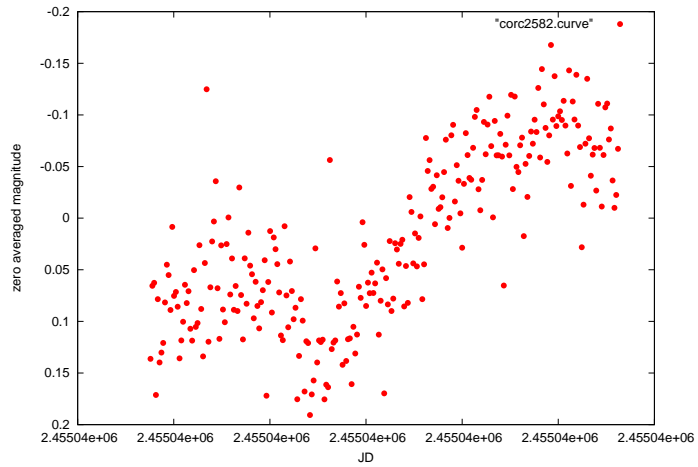
Figure 6.2.7: Light curves



(a) Star ID 12765

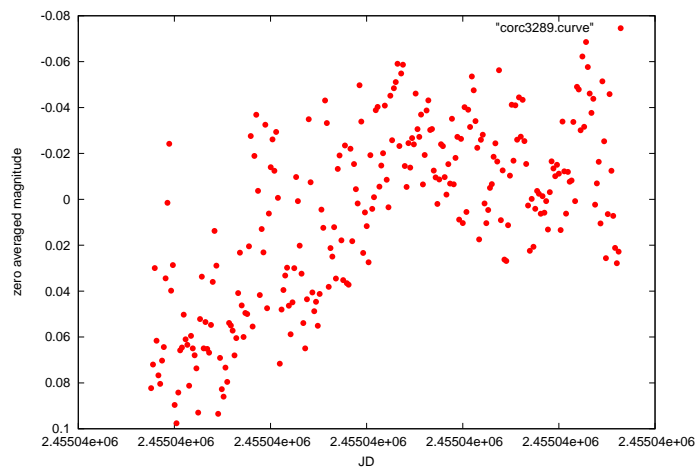


(b) Star ID 2506

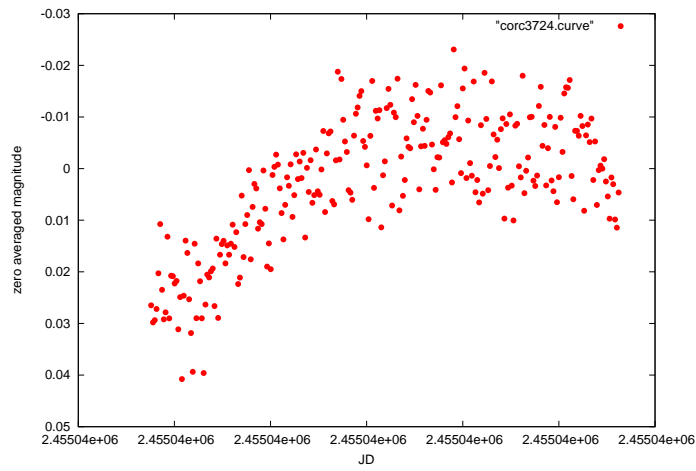


(c) Star ID 2582

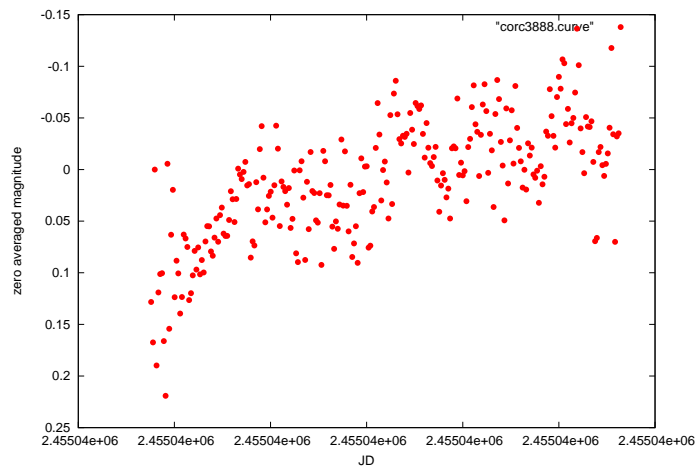
Figure 6.2.8: Light curves



(a) Star ID 3289

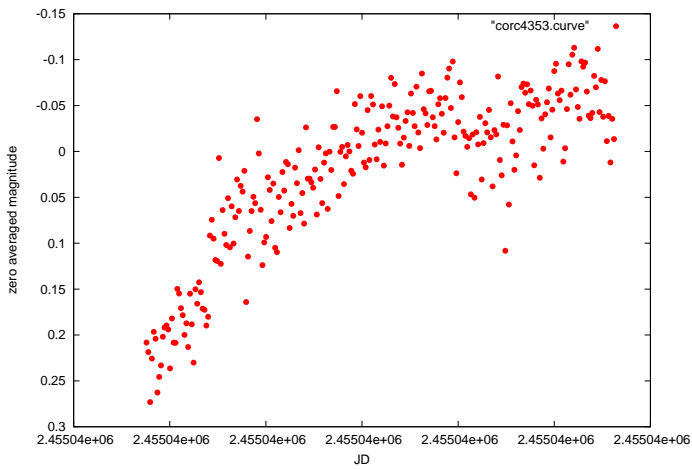


(b) Star ID 3724

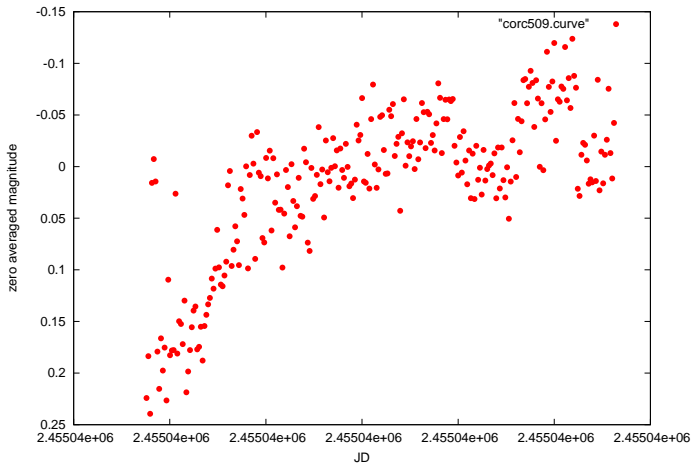


(c) Star ID 3888

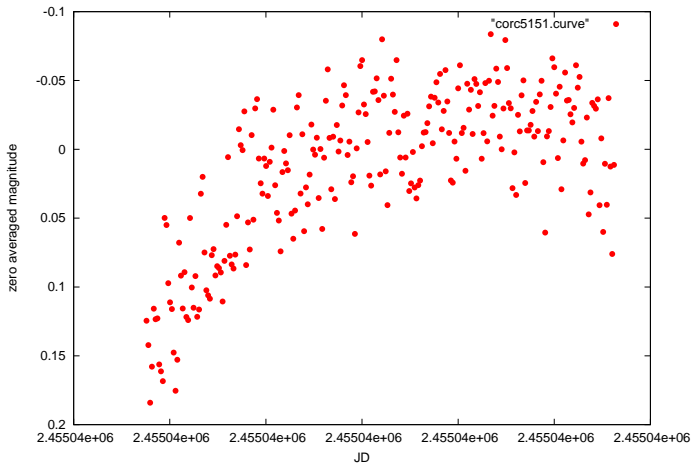
Figure 6.2.9: Light curves



(a) Star ID 4353

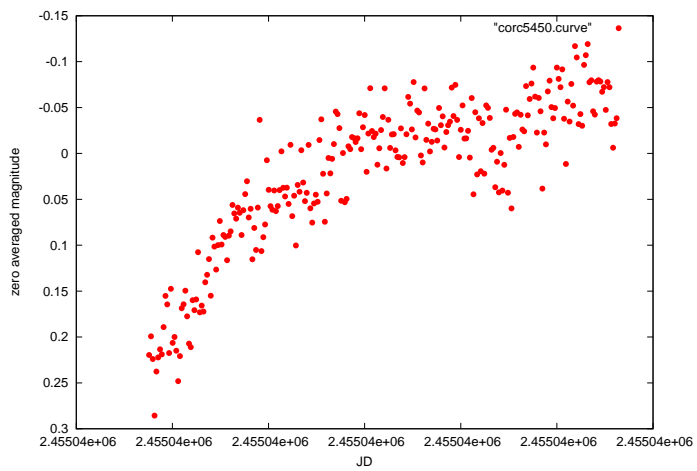


(b) Star ID 509

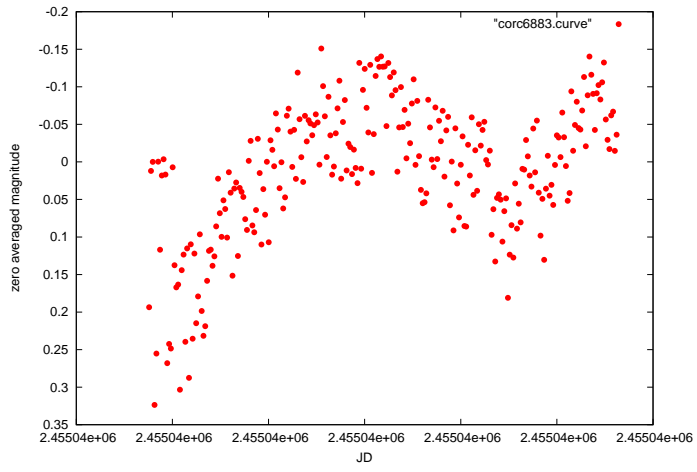


(c) Star ID 5151

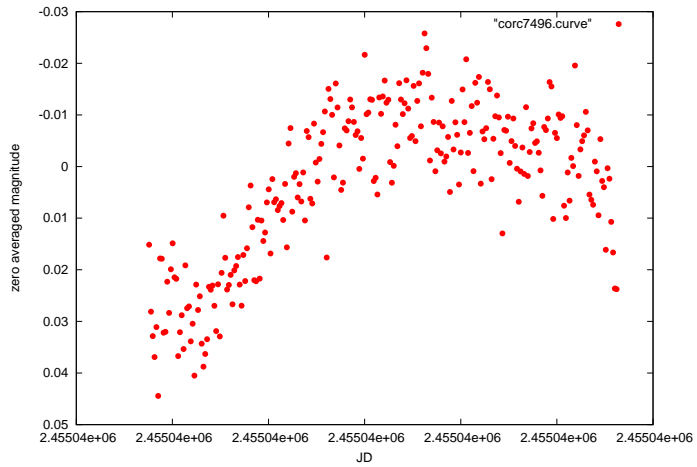
Figure 6.2.10: Light curves



(a) Star ID 5450

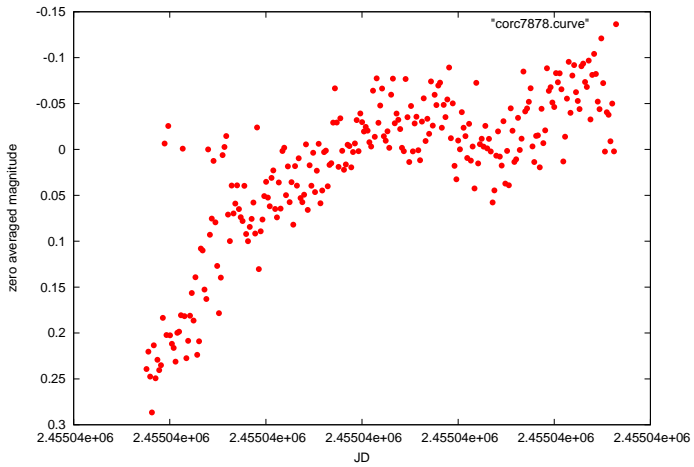


(b) Star ID 6883

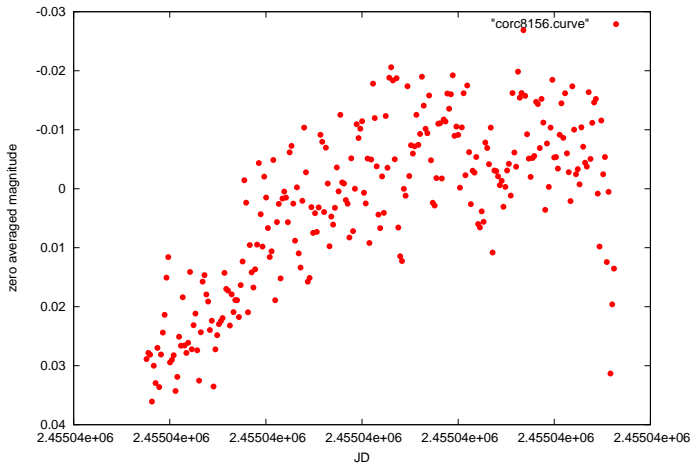


(c) Star ID 7496

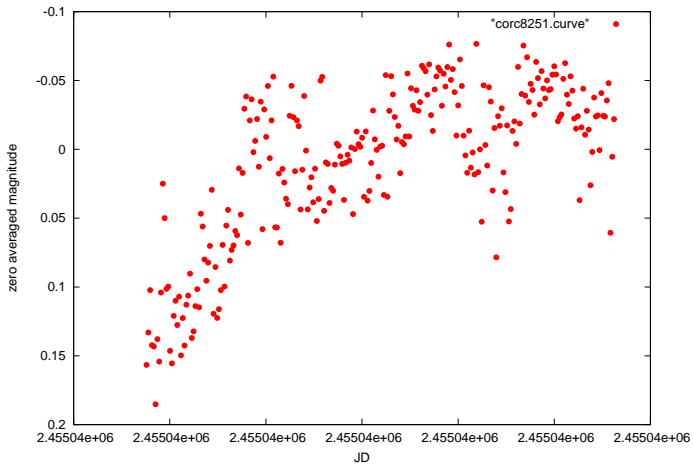
Figure 6.2.11: Light curves



(a) Star ID 7878

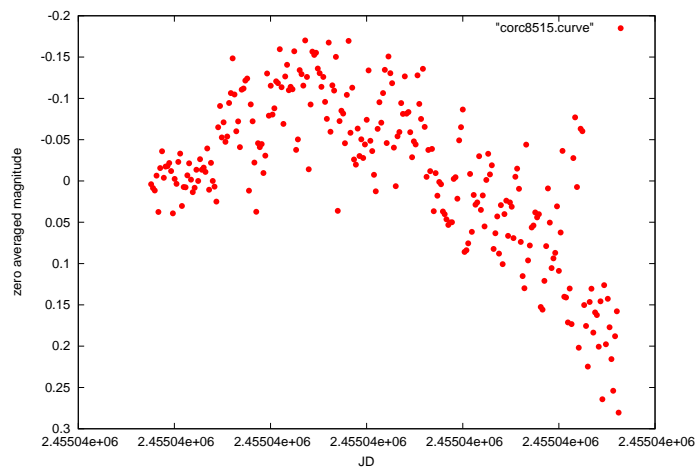


(b) Star ID 8156

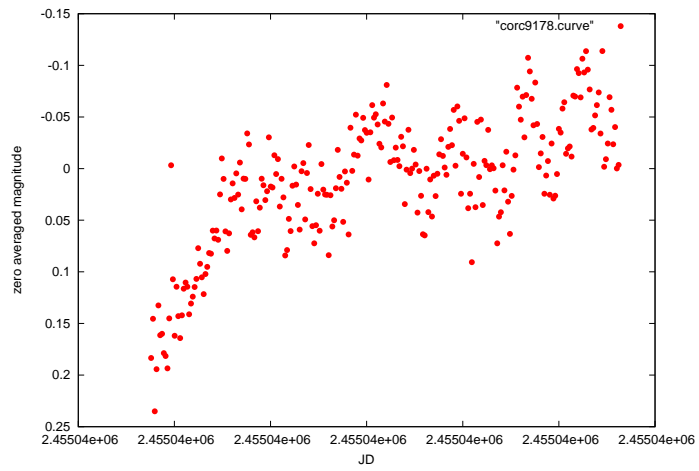


(c) Star ID 8251

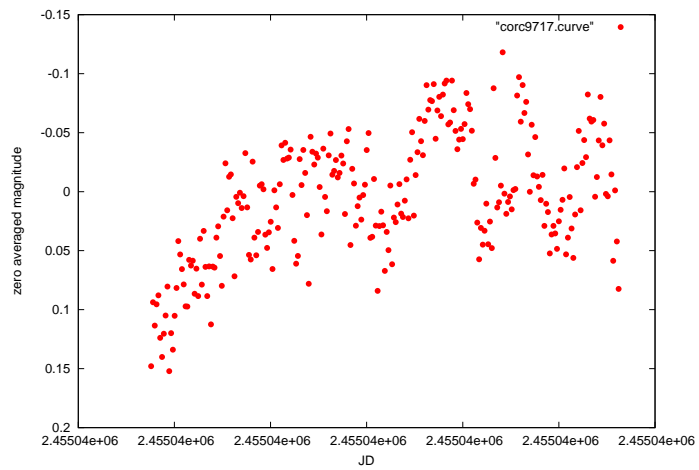
Figure 6.2.12: Light curves



(a) Star ID 8515



(b) Star ID 9178



(c) Star ID 9717

Figure 6.2.13: Light curves

Star ID	frame RA ($^{\circ}$)	frame DEC ($^{\circ}$)	Identifier	object RA ($^h \text{ } ^m \text{ } ^s$)	object DEC ($^h \text{ } ^m \text{ } ^s$)	Sp. type	Remarks
12177	343.927	+45.996	IRAS 22538+4541	22 56 07.6	+45 57 15		Infra-Red source
12517	340.992	+46.115	TYC 3621-1505-1	22 43 57.039	+46 11 33.19		
12610	343.931	+46.044	TYC 3622-2195-1	22 55 59.519	+46 03 08.52		
12765	340.799	+46.144	BD+45 4031	22 43 19.302	+46 08 23.92	A0	
2506	340.771	+44.575	NSV 14286	22 43 00.05	+44 35 19.0		
2582	340.501	+44.591	TYC 3226-1347-1	22 42 17.133	+44 38 50.47		
3289	342.163	+44.686	HD 216016	22 48 38.846	+44 41 13.94	K0	
3724	341.750	+44.774	CCDM J22470+4446AB	22 46 59.359	+44 46 22.59	A0	
3888	341.520	+44.804	TYC 3226-1575-1	22 46 04.911	+44 48 21.44		
4353	344.152	+44.806	BD+44 4280	22 56 16.499	+44 47 49.13	A5	
509	343.526	+44.162	TYC 3227-566-1	22 53 59.276	+44 15 37.72		
5151	342.496	+45.004	V* VY Lac	22 49 59.134	+45 00 16.03	A2	
5450	344.102	+44.997	BD+44 4281	22 56 20.810	+45 03 35.43	F8	
6883	340.790	+45.333	TYC 3621-678-1	22 43 18.408	+45 21 14.82		Eclipsing binary or β Lyr
7496	342.118	+45.408	HD 216003	22 48 28.049	+45 24 25.12	A0	
7878	344.332	+45.395	TYC 3622-1284-1	22 57 16.748	+45 19 48.26		
8156	342.678	+45.501	HD 216249	22 50 42.591	+45 30 03.22	K0	
8251	342.869	+45.511	HD 216339	22 51 28.589	+45 30 39.78	A0	
8515	340.649	+45.597	IRAS 22405+4521	22 42 45.9	+45 36 49		Infra-Red source
9178	340.605	+45.702	1RXS J224245.4+454410	22 42 45.396	+45 44 10.50		X-ray source
9717	341.674	+45.755	HD 215759	22 46 41.709	+45 45 21.54	A0	

Table 6.2.1: A catalogue of variable stars within ExoField #1.

6.3 Conclusions

- We have detected twenty-one (21) candidate variable stars, out of which sixteen (16) lack any bibliographic reference.
- We have added a new variability index, namely the j-index, to the ThReT reduction and analysis pipeline. The j-index performs well, quickly and is able to identify variable stars within a sample of thousands of light curves.
- Astrometric calibration have been performed and these stars have been pinpointed using the SIMBAD database.
- We have established that a survey for variable stars and possibly extra-solar planets can be conducted from Mt. Holomon, Greece.
- The good seeing conditions are also re-established. The mean seeing is 0.8 arcsec.
- Overall weather and seeing conditions at Mt. Holomon are favourable for a survey to start, in a more organized and possibly automated manner.
- Better results would be obtained if the observations of all consecutive nights were "bulk" reduced and analysed collectively. In our case this was not possible due to continuous changes of the instrumental configuration (addition–removal of filters, camera changes etc.) in order to carry out projects running in parallel.
- In this investigation there are several sources for error. The main trend introduced in most of our light curves, comes from the severe under sampling due to the large FoV of our instrument.
- An attempt to reduce the data using the HellasGRID computing infrastructure was made. Should this continue, we would be able to "bulk" reduce data in less time.

6.4 Future Work

This diploma thesis can be extended in various ways. A classification algorithm, for example, would be a significant contribution to the reduction and analysis pipeline. The constant observing runs at Mt. Holomon will provide new data and it is my intention to continue such observations.

One of the most interesting aspects of contemporary computer science is artificial intelligence and machine learning. Neural networks, especially, have been a very successful tool for astronomical research. Their main applications are automated identification and classification [3].

Self-organizing maps (SOM) provide an excellent example of a pattern recognition agent [43], [17]. They perform unsupervised classification and they are described by their inventor Teuvo Kohonen as "maps that reflect topological ordering". Before actually using the SOM, one has to train it. The SOM is a list of weight vectors which is realized as a two-dimensional grid of processing units (neurons). At the first stage each training pattern is assigned to a neuron. The model pattern is described by a vector with dimensionality equal to the number of features of the pattern. For example, a light curve is the pattern while the mean magnitude, the maximum variation and the period is the three dimensional vector that describes it. If more data are available i.e. spectral type, radial velocity etc. then the vector would be of higher dimensions. Next the map attempts to represent all the available data with optimal accuracy using the set of training patterns. This is why the algorithm needs to be trained with high-quality data. At the same time it organizes itself

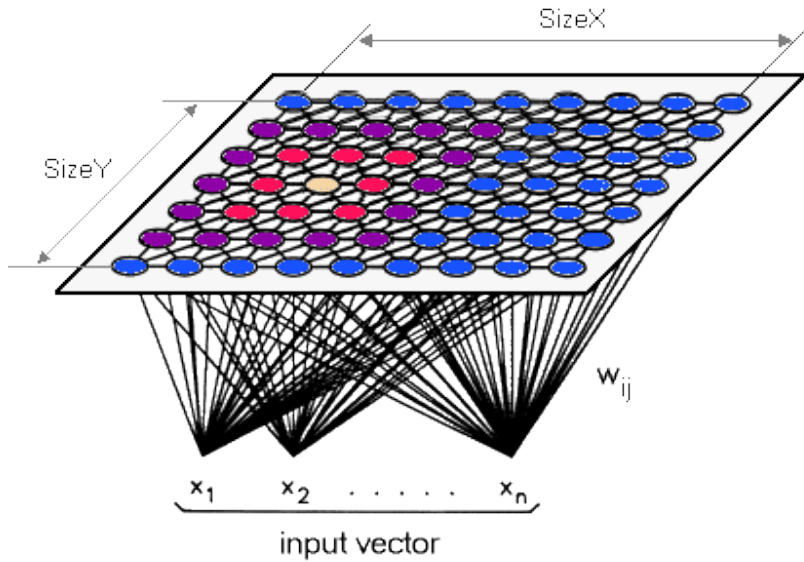


Figure 6.4.1: The Self-Organizing map.

topologically, according to a measure of similarity i.e. the smallest Euclidean distance. The result is a map in which similar patterns are close to each other while dissimilar patterns are far from each other.

Current projects, like OGLE (Optical Gravitational Lensing Experiment), use SOMs for rapid and robust early warning and classification purposes. Future space missions will also employ SOMs for such tasks. GAIA for example, the European Space Agency's cornerstone mission will map the entire sky and accumulate huge data sets comprising of spectroscopic and photometric data. SOMs that support GAIA will be detecting flux variations due to dwarf-novae, supernovae or microlensing events; they will also analyse the vast amount of data gathered in order to detect spectral anomalies due to stellar pulsations or eclipses. Finally new types of spectra are expected to be identified also.

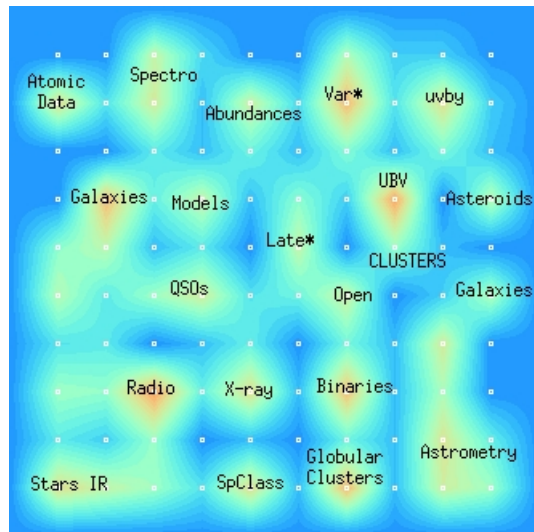


Figure 6.4.2: A SOM provided by the VizieR service to facilitate searching in astronomical catalogues. <http://vizier.cfa.harvard.edu/viz-bin/VizieR>

As it was stressed above it is clear that the continuation of observations is very impor-

tant in order to have new discoveries. As new techniques of observation and noise removal emerge and implemented, the possibilities of detection of low amplitude variability rise significantly. As a result extra-solar planetary transits are detectable from Mt. Holomon. This is further complimented by the outstanding "seeing performance" of the location. Over the years a significant amount of seeing data is gathered. The data argue that Mt. Holomon is an exceptional place for astronomical research. The installation of a professional telescope along with high-grade equipment would be very much appreciated and well-suited, given the overall conditions of the site. The effort will hopefully continue, also by others, and many interesting results are to come.

Appendices

Querying the SIMBAD database

In this appendix I present the results from a multi-object query to the SIMBAD Astronomical Database. The SIMBAD catalogue service can be reached via <http://simbad.u-strasbg.fr/simbad/>.

The search radius around every star is 5.5 arcmin. Only for the last entry, namely star ID 509, had to be used a search radius of 7 minutes of arc. All sources in the database within the search radius are shown. The number of bibliographic references on each entry is also visible.

coord 343.9273124 +45.9957987

Number of objects : 2

#	dist(asec)	identifier	typ	all types	coord1 (ICRS,J2000/2000)	Mag U	Mag B	Mag V	Mag R	Mag I	Sp. T	#bib	#not
-	-	-	--	--	--	--	--	--	--	--	--	--	--
1	269.61	TYC 3622-2195-1	*	* ,IR	22 55 59.5189 +46 03 08.520	~	11.11	10.79	~	~	~	0	0
2	301.04	IRAS 22538+4541	IR	IR	22 56 07.6 +45 57 15	~	~	~	~	~	~	0	0

coord 340.9922695 +46.1148747

Number of objects : 1

#	dist(asec)	identifier	typ	all types	coord1 (ICRS,J2000/2000)	Mag U	Mag B	Mag V	Mag R	Mag I	Sp. T	#bib	#not
-	-	-	--	--	--	--	--	--	--	--	--	--	--
1	279.88	TYC 3621-1505-1	*	* ,IR	22 43 57.0393 +46 11 33.194	~	11.14	10.69	~	~	~	0	0

coord 343.9310308 +46.0443209

Number of objects : 1

#	dist(asec)	identifier	typ	all types	coord1 (ICRS,J2000/2000)	Mag U	Mag B	Mag V	Mag R	Mag I	Sp. T	#bib	#not
-	-	-	--	--	--	--	--	--	--	--	--	--	--
1	169.81	TYC 3622-2195-1	*	* ,IR	22 55 59.5189 +46 03 08.520	~	11.11	10.79	~	~	~	0	0

coord 340.79993219 +46.1440432

Number of objects : 2

#	dist(assec)	identifier	typ	all types	coord1 (ICRS,J2000/2000)			Mag U	Mag B	Mag V	Mag R	Mag I	Sp. T	#bib	#not	
1	78.95	BD+45 4031	*	*_IR	22	43	19.3022	+46	08	23.923	~	11.25	11	~	A0	0
2	290.31	BD+45 4032C	*!	***,*!**	22	43	26.1	+46	04	29	~	~	11.2	~	0	0

coord 340.7713297 +44.5748273

Number of objects : 3

#	dist(assec)	identifier	typ	coord1 (ICRS,J2000/2000)				Mag U	Mag B	Mag V	Mag R	Mag I	Sp. T	#bib	#not
-	-	-	---	---	---	---	---	---	---	---	---	---	---	---	---
1	73.45	NSV 14286	V*	V*,V*,IR	22 43 00.05	+44 35 19.0		~	~	~	~	~	1	0	
2	180.86	TYC 3226-981-1	*	*	22 43 06.8319	+44 31 29.445		~	11.9	10.7	~	~	0	0	
3	272.61	P2 2241+442	Dsd	Dsd	22 43 20.44	+44 31 29.8		~	~	~	~	~	0	0	

coord 340.50008277 +44.59099999

Number of objects : 1

coord 344.152083 +44.8055687

Number of objects : 4

#	dist(asec)	identifier	typ	all types	coord1 (ICRS,J2000/2000)	Mag U	Mag B	Mag V	Mag R	Mag I	Sp. T	Mag	#bib	#not
1	215.11	BD+44 4280	*	,IR	22 56 16.4994 +44 47 49.127	~	11.08	10.7	~	~	A5	0	0	
2	234.04	TYC 3227-1650-1	*	,IR	22 56 56.4455 +44 49 58.726	~	11.44	10.13	~	~	~	0	0	
3	285.06	NVSS J225700+444445	Rad	Rad	22 56 55 +44 44.9	~	~	~	~	~	~	0	1	
4	315.06	TYC 3227-2349-1	*	,IR	22 56 26.0386 +44 43 25.342	~	10.83	10.42	~	~	~	0	0	

coord 342.4963054 +45.0035376

Number of objects : 3

coord 344.1023373 +44.997329

Number of objects : 3

#	dist(assec)	identifier	typ	all types	coord1 (ICRS,J2000/2000)	Mag U	Mag B	Mag V	Mag R	Mag I	Sp. T	#bib	#not
-	-	-	*	* ,IR	22 56 20.8103 +45 03 35.425	~	10.37	9.89	~	~	F8	0	0
1	228.53	BD+44 4281	*	* ,IR	22 56 20.5911 +44 55 16.326	~	11.5	10.9	~	~	0	0	0
2	277.28	TYC 3227-858-1	*	* ,IR	22 56 55.5028 +44 59 41.100	~	11.38	10.06	~	~	0	0	0
3	328.34	TYC 3227-1126-1	*	* ,IR							A	0	0

coord 340.7896747 +45.332825

Number of objects : 8

#	dist(assec)	identifier	typ	all types	coord1 (ICRS,J2000/2000)	Mag U	Mag B	Mag V	Mag R	Mag I	Sp. T	#bib	#not
-	-	-	*	* ,IR	22 43 18.4081 +45 21 14.821	~	12.2	10.4	~	~	~	0	0
1	121.05	TYC 3621-678-1	*	* ,IR	22 43 03.6787 +45 22 57.638	~	11.6	11.1	~	~	~	0	0
2	189.74	TYC 3621-557-1	*	* ,IR	22 42 49.99 +45 21 03.5	~	~	~	~	~	~	0	0
3	216.04	1RXS J224250.0+452103	X	X	22 42 47.726 +45 21 05.21	~	10.81	10.19	10.12	~	~	1	0
4	239.38	TYC 3621-711-1	V?	* ,V?,IR	22 42 47.726 +45 21 05.21	~	10.9	10.2	~	~	G0	0	0
5	257.52	HD 215190	*	*	22 42.8 +45 22	~	11.07	9.7	~	~	G5	0	0
6	292.17	HD 215226	*	* ,IR	22 42 52.5570 +45 16 07.251	~	~	~	~	~	0	0	0
7	308.84	NWSS J224259+452446	Rad	Rad	22 42 59.27 +45 24 47.5	~	10.57	9.33	~	~	A	0	0
8	315.16	BD+44 4212	*	* ,IR	22 43 16.5275 +45 14 51.799	~							

coord 342.1184885 +45.4076024

Number of objects : 7

#	dist(asec)	identifier	typ	all types	coord1 (ICRS,J2000/2000)			Mag U	Mag B	Mag V	Mag R	Mag I	Sp. T	#bib	#not
1	4.66	HD 216003	*	* IR,UV	22 48 28.0492	+45 24 25.121	~	8.45	8.4	~	~	A0	0	0	
2	41.83	BD+44 4239	*	* IR	22 48 25.3658	+45 24 00.839	~	10.39	10.18	~	~	A0	0	0	
3	135.76	NVSS J224841+452417	Rad	Rad	22 48 41.30	+45 24 18.4	~	~	~	~	~	~	0	0	
4	157.31	LP 237-36	PM*	* PM*,IR	22 48 41.82	+45 25 37.3	~	14.33	12.7	11.8	10.7	~	3	0	
5	167.01	BD+44 4237	*	* IR	22 48 15.7821	+45 22 46.762	~	11.34	10.12	~	~	K2	0	0	
6	175.38	2MASS J22484407+4525275PM*	* IR	22 48 44.08	+45 25 27.6	~	20.8	~	18.4	16.2	~	1	0		
7	322.65	LHS 6412	PM*	* PM*,IR	22 48 47.96	+45 20 18.8	~	16.1	~	13.5	11.8	M4	4	0	

coord 344.3316356 +45.3949524

Number of objects : 1

coord 342.6783073 +45.5011943

Number of objects : 2

dist(asec)	identifier	typ	all types	coord1 (ICRS,J2000/2000)			Mag U	Mag B	Mag V	Mag R	Mag I	Sp. T	#bib	#not
1.239	HD 216249	*	*.IR	22 50 42.5909	+45 30 03.224		~ 10.04	8.91	~	~	K0	0	0	
2.258.79	TYC 3621-653-1	*	*.IR	22 50 56.0330	+45 26 26.182		~ 12.3	10.8	~	~	~	0	0	

coord 341.6737167 +45.7547071

Number of objects : 3

#	dist(assec)	identifier	typ	all types	coord1 (ICRS,J2000/2000)	Mag U	Mag B	Mag V	Mag R	Mag I	Sp. T	#bib	#not
-	-	-	--	--	--	--	--	--	--	--	--	--	--
1	4.6	HD 215759	*	,IR	22 46 41.7095 +45 45 21.543	~	9.73	9.65	~	~	A0	0	0
2	61.69	TYC 3621-217-1	*	,IR	22 46 45.9092 +45 44 33.857	~	11.7	10.8	~	~	0	0	0
3	328.98	HD 215685	*	,IR	22 46 13.6786 +45 42 47.935	~	10.65	10.51	~	~	A	0	0

coord 343.5261863 +44.1619413 (FK5, 2000, 2000), radius: 7 arcmin

Number of objects : 2

#	dist(assec)	identifier	typ	all types	coord1 (ICRS,J2000/2000)	Mag U	Mag B	Mag V	Mag R	Mag I	Sp. T	#bib	#not
-	-	-	--	--	--	--	--	--	--	--	--	--	--
1	362.65	TYC 3227-566-1	*	,IR	22 53 59.2761 +44 15 37.723	~	11.09	10.73	~	~	0	0	0
2	392.86	2MFGC 17222	LSB	G,LSB	22 54 35.8 +44 05 52	~	~	~	~	~	3	0	0

Software

This appendix contains the original sigma.csh script which I modified in order to obtain the J-index (Stetson, 1996)[40] for each star. The calculation is performed within the sigma.for fortran routine. This appendix also contains some of the scripts written by me, in order to make the life of others and mine a little easier. The main aim of some scripts is clearly the visual investigation of images or light curves, after plotting.

sigma.csh

```
cd $directory/
cp $home/Analysis/sigma.for .
rm *.txt
rm c*.curve
ls -l $data*.mtA >junk

set k='awk 'END{print NR}' junk'

foreach file(*.curve)
clear
echo
echo
echo
echo
set b='awk 'END{print NR}' $file'

if ($b > 3)then
    echo "CHECKING NUMBER OF POINTS ON FILE $file.....OK"
else
    echo "CHECKING NUMBER OF POINTS ON FILE $file.....REMOVED"
    rm $file
endif
end

if (-e junk)then
rm junk
endif

if (-f time)then
rm time
endif
```

```
if(-f air)then
rm air
endif

if(-f delta)then
rm delta
endif

foreach file(*.jd)
set rr=$file:r
cat $file >>time
cat $rr.air >>air
end
set time='cat time'
set air='cat air'
set tnr='awk 'END{print NR}' time'

gfortran sigma.for

foreach file(*.curve)
echo
echo
echo
set n='awk 'END{print NR}' $file'

#Number of points per star
echo $n > n
echo $n > q
awk '{print $2}' $file > mag
awk '{print $3}' $file >error
./a.out

set mean='cat mean.txt'
set sigma='cat sigma.txt'
set inner='cat inner.txt'
set pulse='cat pulse.txt'
set rms='cat rms.txt'
set lrms='cat logrms.txt'
set jind='cat jind.txt'

set i=1
while ($i <= $tnr)
  set b='cat $file|grep $time[$i]'
  set nb=$#b
  if ($nb == 4)then
    echo $b >> c$file
  else
    echo $time[$i] $mean $sigma $air[$i] >> c$file
  endif
```

```

@ i = $i + 1
end

echo $mean $sigma $inner $pulse $rms $lrms $jind $file >> sigmaplot.txt
echo "          FILE $file UNDER ANALYSIS"
echo "          CALCULATED MEAN : $mean"
echo "          CALCULATED SIGMA: $sigma"
echo "          CALCULATED PULSATION: $pulse"
echo "          J-INDEX: $jind"

end

rm -f cc$file

rm junk
cd $home/Analysis/
#source ensemble.csh

```

sigma.for

```

real*8 s, mean, sum, inner, sum2
real*8 k, ssum, fac, dsum, pulse
real*8 dfac, frac           !for the j index calculation
real*8 Psum, w, wsum, jind, one   !for the j index calculation
real*8 calc, inv, mag, siner, sum3
real*8 rms, lrms
integer n, x, i, m
real*8 A(10000), E(10000), D(10000), Pk(10000)

! Open and Read Input
open (1, file='n')
read (1,*) n
open (11, file='q')
read (11,*) q
open (2, file='mag')
read (2,*) (A(x),x=1,n)
open (3, file='error')
read (3,*) (E(x),x=1,n)

open (33, file='Deltas.txt')
inv= 1/q

! Calculate mean magnitute (x square fitting)
sum2=0

```

```

sum3=0
!
do i=1,n
  sum2 = sum2 + A(i)
!
enddo
mean = sum2*inv

do i=1,n
  sum2 = sum2 + 1/(E(i)**2)
  sum3 = sum3 + A(i)/(E(i)**2)      ! Weighted with the error mean
enddo
mean = sum3/sum2

!Calculate sigma deviation
ssum=0
do i=1,n
  k= A(i) - mean
  ssum = ssum + k**2
enddo
calc = ssum * inv
sigma = calc - mean**2
sigma = sqrt(calc)

!
write (6,*) n, i, k, ssum, calc, sigma !check the output

!Calculate delta magnitude residual
dfac = sqrt(q/(q-1))
do i=1,n
  frac = (A(i) - mean)/sigma
  D(i) = dfac*frac
!
  write (6,*) D(i) !To check the output
enddo

write (33,*) D(i)
close (33)

!Calculate P_k
m=1

do i=1,n,2

!-1 in the paper is to account for mathematical consistency.
!e.g If the number of observations is odd

  Pk(m) = D(i)*D(i+1)
!
  write (6,*) n, D(i), Pk(m), i, m !To check the output
  m=m+1

```

```

enddo

!calculate the j index
w=1
wsum=0
Psum=0
one=1 !This is used so argument a and b in sign() are of the same type.

do i=1,m !afou o pinakas Pk pairnei times apo 1 mehri m, mises apo ta D.

    Psum = Psum + (w * sign(one, Pk(i))) * sqrt(abs(Pk(i)))
    wsum = wsum + w
    write(6,*) Psum, wsum, jind, "#####" ! to check the output

enddo
jind = Psum/wsum
!The function sign(a, b) returns the value of a with the sign of b

!Calculate inner sigma scattering
dsum=0
fac = 1/(2*(q-1))
m = n - 1
dsum = 0
do i=1,m
    dsum = dsum + (A(i)-A(i+1))**2
enddo
siner = dsum*fac
inner = sqrt(siner)

!Calculate Pulsation factor
pulse = sigma/inner

!Calculate rms
rms = 0
do i=1,n
    rms = rms + ((A(i)-mean)/(E(i)))**2
enddo

!Calculate log(rms)

lrms = log(rms)

!Write results to file
open (3,file='mean.txt')
open (4,file='sigma.txt')
open (5,file='inner.txt')

```

```

open (6,file='pulse.txt')
open (7,file='rms.txt')
open (8,file='logrms.txt')
open (9,file='jind.txt')

write (3,*) mean
write (4,*) sigma
write (5,*) inner
write (6,*) pulse
write (7,*) rms
write (8,*) lrms
write (9,*) jind
end

```

sigma2.for

```

real*8 s, mean, sum, inner, sum2
real*8 k, ssum, fac, dsum, pulse
real*8 dfac, frac           !Dilosimou
real*8 Psum, w, wsum, jind, one      ! about the j index
real*8 calc, inv, mag, siner, sum3
real*8 rms, lrms
integer n, x, i, m
real*8 A(10000), D(10000), Pk(10000)

! Open and Read Input
open (1, file='n')
read (1,*) n
open (11, file='q')
read (11,*) q
open (2, file='mag')
read (2,*) (A(x),x=1,n)
i=1

open (33, file='Deltas.txt')
inv= 1/q

! Calculate mean magnitude (x square fitting)

sum2=0
sum3=0
do i=1,n
sum2 = sum2 + A(i)
enddo
mean = sum2*inv

```

```

!
!      do i=1,n
!        sum2 = sum2 + 1/(E(i)**2)
!        sum3 = sum3 + A(i)/(E(i)**2)      ! Weighted mean
!
!      enddo
!      mean = sum3/sum2

!Calculate sigma deviation
ssum=0
do i=1,n
  k= A(i) - mean
  ssum = ssum + k**2
enddo
calc = ssum * inv
sigma = calc - mean**2
sigma = sqrt(calc)

!      write (6,*) n, i, k, ssum, calc, sigma !To check the output

!Calculate delta magnitude residual
dfac = sqrt(q/(q-1))
do i=1,n
  frac = (A(i) - mean)/sigma
  D(i) = dfac*frac
!
!      write (6,*) D(i) !To check the output
enddo

write (33,*) D(i)
close (33)

!Calculate P_k
m=1

do i=1,n,2
  !To -1 to vazei gia to mathimatiko tou pragmatos kai
  !otan den ehei zygo arithmo paratiriseon...
  Pk(m) = D(i)*D(i+1)
!
  write (6,*) n, D(i), Pk(m), i, m !To check the output
  m=m+1

enddo

!calculate the j index
w=1
wsum=0
Psum=0

```

```

one=1 !This is used so argument a and b in sign() are of the same type

do i=1,m !afou o pinakas Pk pairnei times apo 1 mehri m, mises apo ta D

Psum = Psum + (w * sign(one, Pk(i))) * sqrt(abs(Pk(i)))
wsum = wsum + w
!      write(6,*) Psum, wsum, jind, "#####" ! to check the output

enddo
jind = Psum/wsum
!The function sign(a, b) returns the value of a with the sign of b

!Calculate inner sigma scattering
dsum=0
fac = 1/(2*(q-1))
m = n - 1
dsum = 0
do i=1,m
dsum = dsum + (A(i)-A(i+1))**2
enddo
siner = dsum*fac
inner = sqrt(siner)

!Calculate Pulsation factor
pulse = sigma/inner

!Write results to file
open (3,file='mean.txt')
open (4,file='sigma.txt')
open (5,file='inner.txt')
open (6,file='pulse.txt')
open (9,file='jind.txt')

write (3,*) mean
write (4,*) sigma
write (5,*) inner
write (6,*) pulse
write (9,*) jind
end

```

fitsinspect.csh

```
#!/bin/csh

source /star/etc/cshrc
source /star/etc/login

alias echo "echo > /dev/null"
kappa
ccdpack
convert
figaro
unalias echo

#echo Give the path of the dataset
#set path=$<
#cd $path

#echo File name of datafiles to inspect
#set name=$<

gaia &
sleep 3

foreach image (*.fit)
  gaiadisp $image
  sleep 4
end
```

curveobserve.csh

```
#!/bin/csh

foreach file (*.curve)
gnuplot<<EOF
plot "$file" with lines
pause 2
EOF
#sleep 3
end
```

remover.csh

```
#!/bin/csh

mv *.fit tmp/
```

```
rm *<<EOF
y
EOF

cd tmp
mv * ..
```

SeeingPlotter.csh

```
#!/bin/csh

# Check if the directory graphs exists and if yes delete it
if (-d graphs) then
    rm -r graphs
endif

#make directory graphs
mkdir graphs

foreach directory (*)
    set dir=$directory
    cd $dir
    echo "***** Working on file" $dir "*****"

gnuplot<<EOF
set terminal postscript enhanced color
set xlabel "JD 2450000+"
set ylabel "seeing (arcsec)"
set out '$dir.ps'
plot "results_smooth.dat" using 1:3 pointsize 2 pt 9 lt 1
title "FWHM-X", "" using 1:4 title "FWHM-Y" pt 7 pointsize 2 lt 3
exit
EOF

# set format x "%.4f" #this is to change the number of
#decimal places to 4, no need for it here.
#Put it before the plot command.

cp *.ps ../graphs

#rm -f *.eps
#rm -f *.ps      #un-comment this to get rid
# of all the .ps files in all the directories

cd ..
end

end
```

curveplotter.csh

```

#!/bin/csh

#sort -k5 -n sigmaplot.txt > jsigmaplot
#sort -k4 -n sigmaplot.txt > pulse_sigmaplot

#set n = `awk 'END{print NR}' jsigmaplot'
#echo "The file contains" $n "entries"

#set jindex = `awk '{print $5}' jsigmaplot'
#set pulsation = `awk '{print $4}' pulse_sigmaplot'

#Here U define the threshold of variability,
#for the j_index and the pulsation parameter
#awk '{if ($5 >= 0.50) print $5, $6}' jsigmaplot > j_high
#awk '{if ($4 >= 2.5) print $4, $6}' jsigmaplot > puls_high

#mkdir plots

set ID = `awk '{print $2}' j_high'
cp $ID plots

cd plots

foreach file(*.curve)

    set number = $file
    gnuplot<<EOF
    set terminal postscript enhanced color
    set yrangle[0.4:-0.4]
    set autoscale
    set xlabel "JD"
    set ylabel "zero averaged magnitude"
    set out "$number.ps"
    plot "$number"
    exit
EOF

end

```

pdfer.csh

```
#!/bin/csh

#A script to convert multiple .ps files to .pdf

rm -f *.pdf

foreach file (*.ps)
    set f=$file:r
    ps2pdf $f.ps $f.pdf
end

#rm -f *.ps #To keep or not to keep the .ps files? If not uncomment!

end
```

Bibliography

- [1] J. ANTONIADIS, *A survey for extrasolar planets with the method of transits*, Diploma thesis, (2009).
- [2] J. ANTONIADIS, V. KARAMANAVIS, D. MISLIS, A. NITSOS, AND J. H. SEIRADAKIS, *ThReT: A New Survey for Extrasolar Planetary Transits at Mt. Holomon Greece*, in Astronomical Society of the Pacific Conference Series, K. Tsinganos, D. Hatzidimitriou, & T. Matsakos, ed., vol. 424 of Astronomical Society of the Pacific Conference Series, July 2010, pp. 218–+.
- [3] V. BELOKUROV, N. W. EVANS, AND Y. L. DU, *Light-curve classification in massive variability surveys - I. Microlensing*, MNRAS, 341 (2003), pp. 1373–1384.
- [4] F. BONNAREL, P. FERNIQUE, O. BIENAYMÉ, D. EGRET, F. GENOVA, M. LOUYS, F. OCHSENBEIN, M. WENGER, AND J. G. BARTLETT, *The ALADIN interactive sky atlas. A reference tool for identification of astronomical sources*, Astronomy and Astrophysics, 143 (2000), pp. 33–40.
- [5] E. BUDDING AND O. DEMIRCAN, *Introduction to astronomical photometry*, 2007.
- [6] B. W. CARROLL AND D. A. OSTLIE, *An Introduction to Modern Astrophysics*, 1996.
- [7] G. J. CURRIE, M. J. PIVETT AND A. J. CHIPPERFIELD, *CONVERT – A Format-conversion Package*, (1997).
- [8] M. J. CURRIE, *KAPPA – Kernel Application Package*, (1997).
- [9] A. C. DAVENHALL, *Road-Map for CCD Photometry*, Starlink Bulletin, No. 20, pp17–19, 1998.
- [10] P. W. DRAPER, *GAIA – Graphical Astronomy and Image Analysis Tool*, (1997).
- [11] C. J. HANSEN, S. D. KAWALER, AND V. TRIMBLE, *Stellar Interiors - Physical Principles, Structure, and Evolution*, Springer, 2nd ed., 2 2004.
- [12] R. HELLER, D. MISLIS, AND J. ANTONIADIS, *Transit detections of extrasolar planets around main-sequence stars. I. Sky maps for hot Jupiters*, Astronomy and Astrophysics, 508 (2009), p. 1509.
- [13] S. B. HOWELL, *Handbook of CCD astronomy*, Cambridge University Press, 2006.

- [14] P. KABATH, A. ERIKSON, H. RAUER, T. PASTERNAKCI, S. CSIZMADIA, R. CHINI, R. LEMKE, M. MURPHY, T. FRUTH, R. TITZ, AND P. EIGMÜLLER, *Periodic variable stars in CoRoT field LRa02 observed with BEST II*, Astronomy and Astrophysics, 506 (2009), pp. 569–587.
- [15] J. KALLRATH AND E. F. MILONE, *Eclipsing Binary Stars: Modeling and Analysis: Astronomy and Astrophysics Library*, Springer-Verlag New York, 2009.
- [16] H. KARTTUNEN, P. KRÜGER, H. OJA, M. POUTANEN, AND K. J. DONNER, eds., *Fundamental Astronomy*, 2007.
- [17] T. KOHONEN, *Self-Organizing Maps*, 2001.
- [18] G. KOVÁCS, G. BAKOS, AND R. W. NOYES, *A trend filtering algorithm for wide-field variability surveys*, MNRAS, 356 (2005), pp. 557–567.
- [19] D. W. KURTZ, *Stellar pulsation: an overview*, Communications in Asteroseismology, 147 (2006), pp. 6–30.
- [20] D. W. KURTZ, V. G. ELKIN, AND G. MATHYS, *Probing the magnetoacoustic boundary layer in the peculiar magnetic star 33 Lib (HD 137949)**, MNRAS, 358 (2005), pp. L6–L10.
- [21] P. MASSEY AND G. H. JACOBY, *CCD Data: The Good, The Bad, and The Ugly*, in Astronomical CCD Observing and Reduction Techniques, S. B. Howell, ed., vol. 23 of Astronomical Society of the Pacific Conference Series, 1992, pp. 240–+.
- [22] W. J. MERLINE AND S. B. HOWELL, *A Realistic Model for Point-sources Imaged on Array Detectors: The Model and Initial Results*, Experimental Astronomy, (1995).
- [23] D. MISLIS, *Measurements of Atmosphere Turbulence and Detection of Extrasolar Planetary Systems*, Diploma thesis, (2005).
- [24] D. MISLIS, S. PYRZAS, E. T. HARLAFTIS, R. A. STREET, K. HORNE, D. POLLACCO, J. H. SEIRADAKIS, S. R. KANE, T. LISTER, C. CAMERON, AND W. I. CLARKSON, *WASP0: A wide field CCD search for extra solar planets. Instrumentation, data analysis and preliminary results*, in Recent Advances in Astronomy and Astrophysics, N. Solomos, ed., vol. 848 of American Institute of Physics Conference Series, Aug. 2006, pp. 810–815.
- [25] L. MORTARA AND A. FOWLER, *Evaluations of Charge-Coupled Device / CCD / Performance for Astronomical Use*, in Society of Photo-Optical Instrumentation Engineers (SPIE) Conference Series, vol. 290 of Society of Photo-Optical Instrumentation Engineers (SPIE) Conference Series, Jan. 1981, pp. 28–+.
- [26] I. NESTORAS, *Photometric observations and Data Reduction of Contact Binary Systems and of SS433 Long Term Study of the Astronomical Seeing in Mount Xolomon Chalkidikis*, Diploma thesis, (2007).
- [27] J. S. NESTORAS, D. MISLIS, S. PYRZAS, E. TREMOU, J. H. SEIRADAKIS, AND S. I. AVGOLOUPI, *Seeing Measurements from Mt. Holomon*, in Recent Advances in Astronomy and Astrophysics, N. Solomos, ed., vol. 848 of American Institute of Physics Conference Series, Aug. 2006, pp. 906–909.
- [28] J. PALMER AND A. C. DAVENHALL, *The CCD Photometric Calibration Cookbook*, (1997).

- [29] J. R. PERCY, *Understanding variable stars*, Cambridge University Press, 2007.
- [30] A. C. PHILLIPS, *The Physics of Stars, 2nd Edition*, July 1999.
- [31] G. J. PIVETT, *The 2-D CCD Data Reduction Cookbook*, (1997).
- [32] S. PYRZAS, *Photometric study and detection of periodicities in cataclysmic variable stars*, Diploma thesis, (2009).
- [33] A. REBASSA-MANSERGAS, *Post-common-envelope binaries from the Sloan Digital Sky Survey*, PhD thesis, (2008).
- [34] A. REBASSA-MANSERGAS, B. T. GÄNSICKE, M. R. SCHREIBER, J. SOUTHWORTH, A. D. SCHWOPE, A. NEBOT GOMEZ-MORAN, A. AUNGWEROJWIT, P. RODRÍGUEZ-GIL, V. KARAMANAVIS, M. KRUMPE, E. TREMOU, R. SCHWARZ, A. STAUDE, AND J. VOGEL, *Post-common envelope binaries from SDSS - III. Seven new orbital periods*, MNRAS, 390 (2008), pp. 1635–1646.
- [35] W. K. ROSE, *Advanced Stellar Astrophysics, ISBN 0521581885*. Cambridge, UK: Cambridge University Press., May 1998.
- [36] M. SARAZIN AND F. RODDIER, *The ESO differential image motion monitor*, Astronomy and Astrophysics, 227 (1990), pp. 294–300.
- [37] J. H. SEIRADAKIS AND S. AVGOLOUPI, *Observational Anstronomy*, AUTH, 1986.
- [38] K. T. SHORTRIDGE, H. MEYERDIERKS, M. J. CURRIE, M. J. CLAYTON, AND J. J. LOCKLEY, *FIGARO – A general data reduction system*, (1997).
- [39] C. STERKEN AND C. JASCHEK, eds., *Light Curves of Variable Stars: A Pictorial Atlas*, Cambridge University Press, 2005.
- [40] P. B. STETSON, *On the Automatic Determination of Light-Curve Parameters for Cepheid Variables*, PASP, 108 (1996), pp. 851–+.
- [41] H. VARVOGLIS AND J. H. SEIRADAKIS, *Introduction to Contemporary Astronomy*, 3rd ed., Gartaganis, Thessaloniki, 1994.
- [42] M. VISKUM, M. M. HERNANDEZ, J. A. BELMONTE, AND S. FRANDSEN, *A search for delta Scuti stars in northern open clusters. I. CCD photometry of NGC 7245, NGC 7062, NGC 7226 and NGC 7654*, Astronomy and Astrophysics, 328 (1997), pp. 158–166.
- [43] L. WYRZYKOWSKI AND V. BELOKUROV, *Self-Organizing Maps. An application to the OGLE data and the Gaia Science Alerts*, AIP Conf. Proc., 1082 (2008), pp. 201–206.
- [44] X. ZHANG, L. DENG, Y. XIN, AND X. ZHOU, *Searching for Variable Stars in the Field of NGC 7789*, Chin. J. Astron. Astrophys., 3 (2003), pp. 151–165.

Index

- ϵ -mechanism, 10
- accretion column, 36
- ADU, analog-to-digital units, 53
- AI Vel stars, 32
- Ap stars, 33
- Argelander, 3
- astrometric binaries, 14
- bias, 63
- Blazhko effect, 32
- Bonner Durchmusterung, 2, 3
- cataclysmic variables, 12, 35
- chemically peculiar, CP stars, 19, 33
- cluster-type variables, 31
- common envelope binary, 15
- common-envelope, CE, 36
- contact binary, 15
- core-collapse supernovae, 38
- counts, 53
- dark current, 63
- David Fabricius, 2
- detached systems, 15
- differential rotation, 18
- dwarf Cepheids, 32
- dwarf novae, 12, 36
- eclipsing binaries, 14
- FG Serpentis, 37
- flare stars, 12
- flat fields, 63
- FU Orionis, 40
- gain, 53
- gravity darkening, 43
- Hipparchus, 1
- HM Sagittae, 37
- IBVS, Information Bulletin on Variable Stars, 4
- intermediate polars, 36
- Isoplanatic angle, 47
- j-index, 66, 101
- jets, 40
- k-mechanism, 10
- Kepler's supernova, 2
- lighthouse effect, 30, 42
- linearity, 53
- meridional circulation, 19
- micro flares, 35
- Name List of Variable Stars, 4
- nebular variables, 12
- Non-radial Pulsations, 12
- nova-like stars, 12
- novae, 12, 35
- NSV, New catalog of Suspected Variables, 4
- oblique-pulsator model, 33
- oblique-rotator model, 33
- over-contact binary, 15
- Poisson noise, 56, 64
- polars, 36
- post-common-envelope binaries, PCEBs, 36
- primary component, 15, 17
- primary minimum, 15
- pulsation parameter, 66
- QE, Quantum efficiency, 53

- R Coronae Borealis stars, 12
- Radial Pulsations, 11
- readout noise, 55
- Roche geometry, 14
- Roche lobes, 14
- RR Telescopii, 37
- RRs variables, 32
- RS Canum Venaticorum, 25
 - scintillation, 47
 - secondary component, 15
 - seeing, 47
 - self-organizing maps, SOM, 85
 - semi-detached binary, 15
 - shot noise, 64
 - Signal-to-Noise Ratio, S/N, 55
 - spectroscopic binaries, 14
 - spotted-pulsator model, 33
 - starspot or distortion wave, 26
 - stochastic driving, 10
- SX Phe stars, 32
- symbiotic phenomenon, 37
- trends, 64
- Tycho Brahe's supernova, 2
- ultra-short period Cepheids, 32
- V1016 Cygni, 37
- visual binaries, 13
- white noise, 64
- YY Geminorum, Castor C, 29
- Z Andromedae, 37
- zero-phase, 15